Université d'Ottawa · University of Ottawa

Université d'Ottawa - University of Ottawa

FACULTÉ DES ÉTUDES SUPÉRIEURES ET POSTDOCTORALES

FACULTY OF GRADUATE AND POSTDOCTORAL STUDIES

EDNIE, Mark

AUTEUR DE LA THÈSE - AUTHOR OF THESIS

M.Sc. (Geography)

GRADE - DEGREE

Department of Geography

FACULTÉ, ÉCOLE, DÉPARTEMENT - FACULTY, SCHOOL, DEPARTMENT

TITRE DE LA THÈSE - TITLE OF THE THESIS

Evaluation of the Basal Temperatures of Snow (BTS) Method to Map Permafrost in Complex Mountainous Terrain, Wolf Creek, Y.T.

A. Lewkowicz

DIRECTEUR DE LA THÈSE - THESIS SUPERVISOR

EXAMINATEURS DE LA THÈSE - THESIS EXAMINERS

C. Burn

M. Sawada

J.-M. De Koninck, Ph.D.

LE DOYEN DE LA FACULTÉ DES ÉTUDES SUPÉRIEURES ET POSTDOCTORALES

SIGNATURE

DEAN OF THE FACULTY OF GRADUATE AND POSTDOCTORAL STUDIES

Evaluation of the basal temperature of snow (BTS) method to map permafrost in complex mountainous terrain, Wolf Creek, Y.T.

Mark Ednie

Masters of Science Thesis submitted to the Faculty of
Graduate and Post Doctoral Studies

Department of Geography
University of Ottawa

Your file Votre référence
ISBN: 0-612-90066-5
Our file Notre référence
ISBN: 0-612-90066-5

ABSTRACT

This study is the first known attempt in North America to use the basal temperature of snow (BTS) method to predict the distribution of mountain permafrost. The study site, Wolf Creek Research Basin, Yukon Territory (60°30'N, 135°13'W), is a 195 km^2 basin ranging in elevation from 650-2100 m with a mean annual air temperature of about -4°C at 1235 m a.s.l.

A modeled BTS surface, based on 394 measured BTS values and with elevation and potential incoming solar radiation as independent variables, was created within a GIS environment with an r^2 value similar to European results. The distribution of permafrost within the basin was identified from pits and boreholes. A subsequent logistic regression was used to compare modeled BTS values to the actual permafrost distribution in order to produce a map of permafrost probability in the basin. A significantly higher likelihood of permafrost, observed in a confined valley bottom, was attributed to cold air drainage. This occurrence was not predicted by the BTS model and data from the affected area were removed from later analyses.

Based on the predicted permafrost distribution, continuous permafrost (>90%) is present above 1600 m, widespread discontinuous permafrost (50-90%) is predicted between 1400-1600 m, sporadic discontinuous permafrost (10-50%) is predicted between 800-1400 m, and isolated permafrost (<10%) is predicted below 800 m. Slope orientation and gradient affect the probability of permafrost so that on north-facing 20° slopes >90% probability extends to below 1500 m, while on south-facing slopes with a similar gradient, the same probability is 200 m higher. An estimated 43% of the basin is underlain by permafrost.

Separate logistic regressions were used to predict permafrost probability under deep snow conditions (>80 cm) and shallow snow conditions (<80 cm). Under shallow

snow conditions, 55% of the basin would be underlain by permafrost compared to only 34% under deep snow conditions.

It is concluded that BTS modeling is possible in mountainous parts of the Yukon Territory and that a quantitative probabilistic approach employing logistic regression is the most logical given variable terrain, vegetation and snow cover in this region.

RÉSUMÉ

Cette étude est le premier essai connu de la méthode température de la base de la couverture de neige (TBCN) en Amérique du Nord pour prédire la distribution du pergélisol alpin. La région d'étude choisie, le bassin de Recherche Wolf Creek dans le territoire du Yukon (60°30'N, 135°13'W) est un bassin de 195 km^2 comprenant des altitudes qui varient entre 650-2100 m et une température moyenne annuelle de l'air d'environ -4°C à 1235 m au-dessus du niveau de la mer.

Une surface modélisée de la TBCN basée sur 394 données de la TBCN avec des données d'altitude et de rayonnement solaire potentiel comme variables indépendantes, a été créé dans un environnement de SIG avec une donnée du r^2 semblable aux résultats européens. La distribution du pergélisol dans le bassin a été identifiée à l'aide de trous et de forages creusés dans le sol. Une régression logistique a été employée afin de comparer les données TBCN modélisées avec la véritable distribution du pergélisol et produire une carte de la probabilité du pergélisol dans le bassin. Une probabilité significativement plus élevée de la présence du pergélisol, observée dans une vallée close, a été attribuée au drainage d'air froid. Cet événement n'était pas prédit par le modèle TBCN et les données provenant de cet endroit ont été supprimées des analyses subséquentes.

À partir de la distribution prédite du pergélisol, le pergélisol continu (>90%) est présent au-delà de 1600 m, le pergélisol étendu discontinu (50-90%) est prédit entre 1400-1600 m, le pergélisol sporadique discontinu (10-50%) est prédit entre 800-1400 m, et le pergélisol isolé (<10%) est prédit en deçà de 800 m. L'orientation et le gradient de pente d'un versant influencent la probabilité du pergélisol de sorte que sur un versant sud de 20°, la probabilité de pergélisol de >90% s'étend jusqu'à 1500 m, tandis que sur un versant nord avec un gradient de pente semblable la même probabilité se trouve 200 m plus haut. Il est estimé que le pergélisol est présent sur 43% de l'étendue du bassin.

Des régressions logistiques séparées ont été utilisées pour prédire la probabilité du pergélisol sous des conditions de neige profonde (>80 cm) et des conditions de neige peu profonde (<80 cm). Sous des conditions de neige peu profonde, le pergélisol est présent sur 55% de l'étendue du bassin, comparativement à seulement 34% sous des conditions de neige profonde.

Il est conclut qu'il est possible d'utiliser le modèle TBCN dans les régions montagneuses du territoire du Yukon et qu'une approche quantitative probabiliste qui emploie une régression logistique est la plus appropriée étant donné le terrain variable, la végétation et la couverture de neige dans cette région.

ACKNOWLEDGEMENTS

This Masters thesis proved to be both a difficult and exhilarating experience with many ups and downs. Many thanks to my supervisor Antoni Lewkowicz for his never-ending support and enthusiasm for the project. The many times discussing aspects and new ideas of the thesis together in his office and around the University will be warmly remembered.

Financial support was provided by the Northern Scientific Training Program and NSERC funds (Dr. A. Lewkowicz). Radiation modeling was made possible thanks to support from Helios Environmental Modeling Institute. An additional thanks is given to Rick Janowicz (Environment Canada) for logistic support in the field, especially for the fresh eggs and bacon.

Many warm thanks are given to those who conducted winter fieldwork, without which this project would not be possible. Thanks to Antoni Lewkowicz (winters 2001,2002), Marica Philips (winter 2001) and Andje Lewkowicz-Lalonde (2002). A special thanks to my personal assistant Reid Van Brabant, who painstakingly helped dig an endless number of pits over a 39-day period; thank you for your help and enthusiasm. Additional thanks to Mike Sawada whose GIS knowledge and generous help in times of need was a lucky treat.

Special thanks to my family, whose support both moral and financial, made the difference. Last but not least, a warm thanks to Kimberley Mason, my loving wife who stood by me throughout the whole experience; thank you for your support and love.

TABLE OF CONTENTS

ABSTRACT ii

RÉSUMÉ iv

ACKNOWLEDGEMENTS vi

TABLE OF CONTENTS vii

LIST OF FIGURES ix

LIST OF TABLES xi

CHAPTER 1. INTRODUCTION AND BACKGROUND 1
1.1. Introduction 1
1.2. Objectives 2
1.3. Mountain permafrost distribution modeling 2

CHAPTER 2. STUDY AREA 7
2.1. Location 7
2.2. Climate 8
2.3. Permafrost 9
2.4. Vegetation 10
2.5. Geology and Quaternary History 10

CHAPTER 3. METHODOLOGY 12
3.1. Steps employed in the methodology 12
3.1.1. BTS measurement points 14
3.1.2. Develop a map of potential incoming solar radiation. 17
3.1.3. Regress the BTS values against elevation and potential incoming solar radiation. 18
3.1.4. Verify the presence or absence of permafrost. 18
3.1.5. Evaluate the relationship between the modeled BTS values and actual permafrost distribution. 23
3.1.6. Develop a preliminary permafrost map of Wolf Creek basin. 24

CHAPTER 4. RESULTS 25
4.1. Measured BTS values 25
4.2. Potential incoming solar radiation 26
4.3. Regression analyses to predict BTS values 28
4.3.1. Preliminary analyses 28
4.3.2. Final analysis 31
4.4. Observations of late-summer frozen ground 36
4.5. Use of logistic regression to predict permafrost probability 39
4.6. Refinement of predictive model 46
4.7. Description of permafrost distribution 55
4.8. Micro-scale variations in permafrost distribution 61

CHAPTER 5. DISCUSSION **66**
5.1. Impact of snow on permafrost distribution 66
5.2. Inter-annual variations in BTS values 74

CHAPTER 6. CONCLUSION **81**
6.1. Conclusions 81
6.2. Future research 83

References **84**

LIST OF FIGURES

Figure 1.3.1: Schematic illustration of steps in process-oriented permafrost distribution models (Hoelzle *et al.*, 2001) 5
Figure 2.1.1: Location of Wolf Creek study site. 7
Figure 2.2.1: Mean annual air temperatures for Whitehorse, Yukon Territory (60°42'N, 135°04'W) at elevation of 703 m a.s.l from 1943-1993 (Canadian climate normals, 1994) 8
Figure 2.2.2: Hourly temperatures recorded at a palsa site in Wolf Creek basin at 1250 m from April 6th 2001 to August 28th 2002 9
Figure 3.1: Schematic of the major steps used to evaluate the BTS method in Wolf Creek. 13
Figure 3.2: Location of BTS measuments for both 2001 (blue) and 2002 (red). 14
Figure 3.3: Ground surface temperatures at three different data-logger sites. 15
Figure 3.4: Example of clast-rich pit with a sandy matrix below 25 cm depth. 19
Figure 3.5: The location of pits excavated in late summer 2002 in the Wolf Creek basin. 20
Figure 3.6: Example of a pit excavation with the temperature probe (1.5 m in length) and multimeter. 22
Figure 4.1.1: Histogram of measured BTS values. 25
Figure 4.2.1: Map of PISR density for May 15th – September 30th produced using a 30 m digital elevation model (Yukon. Dept of Renewable Resources, 2000) and Solar Analyst extension in Arcview 3.2 (Fu and Rich, 1999). 26
Figure 4.2.2: Histogram of PISR density for Wolf Creek Basin generated using Figure 4.2.1 27
Figure 4.2.3: Map showing differences in potential incoming solar radiation density in relation to aspect. 28
Figure 4.3.1: 3D graph of measured BTS, elevation and potential incoming solar radiation. 29
Figure 4.3.2: Visual representation of BTS surface predicted using the modified BTS data set. 31
Figure 4.3.3: Distribution of the BTS regression model residuals. 32
Figure 4.3.4: Plotted residual data from the BTS regression model 33
Figure 4.3.5: Measured BTS versus fitted BTS values. 33
Figure 4.3.6: Map of modeled BTS values for Wolf Creek basin. 34
Figure 4.3.7: Map of modeled BTS values +1 standard error for Wolf Creek basin. 35
Figure 4.3.8: Map of modeled BTS values –1 standard error for Wolf Creek basin. 35
Figure 4.4.1: Frozen ground observed at a depth of 40 cm at site 2002/07/24/A24B. 36
Figure 4.4.2: Examples of ground temperature predictions. 37
Figure 4.4.3: Histogram of excavated pits at modeled BTS values 38
Figure 4.4.4: Organic mat thickness at permafrost and non-permafrost sites. 39
Figure 4.5.1: Permafrost probability curve generated from logistic regression analysis (LM-1) that uses all the accepted pits. 40
Figure 4.5.2: Observed permafrost percentages versus predicted permafrost probabilities for LM-1 at specific BTS values. 41
Figure 4.5.3: Map of permafrost probability for the Wolf Creek basin. 42
Figure 4.5.4: Percentage of elevation bands in Wolf Creek underlain by permafrost according to LM-1. 43

Figure 4.5.5: Permafrost probability curve of best fit and ± 1BTS standard error according to LM-1. 44
Figure 4.5.6: Map of permafrost probability calculated using +1 BTS standard error. 45
Figure 4.5.7: Map of permafrost probability calculated using -1 BTS standard error. ..45
Figure 4.6.1: Southwest-facing picture of the confined valley that is subject to cold air drainage or atmospheric temperature inversions. 47
Figure 4.6.2: Overlay of excavated pits and digitized air photograph. 48
Figure: 4.6.3 Observed permafrost percentages versus predicted permafrost probabilities for LM-2 at specific BTS values. 50
Figure 4.6.4: Permafrost probability curves for LM-1 and LM-2. 51
Figure 4.6.5: Permafrost probability map of the Wolf Creek basin created using LM-2 and measured probabilities in the valley west of Coal Ridge. 53
Figure 4.6.6. Large-scale map of the area affected by cold air drainage. 54
Figure 4.6.7: Predicted percentage of area underlain by permafrost for LM-2. 55
Figure 4.7.1: Trends in permafrost probabilities in relation to elevation. 56
Figure 4.7.2: Extent of permafrost probability classes in km^2. 57
Figure 4.7.3: The lower limit of permafrost probabilities (90%, 50%, 10%) in relation to slope angle and aspect. 59
Figure 4.7.4: Radar chart showing the lower limit of permafrost probability (90%, 50%, 10%) on different slope angles over 8 compass directions. 60
Figure 4.8.1: Picture showing the north slopes of Mount Granger. 62
Figure 4.8.2: Schematic of typical bench characteristics. 63
Figure 4.8.3: The presence of *Cassiope tetragona* indicates the existence of late-lying snow cover. 63
Figure 5.1.1: Observed permafrost percentages versus predicted permafrost probabilities for (A) LM-2, (B) LM-4, and (C) LM-5 at specific BTS values. 67
Figure 5.1.2: Permafrost probability curves generated from logistic regression analyses LM-2, LM-4 and LM-5. 68
Figure 5.1.3: Map of permafrost probability for the Wolf Creek basin under (A) deep snow conditions and (B) shallow snow conditions. 69
Figure 5.1.4: Predicted percentage of area underlain by permafrost for (A) LM-2, (B) LM-4, and (C) LM-5. 71
Figure 5.2.1A: Surface and ground temperature from data-loggers Crest, Cassiope 1, and C6. 76
Figure 5.2.1B: Surface and ground temperature from data-loggers C17, C30, and C40. 77
Figure 5.2.1C: Surface and ground temperature from data-loggers Drainage divide, Plateau 3, and Semi-permanent snow bank. 78
Figure 5.2.2: Possible effect of ground water infiltration on surface and ground temperatures at data-logger C6. 79
Figure 6.1.1: Steps of the methodology employed by the study. 82

LIST OF TABLES

Table 4.3.1: BTS regression coefficients and P-values for the intercept, PISR density and elevation (n = 386). 29
Table 4.3.2: BTS regression coefficients and P-values for the intercept, PISR and elevation (n = 317). 31
Table 4.5.1: Variables defined in LM-1 regression model..... 40
Table 4.6: Variables defined in LM-2 regression model..... 49
Table 5.1.1: Variable defined in LM-2, LM-4 and LM-5 regression models..... 66
Table 5.1.2: Elevation boundaries of permafrost classifications for LM-2,LM-4 and LM-5..... 70
Table 5.2.1: Average yearly temperature for data-loggers. 80

CHAPTER 1. INTRODUCTION AND BACKGROUND

1.1. Introduction

Permafrost is defined as earth materials which remain at temperatures of less than or equal to 0° C for two years or more (ACGR, 1988; Washburn, 1979). Mountain or alpine permafrost usually refers to occurrences in mountainous regions where permafrost is absent in adjacent lowlands (Harris and Corte, 1992). Mountain permafrost distribution is controlled by a multitude of factors that include snow cover, mean annual air temperature, incoming solar radiation, vegetation, geology and soil characteristics.

A warming climate in mountainous regions will have a significant impact on the existence and distribution of permafrost (Haeberli *et al.*, 1993), especially in areas where permafrost is discontinuous or sporadic. It must be noted that climate change may affect meteorological phenomena other than temperature, including precipitation (IPCC, 1996), and this will increase the complexity of alpine permafrost reaction to climate change (Haeberli *et al.*, 1993).

Warming trends and associated changes in permafrost and glaciers have been observed in several mountainous regions. Warming has been observed in rock glacier permafrost in the Kluane Range, Yukon Territory with permafrost degrading from both the top and the base (Johnson and Nickling, 1979). Harris (1988) measured a near-zero temperature gradient and heat flow in a borehole on Plateau Mountain, Alberta, in permafrost more than 150 m in thickness. Large inter-annual variations in alpine permafrost temperatures have been observed in the European Alps. Borehole investigations on the Murtel-Corvatsch rock glacier showed a warming trend until 1994 when the permafrost began to cool, indicating the possibility of unstable climatic conditions (Vonder Muhll *et al.*, 1998).

A warming climate has the potential to cause an increase in active-layer thickness, basal melting causing permafrost thinning, hydrogeological changes, a rise in the lower limit of permafrost and a warming of surface temperatures (Haeberli *et al.*, 1993; Harris *et al.*, 2001). On slopes, the thawing of permafrost could lead to deep-seated bedrock failures, creep-related processes, rockslides, rock fall, mudslides or active layer detachment failures, increased debris flows and accelerated gelifluction (Evans and Clague, 1994; Harris *et al.*, 2001). These reactions to climate change illustrate the need to examine the present distribution of mountain permafrost in order to be able to identify future changes in distribution.

1.2. Objectives

The aim of this study is to evaluate the basal temperature of snow method as a means to indicate the distribution of permafrost in the Wolf Creek basin, south central Yukon. A secondary objective is to produce a preliminary map of permafrost distribution in Wolf Creek that will be of use to hydrologists conducting research in the basin.

1.3. Mountain permafrost distribution modeling

Permafrost distribution models are of two main types: empirical-statistical models and process-oriented models (Hoelzle *et al.*, 2001). Empirical-statistical models use calculated climate factors as proxies for permafrost, such as freezing or thawing indexes (Nelson and Outcalt, 1987), potential direct solar radiation (Hoelzle, 1992; Gruber and Hoelzle, 2001) and mean annual air temperature (Etzelmuller *et al.*, 1998).

Process-oriented permafrost distribution models use two main approaches: an energy balance approach and a thermal offset approach (Figure 1.3.1). Energy balance models are based on the main energy exchanges between the atmosphere and the

surface, including calculations of short-wave and long-wave radiation, turbulent fluxes and snow distribution. An extensive set of input parameters is required for energy balance models that may be difficult to collect in remote regions. Modeled surface temperatures produced as outputs from the energy balance model can then be used in a thermal offset model. Thermal offset models examine and predict the difference between mean annual ground surface temperature (MAGT) and mean annual temperature at the permafrost table (MAPT) (Burn and Smith, 1988). The relationship between ground surface temperature and top of permafrost is primarily determined by conductive heat flow and is described by Smith and Riseborough (1996) as:

$$TTOP = \frac{k_T DDT_s - k_F DDF_s}{k_F P}$$

where

DDT_A = surface thawing degree days (seasonal thawing index)

DDF_S = suface freezing degree days (seasonal freezing index)

K_T = thermal conductivity of ground (thawed)

K_F = thermal conductivity of ground (frozen)

P = period (365 days)

Thermal offset models have been used to examine the impact of climate change on permafrost distribution (e.g. Smith and Riseborough, 1983; 1996; 2002). Small-scale variability in microclimate conditions and surface characteristics in complex alpine regions, however, limit the application of thermal offset models in mountainous areas (Hoelzle *et al.*, 2001).

There are a number of field techniques that can be used to investigate the distribution of mountain permafrost in a given area: direct probing, refraction seismic

techniques, DC resistivity, ground penetrating radar, electromagnetic induction, radiometry and basal temperature of snow (BTS) (Vonder Mühill *et al.*, 2000; King, 1992). Of these, only the BTS method and probing can be used over extensive areas.

The basal temperature of snow method was first introduced by Haeberli (1973) to map mountain permafrost in the European Alps and has since been refined and proved to be a reliable and accurate tool (Hoelzle, 1992; Hoelzle *et al.*,1993; King, 1992). Deep snow cover, with its low heat transfer capacity, insulates the ground from short-term variations in the surface energy balance (Hoelzle *et al.*, 1993). A snow depth of at least 80 cm is required to fully insulate the ground from diurnal temperature variations (Keller and Grubler, 1993). BTS is an index of the heat flow from the ground (King, 1992) and has been used to indicate not only permafrost distribution but also the mean annual ground temperature, allowing an estimation of permafrost thickness (King, 1992). Observations of BTS values must be undertaken in late winter or early spring when a thermal equilibrium at the base of the snow cover has developed (Imhof *et al.*, 2000). A classification system based on ranges of ground/snow interface temperatures is used to determine the presence of permafrost. BTS values of < -3°C indicate the probable presence of permafrost, values of -2°C to –3°C indicate permafrost is possible and values >-2°C indicate permafrost is improbable (Hoelzle, 1992).

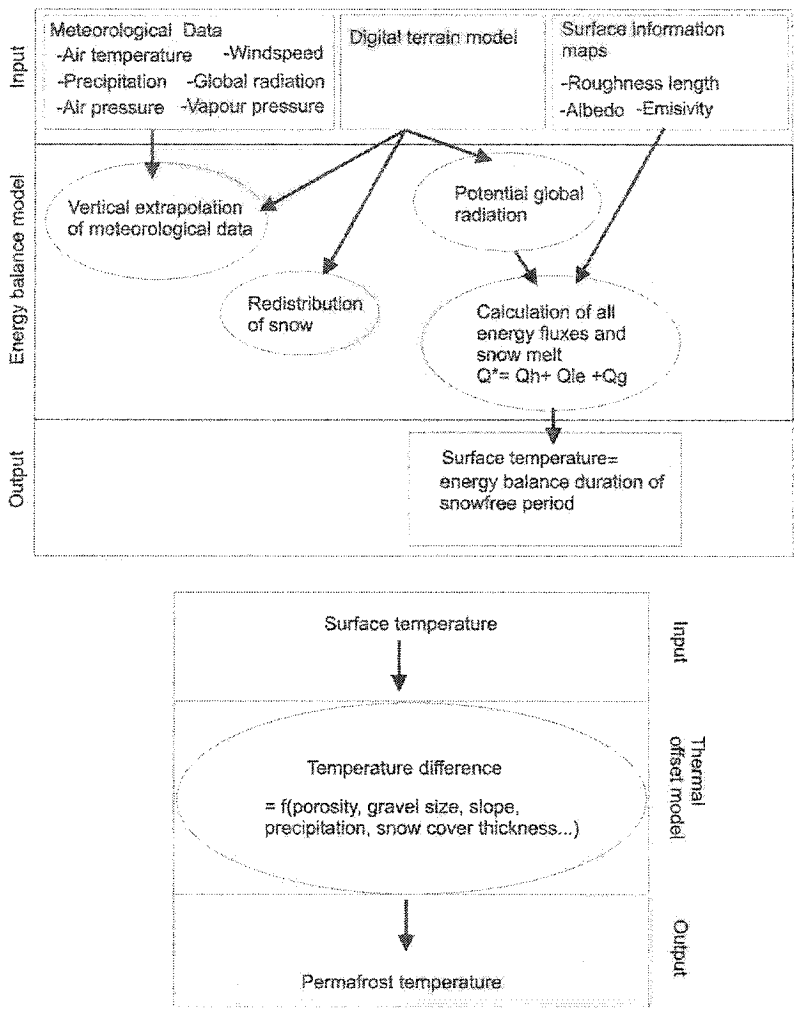

Figure 1.3.1: Schematic illustration of steps in process-oriented permafrost distribution models (Hoelzle *et al.*, 2001).

A major limitation on the use of the BTS method is the lack of sufficient snow cover in many arctic and continental areas (King, 1992). A further difficulty, identified by Imhof *et al.* (2000), is the effect of timing of snow cover establishment on BTS values (Vonder Muhll *et al.*, 1998). Indications of permafrost at a given location may vary on an annual basis depending upon when snow falls over the winter. An early deep snow cover insulates the active layer from the atmosphere, retards the release of heat and may result in a BTS value that indicates no permafrost when the latter is present (Keller and Grubler, 1993). In cases where there is an absence of snow cover well into winter,

the soil may have sufficient time to freeze deeply, resulting in a BTS value indicating permafrost when it is absent. Notwithstanding these points, BTS measurements, together with empirical statistical models, have the potential to directly relate permafrost distribution to topo-climatic factors (altitude, slope, aspect, mean annual air temperature (MAAT) and solar radiation). The advantages of this predictive method are that the methodology can be easily applied, input parameters are limited (altitude, slope, mean annual air temperature, solar radiation) and the method appears to be reliable if locally calibrated (Hoelzle *et al.*, 2001).

Although BTS is a winter indicator of permafrost, the permafrost distribution itself is controlled by both winter conditions (especially snow depth and air temperature) and summer surface energy exchange (Gruber and Hoelzle, 2001). In terms of the latter, elevation (through lapse rate) and solar radiation (affected by aspect, slope and shading from surrounding topography) are the most crucial factors. In Europe, Hoelzle (1992) found a good correlation between elevation, potential incoming summer solar radiation and permafrost distribution, indicating that permafrost may exist below the 0°C MAAT isotherm in shaded areas. The development of a potential solar radiation map that incorporates shading aids in the mapping of permafrost distribution and removes the need to examine slope and aspect.

Researchers using the BTS method to investigate permafrost outside the European Alps have employed the threshold values derived by Haeberli (1973). BTS investigations have been performed in the Polish Tatra Mountains (Dobinski, 1998), in the Daisetsu Mountains, Hokkaido, Japan (Ishikawa and Hirakawa, 2000) and in Lapland, Norway (Jeckel, 1988). No investigations of the BTS method are known for North America.

CHAPTER 2. STUDY AREA

2.1. Location

The Wolf Creek watershed is a 190 km^2 basin situated 15 km south of Whitehorse in the southern Yukon Territory (60°8'N, 135°1'W) (Figure 2.1.1).

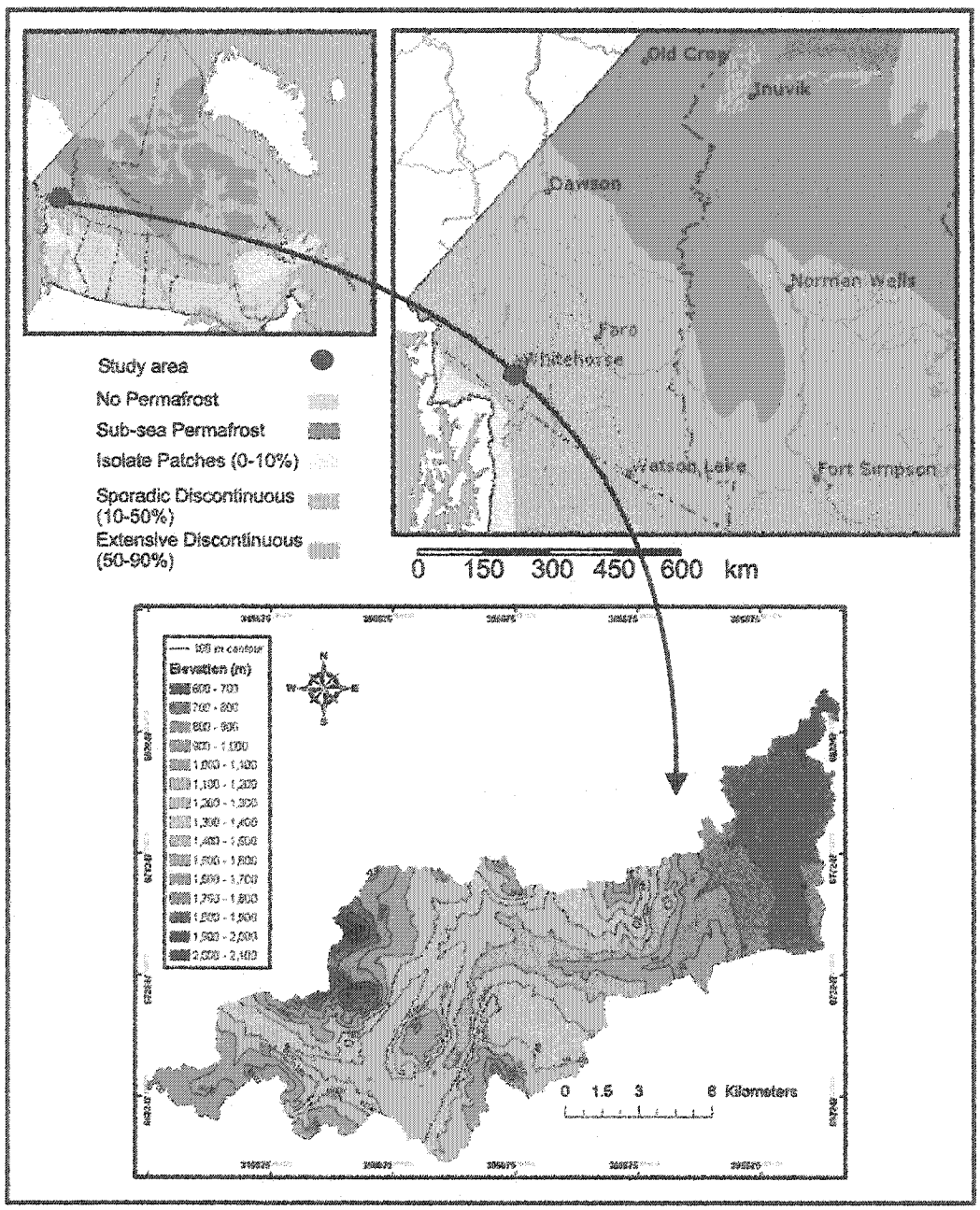

Figure 2.1.1: Location of Wolf Creek study site.
Inset map shows location relative to permafrost zones (after Heginbottom *et al.*, 1995).

Elevations in the basin range from 659 m to 2079 m, with an tree line at approximately 1300 m. The basin's terrain is complex and is characterized by steep-sided U-shaped valleys and gently rolling upland terrain with rounded peaks.

2.2. Climate

The climate of the basin is classified as dry sub-arctic continental with a large seasonal temperature range (Seguin *et al.*, 1999). The temperature in Whitehorse at an elevation of 703 m averages -1°C (1943-1993) (Canadian Climate Normals, 1994) (Figure 2.2.1). The mean air temperature of a palsa site in Wolf Creek at 1250 m for 2001-2002 was -4°C with a range of 60°C, from -35°C to 25°C (Figure 2.2.2). Temperature inversions resulting from cold air drainage occur in some valleys within the basin (Janowicz, 1999).

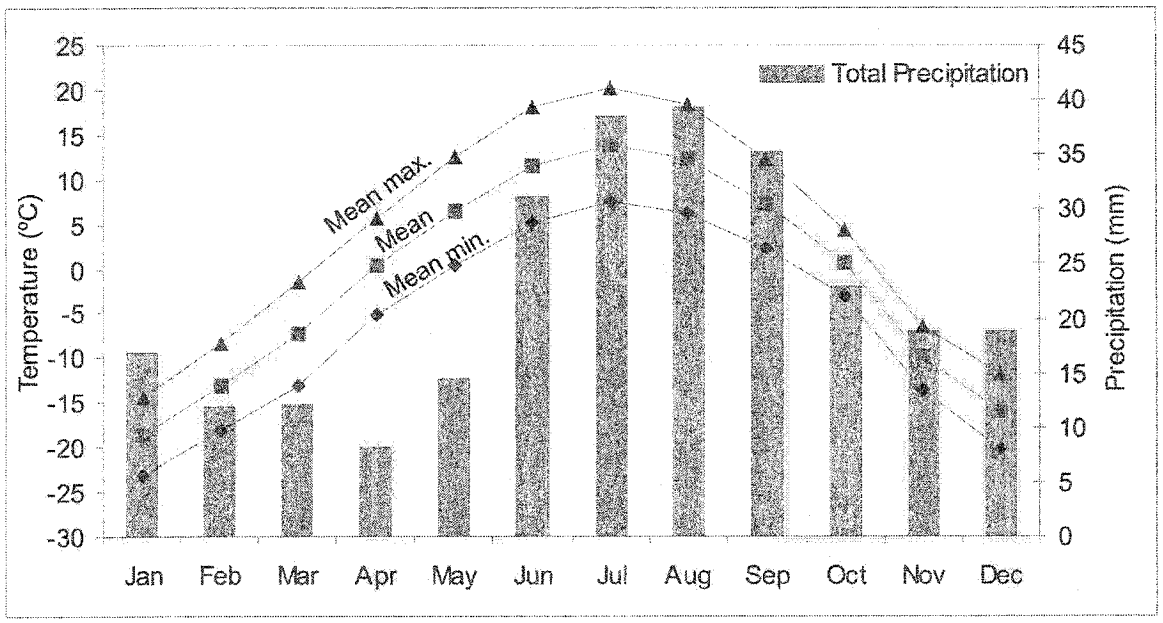

Figure 2.2.1: Mean annual air temperatures for Whitehorse, Yukon Territory (60°42'N, 135°04'W) at elevation of 703 m a.s.l from 1943-1993 (Canadian climate normals, 1994).

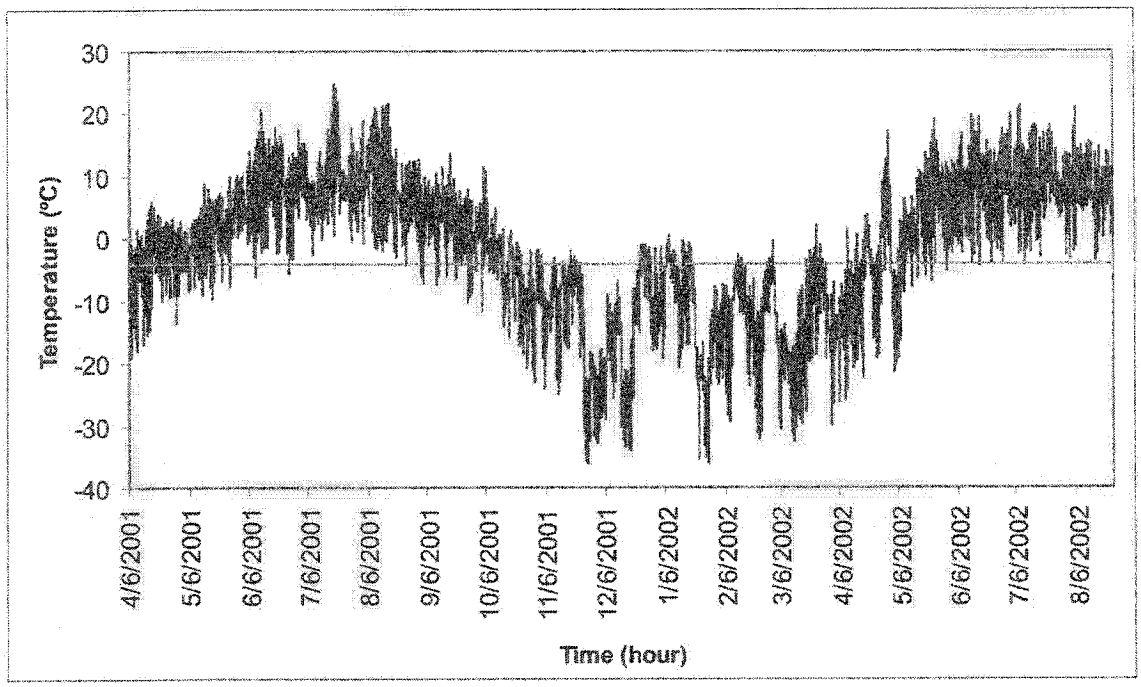

Figure 2.2.2: Hourly temperatures recorded at a palsa site in Wolf Creek basin at 1250 m from April 6th 2001 to August 28th 2002.

Mean annual precipitation varies from 300 to 400 mm (see Figure 2.2.1) with approximately 40% falling as snow (Janowicz, 1999). During summer, rainfall typically occurs as low magnitude events lasting up to several days. Snow cover is greater on north-facing slopes while on south-facing slopes, snow accumulation is moderated by high sublimation rates (Woo and Carey, 1999).

2.3. Permafrost

The area is within the sporadic discontinuous permafrost zone (Heginbottom *et al.*, 1995) (see Figure 2.1.1). No intensive investigation into the extent of permafrost has been undertaken. A preliminary report suggested that permafrost occupies approximately 25-32% of the basin, occurring at higher elevations on south-facing slopes and slightly lower on north-facing slopes (Seguin *et al.*, 1999). Widespread

permafrost and palsas were observed in a confined valley at ~1250 m (Coultish, 2002). Permafrost is also present around thermokarst lakes south of Coal Lake at approximately 1150 m a.s.l. An exposure investigated on August 17th 2001, revealed regular and irregular reticulate ice lenses ranging from 0.5 to 20 cm in thickness (Coultish, 2002). However, the majority of the permafrost in the basin is probably not ice-rich (see Heginbottom *et al.*, 1995).

2.4. Vegetation

The basin spans three major ecological zones based primarily on elevation: boreal forest at low elevations, sub-alpine forest and shrub-lands at mid-elevations, and an alpine zone at high elevations (Francis, 1997). The boreal forest zone represents 22% of the total watershed and is dominantly comprised of white spruce and lodgepole pine communities. The sub-alpine makes up the majority of the basin, accounting for 58% of the total area. Sub-alpine vegetation communities are dominated by willow and dwarf birch shrub-lands. The highest elevations of the watershed are classified as alpine tundra and unvegetated areas, and account for 20% of the total basin. The transitions between these three broad ecological zones are often gradual and difficult to delineate spatially due to the complex topographic characteristics of the watershed (Francis, 1997).

2.5. Geology and Quaternary History

The bedrock geology of the area is heterogeneous. The basin is underlain by sedimentary rocks, consisting of limestones, sandstones, siltstones and conglomerates of Upper Jurassic and middle to lower Cretaceous age (Gordey and Makepeace, 1999). Volcanic rocks, including andesite and basalt with granite intrusions are also present in the basin (Gordey and Makepeace, 1999; Janowicz, 1999). The bedrock is covered by a

layer of till ranging from a thin veneer to thicknesses of one to two meters according to Janowicz (1999). However, based on geophysical investigations, Seguin *et al.* (1999) suggested that the till might range in depth up to 30 m. Other surficial deposits are of glacio-fluvial, glacio-lacustrine, colluvial, fluvial and aeolian origin. Fine-grained colluvial and fluvial deposits cover most valley floors while thinner deposits of colluvium together with bedrock outcrops occur at higher elevations (Janowicz, 1999).

The basin was last covered by the Cassiar and Coast Mountain lobes of the Cordilleran ice sheet around 23 ky B.P. These ranged in elevation from 1828 m to 1981 m a.s.l (Wheeler, 1961; Duk-Rodkin, 1999). Melting of the ice sheet well before 9 ky BP led to the development of deglaciation features such as abandoned meltwater channels, proglacial lakes, eskers, and elongate drift ridges (Wheeler, 1961). Local glaciations may have occurred during the retreat of the ice lobes and during the "Little Ice Age" resulting in the formation of cirques, an example being the Coal Ridge cirque (Wheeler, 1961).

CHAPTER 3. METHODOLOGY

3.1. Steps employed in the methodology

A summary of the major steps used to evaluate the BTS method in Wolf Creek is given below and is followed by a discussion of each step individually. A schematic detailing the following procedure is presented in Figure 3.1.

3.1.1. A geo-referenced network of BTS measurements was established for the basin.

3.1.2. A map of potential incoming solar radiation (PISR) for the basin was created using the Solar Analyst extension and a 30 m digital elevation model in Arcview 3.2 (Fu and Rich, 1999).

3.1.3. The BTS values were regressed against elevation and potential incoming solar radiation to develop a model of BTS values for the entire basin.

3.1.4. The presence or absence of permafrost was verified at selected sites during late summer by probing or digging pits.

3.1.5. The relationship between the modeled BTS values and actual permafrost distribution identified in the excavations was evaluated using logistic regression analysis.

3.1.6. A preliminary permafrost map of Wolf Creek basin was developed based on the relationships between the BTS model of permafrost and the physically verified sites.

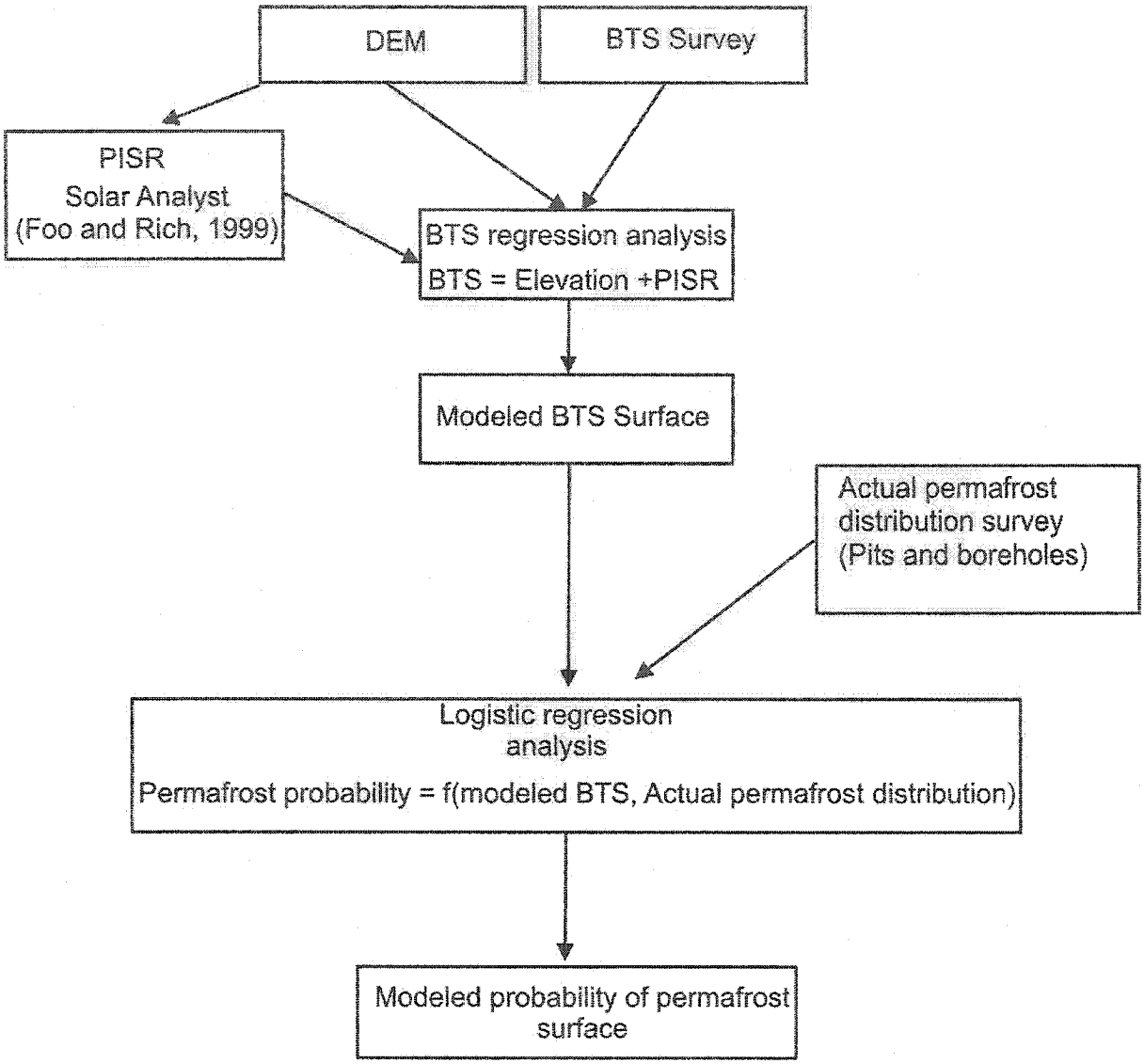

Figure 3.1: Schematic of the major steps used to evaluate the BTS method in Wolf Creek.

3.1.1. BTS measurement points

BTS data were collected by Dr. A. Lewkowicz and Dr. M. Philips during early April 2001. Additional data were collected by A. Lewkowicz and A. Lewkowicz-Lalonde in March-April, 2002 (Figure 3.2). The first set of measurements was collected mainly in the Granger sub-basin where hydrological research is presently being conducted (*e.g.*, Wolf Creek Basin Research Project, http://www.taiga.net/wolfcreek/). The second set occupied a wider range of orientations, and in addition, some measurement points were located at previously measured sites in the Granger basin in order to examine inter-year variability in BTS values (Ishikawa and Hirakawa, 2000).

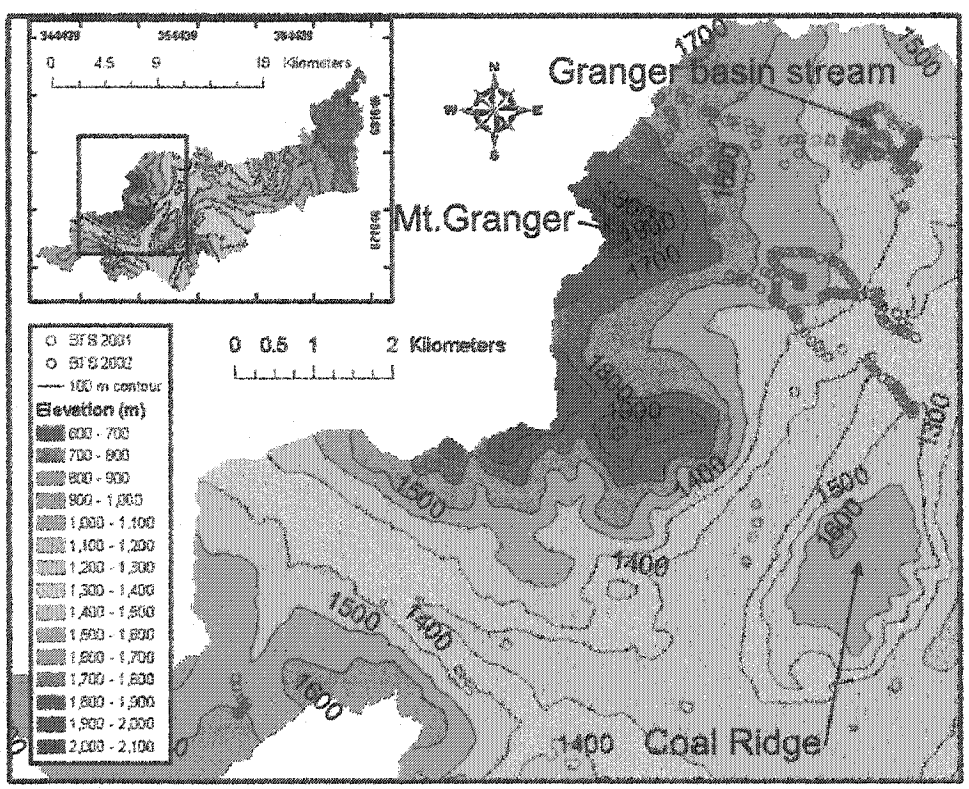

Figure 3.2: Location of BTS measuments for both 2001 (blue) and 2002 (red).

BTS data collection must take place in late winter when the snow cover is thickest and before the snow begins to warm to an isothermal condition (Imhof *et al.*, 2000). Miniature data-loggers (Onset Hobo Pro) were deployed to measure the temporal changes in temperature at the snow/ground interface throughout the winter and thereby validate the timing of the BTS survey. Fourteen data-loggers, installed mainly in the Granger basin by Lewkowicz in August 2000, indicated that minimum steady state temperatures were reached at sites with sufficient snow at the time of the BTS survey in April 2001 (Figure 3.3). A number of the data-loggers were left in place to record annual variations and to ensure valid BTS values for winter of 2001-02.

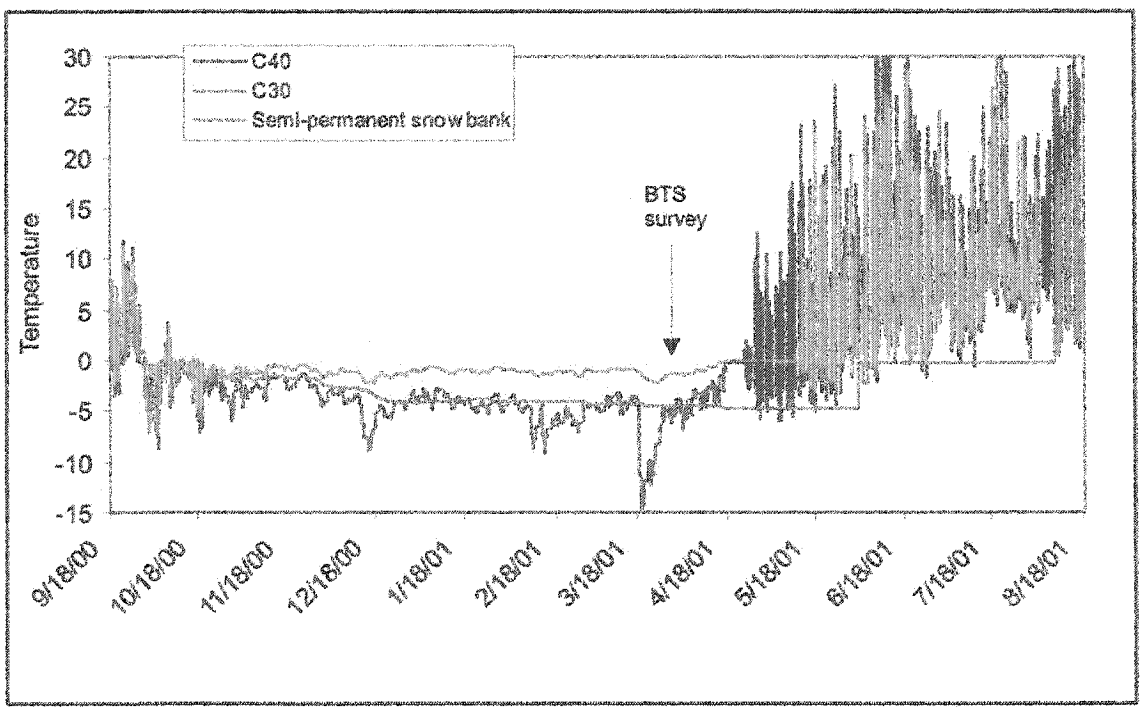

Figure 3.3: Ground surface temperatures at three different data-logger sites.
Orange and green lines represent deep snow cover insulating the ground from diurnal temperature fluctuations. Steady state temperature regimes were reached by late-March and early April at the time of the BTS survey. The blue line represents a site where snow was not deep enough to insulate the ground from diurnal temperature fluctuations.

BTS data were collected using a Fluke multimeter to measure the resistance of a YSI 44033 thermistor inserted into the steel tip of a probe pushed to the base of the snowpack. Snow depth was read from the probe, and using a standard curve, the resistance value was converted into temperature (°C). Thermistor calibrations had been checked in an ice-bath at 0°C in 2001 and were within the desired precision of ± 0.1°C. The location of each sample point was recorded with a handheld GPS (Etrex Summit) in UTM WGS 84 coordinates with precision ranging from 2 to 10 m. Haeberli and Epifini (1986) noted that the minimum snow depth required to insulate the ground from atmospheric disturbances is 1 m, but subsequent research showed that a minimum depth of 0.8 m is sufficient (Hoelzle *et al.*, 1993; King, 1990). A minimum snow depth of 0.8 m was used for this study. Any BTS values with less than the minimum snow depth were rejected since they could have been subjected to diurnal temperature variations.

The accuracy of the BTS values depends on the probe temperature equilibrating with the surrounding snow. In 2001, the probes were left for 5 minutes or more until resistance changes were slow or imperceptible. In 2002, a more rigorous procedure was followed. Resistance values were recorded every minute for a minimum of five minutes until change equaled 0.02kΩ/minute (<0.1°C/minute). The resistance values were converted to temperatures and an exponential curve fitted to the Δ temperature values. This curve was used to estimate additional changes in temperature of the probe tip after the 5-minute period in order to arrive at equilibrium BTS value. It is interesting to note that no discussion could be found in the BTS literature on equilibrating the probe and snow temperatures. The more rigorous measurement procedure followed in 2002 likely produced a greater accuracy than in 2001, but data for both years are acceptable according to standard BTS procedures.

3.1.2. Develop a map of potential incoming solar radiation.

The potential incoming solar radiation map of Wolf Creek basin was created using the Solar Analyst program developed by Fu and Rich (1999). The Solar Analyst generates an upward-looking hemispherical viewshed (fisheye photograph) for each location on the DEM using 32 directions. Merging the hemispherical viewsheds that are calculated for each pixel on the DEM (Yukon. Dept. of Renewable Resources, 2000) produces a total potential incoming solar radiation (PISR) density map in MJ/m^2 based on calculations made at 15-minute intervals.

The program allowed a number of user-defined conditions. The model required the input of a single latitude on which to base calculations. The centre of the basin was chosen to best represent the area and the latitude was therefore set to 60.5° N. Total cumulative potential incoming solar radiation was calculated for the period of the year when the albedo of snow does not influence the radiation balance (Hoelzle, 1992). Based on the data-logger information for 2000-2002 and literature for Wolf Creek (e.g. Granger, 1999), this period was set to May 15th through September 30th.

The program can take cloud cover into account in its apportioning of direct beam and diffuse radiation. Based on data from Environment Canada's Whitehorse weather station, the cloud cover model was given a value of 0.6 out of a possible range of 0 to 1, with 0 representing clear skies and 1 representing complete cloud cover. Thus 40% of the PISR was regarded as direct beam and 60% as diffuse radiation. To avoid the problem of edge calculation accuracy (where the model cannot calculate boundary edge shading due to lack of data outside the study region) the initial elevation grid that was used in calculating PISR was greater in extent than the basin boundaries.

In this study the effects of differential shading by vegetation on potential incoming solar radiation were ignored.

3.1.3. Regress the BTS values against elevation and potential incoming solar radiation.

The variables were tested for normality to a 95% confidence level using Kolmogorov-Smirnov normality test. BTS, elevation and PISR for the sample sites were not significantly different from normal distributions. Multiple regression analysis of BTS (dependent variable) against elevation and PISR was performed using S+ (V.6.0 lm). A linear multiple regression model was fitted to all 396 data points.

3.1.4. Verify the presence or absence of permafrost.

Physical verification of permafrost was performed by probing and/or excavating pits and boreholes at specific locations (e.g. Leverington and Duguay, 1996). Simple probing for frost table (see Mackay and Burn, 2002) was not possible in Wolf Creek because of high clast contents in the surficial material (Figure 3.4).

A total of 200 pits were dug to establish the presence or absence of frozen ground between July 20th and August 28th, 2002 (Figure 3.5). The locations of the pits were selected based on accessibility of terrain and proximity to previously recorded BTS values. Wherever possible, exploratory pits were excavated in transects running across valleys. The location of the exploratory pits was designed to cover a wide range of BTS values. More exploratory pits were excavated in regions with BTS values of -4°C through -1°C than in high elevation locations with low BTS values, -6°C through -11°C.

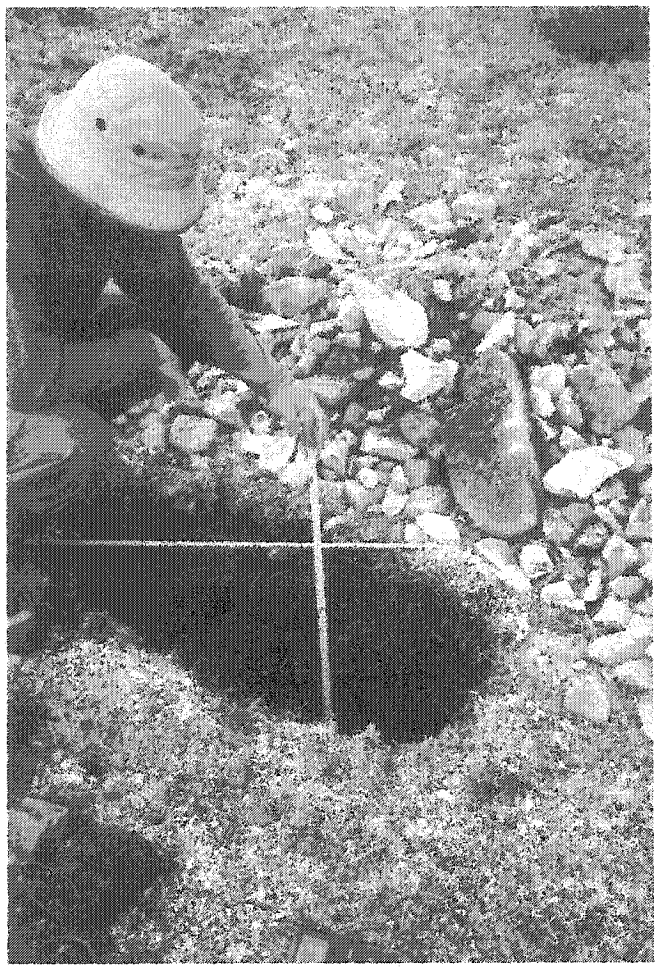

Figure 3.4: Example of clast-rich pit with a sandy matrix below 25 cm depth. Site 2002/07/23/A9A was classified as permafrost and was located on a flat plateau at 1682 m elevation.

To minimize the possibility that seasonal frost could be identified as permafrost, the measurements were made in late-summer. Data from 2001 from a site at 1250 m show that by August 1, 60 % of the thawing degree-days had accumulated and from a modified Stefan equation (*e.g.* Lewkowicz, 1994), this indicates that approximately 78% of the maximum thaw depth would have been attained. By August 31, the numbers reached 90% and 95% respectively.

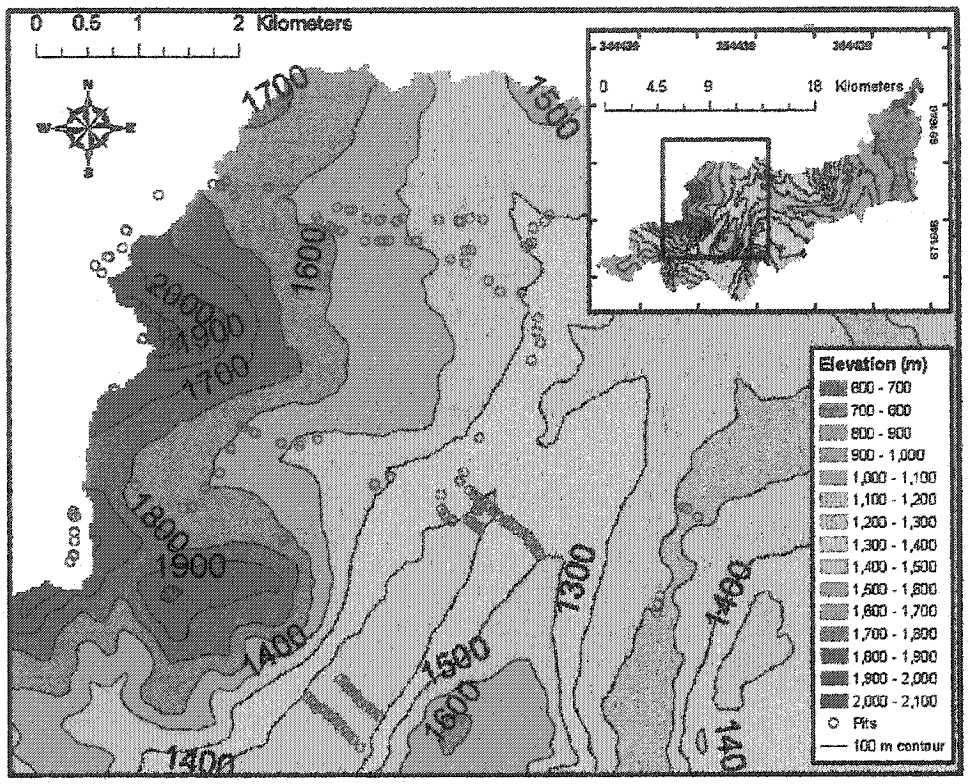

Figure 3.5: The location of pits excavated in late summer 2002 in the Wolf Creek basin.

A frost table depth of 2 m or less was taken as being a critical indicator of permafrost. This was based on several lines of evidence. First, Leverington and Duguay (1996) showed that at Yukon lowland sites, the permafrost table tends to be within 1.5 m of the surface or else permafrost is absent. Similarly, at a palsa site within the basin, even where organic mat was thin, the active layer was less than 1.45 m (Coultish, 2002). Moreover, high specific conductances in water within the upper part of the permafrost were interpreted by Coultish (2002) as indicators of deeper thaw in certain years. The maximum depth of these elevated conductances was 2 m in a degrading palsa that was at least 75 years old. Furthermore, depths of freezing are not necessarily great, even at this elevation: data-logger records show that some non-permafrost sites on a south-facing slope in the Granger Basin froze to a depth of only

65 cm in winter 2000-01. Thus it is believed that it is unlikely that permafrost exists where cryotic soil is absent in late-summer within the upper 2 m.

The presence or absence of frozen ground within the top 2 m was either observed directly or inferred from temperature measurements within the pits. A thermistor was inserted into the soil at the base of the pit and its resistance was recorded in kΩ (Figure 3.6). The kΩ were converted into degrees Celsius in the same way as with the BTS values. Boreholes and pits were dug to a target depth of 1.5 m. A soil temperature < 0.5°C at these depths was taken as an indication of frozen ground within 2 m of the surface and hence of permafrost. If this temperature was not reached by a depth of 1.5 m, or if clast-rich sediments impeded further digging at shallower depths, a temperature profile was recorded within the borehole or pit. A strong temperature gradient and low basal temperatures indicate that frozen ground is present at depth, while a weak gradient or higher temperatures suggest an absence of permafrost.

The temperatures used to develop the profile were recorded at the base of the pit, and at 10 cm, 20 cm, 40 cm and 80 cm above the base. A exponential line was fitted by bivariate regression to the data to predict the temperature to depths of 2 m. If 0°C was predicted within 2 m of the surface, the exploratory pit was classified as being a permafrost site. If 0°C was not predicted within 2 m, the pit was classified as being non-permafrost. If the prediction of 0°C was within ±10 cm of 2 m, the pit was removed from the data-set because the presence or absence of permafrost could not be confidently stated. A total of 16 pits fell into this group.

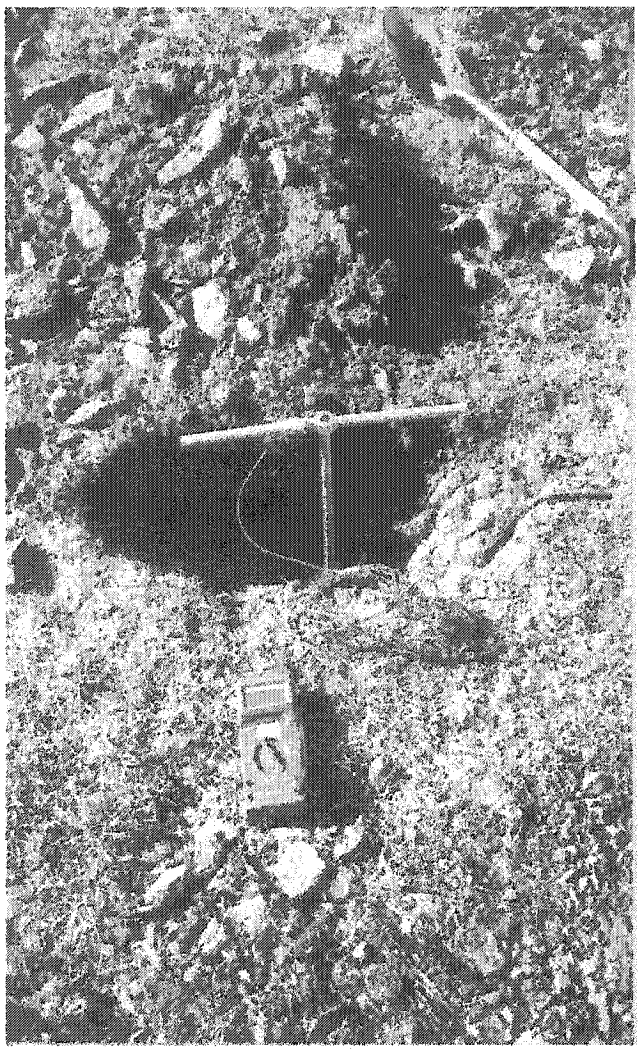

Figure 3.6: Example of a pit excavation with the temperature probe (1.5 m in length) and multimeter.

At each exploratory excavation, a brief description was made of vegetation cover, organic mat thickness and soil characteristics. These data were gathered to assist in the later analysis of permafrost distribution.

A large number of pits were excavated in pairs, each pair located within a 30 m radius, in order to analyze intra-cell (sub-30 m^2) variability in the presence or absence of permafrost. At each paired site, one of the pits was located in a depression or hollow

where snow probably accumulates. The second pit was excavated in an exposed location where shallow snow is likely.

3.1.5. Evaluate the relationship between the modeled BTS values and actual permafrost distribution.

Logistic regression analysis (Pereira and Itami, 1991) was used to evaluate the relationship between BTS values and the presence or absence of permafrost data. Binomial logistic regression is a form of regression that is used when the dependent variable is a dichotomy and the independent variables are either continuous or categorical in nature. Multinomial logistic regression exists to handle the case of dependents with more classes (Kleinbaum *et al.*, 1998). Logistic regression is applicable as the data describing the presence or absence of permafrost is of binary nature. A total of 185 excavations were used in the logistic regression analysis. Predicted BTS values were extracted from the map for locations where excavations were performed. The linear logistic regression was computed using S+ (V.6.0 lm) on all 185 excavations.

Logistic regression applies maximum likelihood estimation after transforming the dependent into a logit variable (the natural log of the odds of the dependent occurring or not). Consequently, logistic regression estimates the probability of a certain condition occurring. Logistic regression calculates changes in the log odds of the dependent variable, not changes in the dependent itself. The analysis does not assume linearity of relationship between BTS, PISR and elevation, does not require normally distributed variables, does not assume homoscedasticity, and in general has less stringent requirements than ordinary linear regresssion (Kleinbaum *et al.*, 1998). Goodness-of-fit tests such as model chi-square are available as indicators of model appropriateness as is the Wald statistic to test the significance of individual independent variables

(Kleinbaum *et al.*, 1998). Logistic regression has been used recently in permafrost research: Luoto and Seppäla (2003) used linear logistic regression analysis to examine the distribution of palsas in Lapland, Finland.

3.1.6. Develop a preliminary permafrost map of Wolf Creek basin.

A permafrost probability map was created by applying the regression equation developed in step 5 to each 30x30 m grid cell. The raster calculator in ArcGIS v.8.2 was used to undertake this step. The resultant values were displayed as a permafrost probability map for the entire basin.

CHAPTER 4. RESULTS

4.1. Measured BTS values

Following procedures identified in step 1 of the methodology a total of 386 BTS measurements were recorded during late winter 2001 and 2002. The BTS values ranged from -9.2°C to -0.3°C with a mean of -3.8° and a standard deviation of 1.7°C. The majority of BTS measurements gathered were in the -4 °C to -1°C range (Figure 4.1.1).

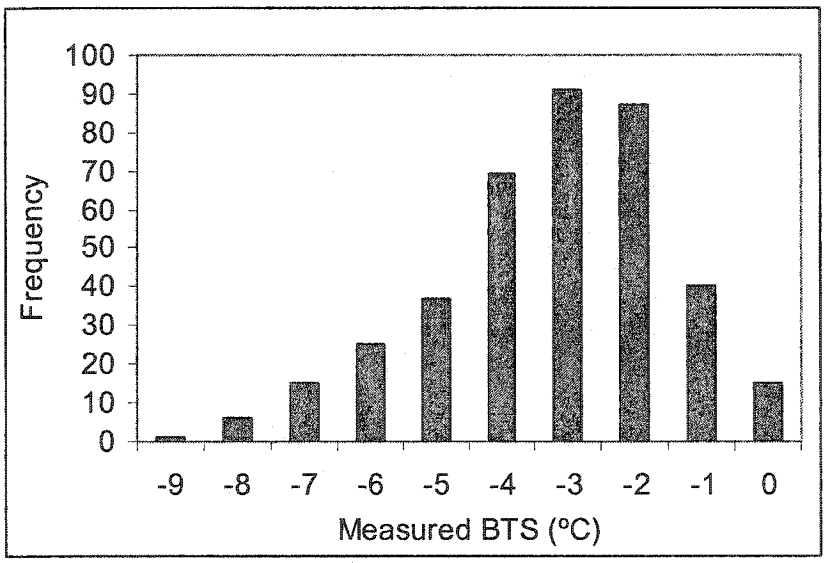

Figure 4.1.1: Histogram of measured BTS values.
Note: Values shown are the upper temperature in the range.

The majority of the BTS measurements were undertaken in the western part of the basin (see Figure 3.2). In 2001, BTS measurements were mostly made north of Mount Granger with heavy concentrations in the Granger basin. In 2002, BTS measurement points were mainly located east of Mount Granger and on Coal Ridge. Some isolated BTS measurements from both years were recorded on palsas in the valley west of Coal Ridge.

As illustrated in Figure 3.2, a number of BTS measurements were taken at the same location in both years to measure inter-annual variation. Most of these BTS measurements are in the Granger sub-basin in the northwestern part of the Wolf Creek Basin.

4.2. Potential incoming solar radiation

Using Solar Analyst and a 30 m digital elevation model, a grid of potential incoming solar radiation density (PISR) was developed for the Wolf Creek Basin (Figure 4.2.1).

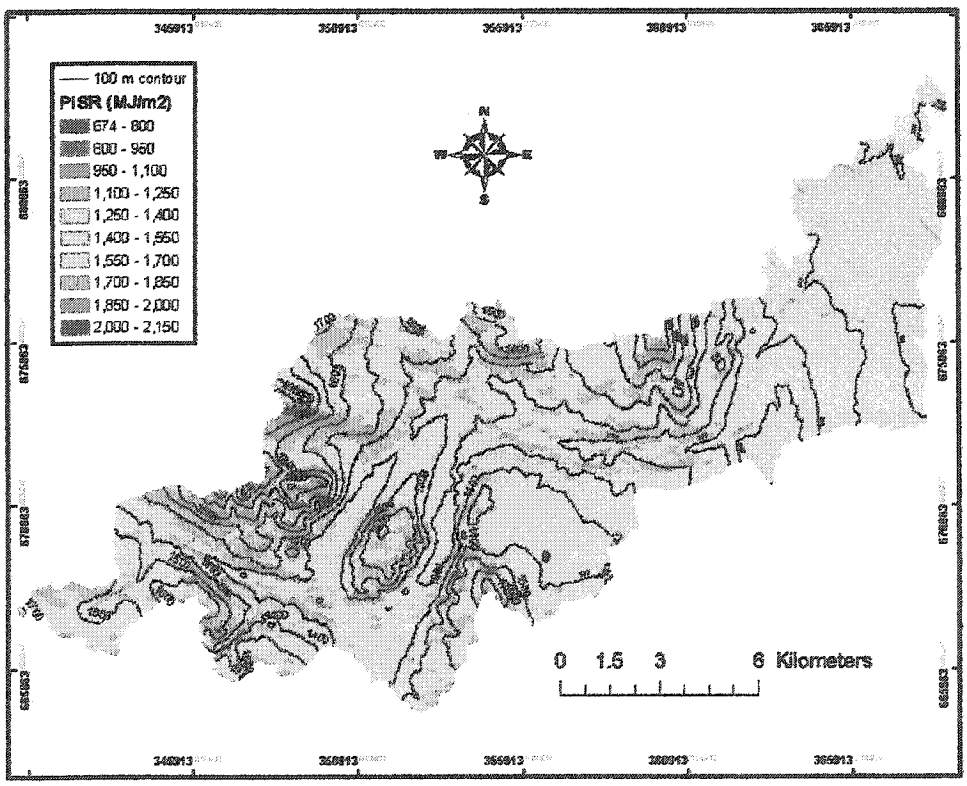

Figure 4.2.1: Map of PISR density for May 15th – September 30th produced using a 30 m digital elevation model (Yukon. Dept of Renewable Resources, 2000) and Solar Analyst extension in Arcview 3.2 (Fu and Rich, 1999).

PISR values range from a minimum of 675 MJ/m^2 to a maximum of 2100 MJ/m^2 with a mean of 1540MJ/m^2 and a standard deviation of 170 MJ/m^2 (Figure 4.2.2). The influence of aspect on the density of PISR received at the surface can be seen in Figure 4.2.3. On south-facing slopes, PISR density at the ground can be twice that of north-facing slopes. For example, the PISR density calculated for site A in Figure 4.2.3, a north-facing slope, was about 750 MJ/m^2 while at a similar elevation on a south-facing slope the calculated PISR was about 2000 MJ/m^2.

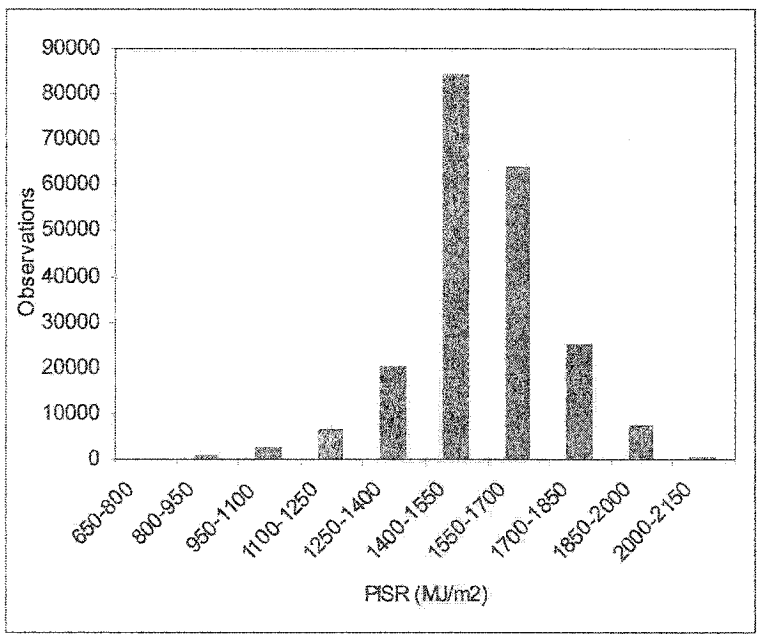

Figure 4.2.2: Histogram of PISR density for Wolf Creek Basin generated using Figure 4.2.1.

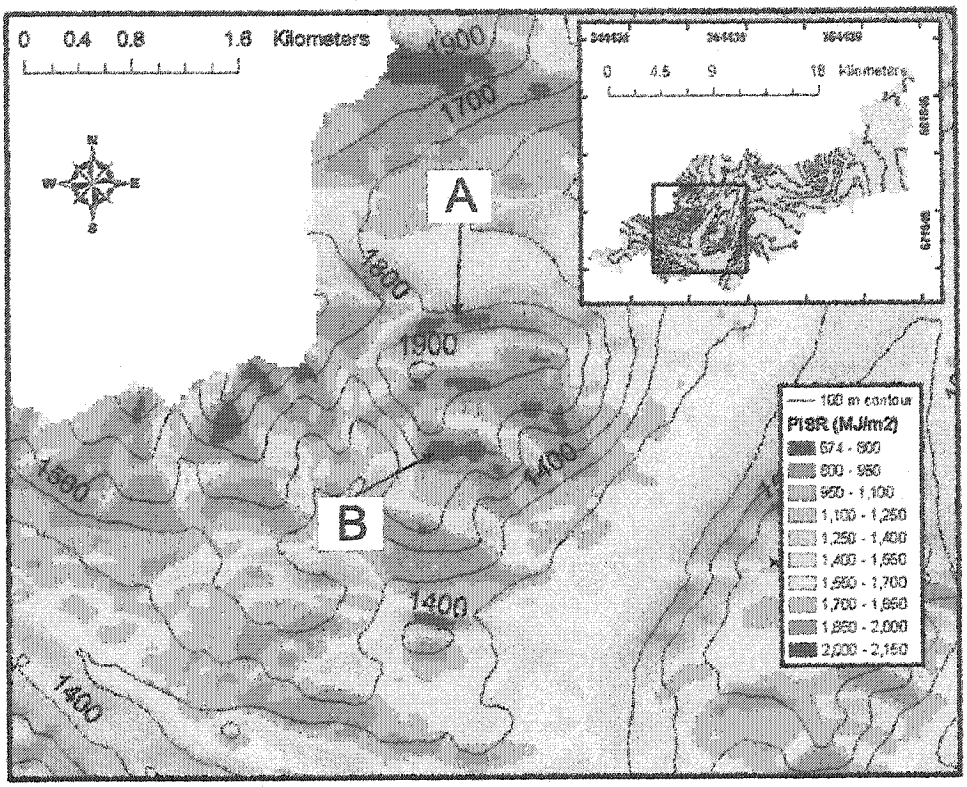

Figure 4.2.3: Map showing differences in potential incoming solar radiation density in relation to aspect.

4.3. Regression analyses to predict BTS values

4.3.1. Preliminary analyses

An initial multiple linear regression analysis between BTS, PISR density and elevation resulted in BTS predictions greater than 0°C in the lower regions of the basin. Values greater than 0°C are not possible in reality and indicate a flaw in the model's predictions. This was attributed to the lack of BTS measurements in the lowest parts of the basin which resulted in relatively steep elevation gradients. To reduce the elevation gradient and prevent BTS values > 0°C in the lower regions of the basin, elevation was

cubed. The resultant model incorporating the transformed elevation variable generated BTS values < 0°C throughout the basin and gave a statistically significant fit with an r^2 value of 0.38 (Table 4.3.1): BTS = $1.37x10^{-5}$(PISR)-$1.30x10^{-9}$(elevation^3)-5.59

Table 4.3.1: BTS regression coefficients and P-values for the intercept, PISR density and elevation (n = 386).

R^2 = 0.38	Coefficient	P- value	Standard Error
Intercept	-5.59	<0.001	0.78
PISR density (MJ/m^2)	$1.37x10^{-5}$	<0.001	$1.6x10^{-6}$
Elevation^3 (m a.s.l)	$-1.30x10^{-9}$	<0.001	$1.02x10^{-10}$

The data set of measured BTS values, elevations and calculated potential incoming solar radiation are graphically presented in Figure 4.3.1.

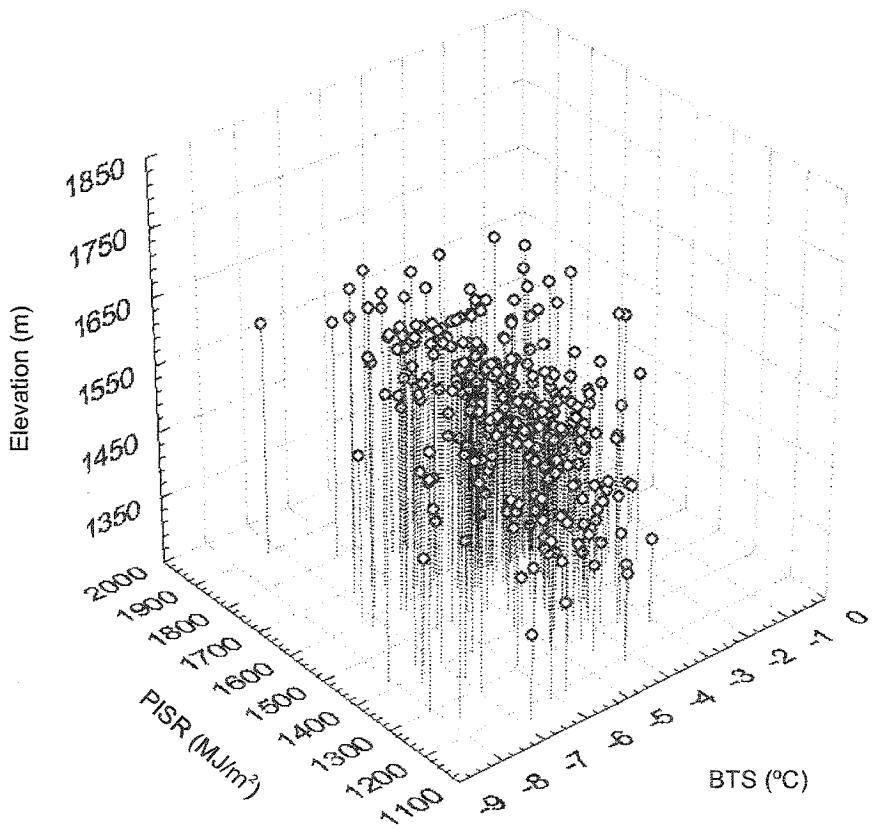

Figure 4.3.1: 3D graph of measured BTS, elevation and potential incoming solar radiation.

Due to the spatial nature of the BTS data set, a spatial statistical analysis of the data was necessary in order to determine if the residuals exhibit spatial autocorrelation. Spatial autocorrelation occurs when a value of the variable at one locality is dependent on the values of neighbouring localities (Sokal and Oden, 1978). A spatial autocorrelation analysis, using global Moran's I, was performed using Rookcase (Sawada, 1999). The lag distance — the distance radius search around each locality to compare residual values — was 39 m, which is the average nearest neighbour distance between BTS sites. The global Moran's I indicated that the linear regression residuals were significantly spatially auto-correlated (p-value = 0.0001) with a value of I = 0.35, with a value of 1 being dependent and 0 being no dependence.

The presence of significant spatial autocorrelation among residuals creates spatially dependent trends that may violate the standard assumptions of linear regression (Kerr *et al.*, 2001). It is evident from the global Morin's I that the BTS data set needs to be filtered (Getis and Griffith, 2002; Mikusinski *et al.*,2000). The filtering of the BTS data was performed in Arc GIS using Rookcase (Sawada, 1999). Individual residuals were evaluated using local spatial autocorrelation techniques with the selected BTS points being removed based upon their proportional influence on spatial autocorrelation. A total of 69 BTS points (18%) were selectively removed in order to statistically reject the hypothesis that the residuals are spatially autocorrelated (Morin's I = 0.053, p-value = 0.1515). The new average nearest neighbour distance between BTS sites increased to 45 m.

4.3.2. Final analysis

After the removal of the selected BTS values, the multiple regression analysis was re-run. The regression coefficients changed and the r^2 value increased to 0.40 (Table 4.3.2).

Table 4.3.2: BTS regression coefficients and P-values for the intercept, PISR and elevation (n = 317).

$r^2 = 0.40$	Coefficient	P- value	Standard Error
Intercept	-4.93	< 0.001	0.71
PISR (MJ/m^2)	$1.11x10^{-5}$	< 0.001	$1.44x10^{-6}$
Elevation^3 (m a.s.l)	$-1.20x10^{-9}$	< 0.001	$9.47x10^{-11}$

A visual representation of the predicted BTS surface against PISR and elevation is shown in Figure 4.3.2.

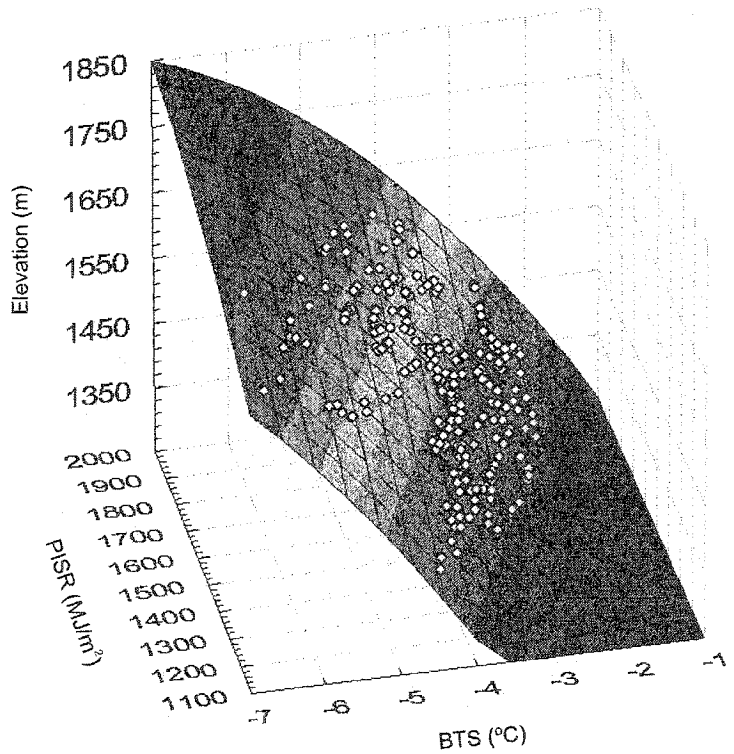

Figure 4.3.2: Visual representation of BTS surface predicted using the modified BTS data set.
Predicted BTS values shown for all locations based on elevations from DEM and modeled PISR.

A number of tests were conducted on the residuals to evaluate the strength and fit of the linear regression model. Figure 4.3.3 indicates that the residual error is close to normally distributed. There are some exceptions at both tails of the residual errors where they tend to deviate from the rest of the data. This identifies some of the outliers that are not similar to the rest of the data. There are no strong trends in the plotted residual data (Figure 4.3.4) although there is some clustering of residual points between the -4°C and -5°C modeled BTS values.

A scatter plot showing the fitted BTS vs. measured BTS has equal scatter above and below the 1:1 line except in the coldest and warmest regions (Figure 4.3.5). Overall, the model predicts a smaller range in values than those that were actually measured. This suggests a systematic variation in other factors that are not included in the model, such as snowpack history and vegetation cover.

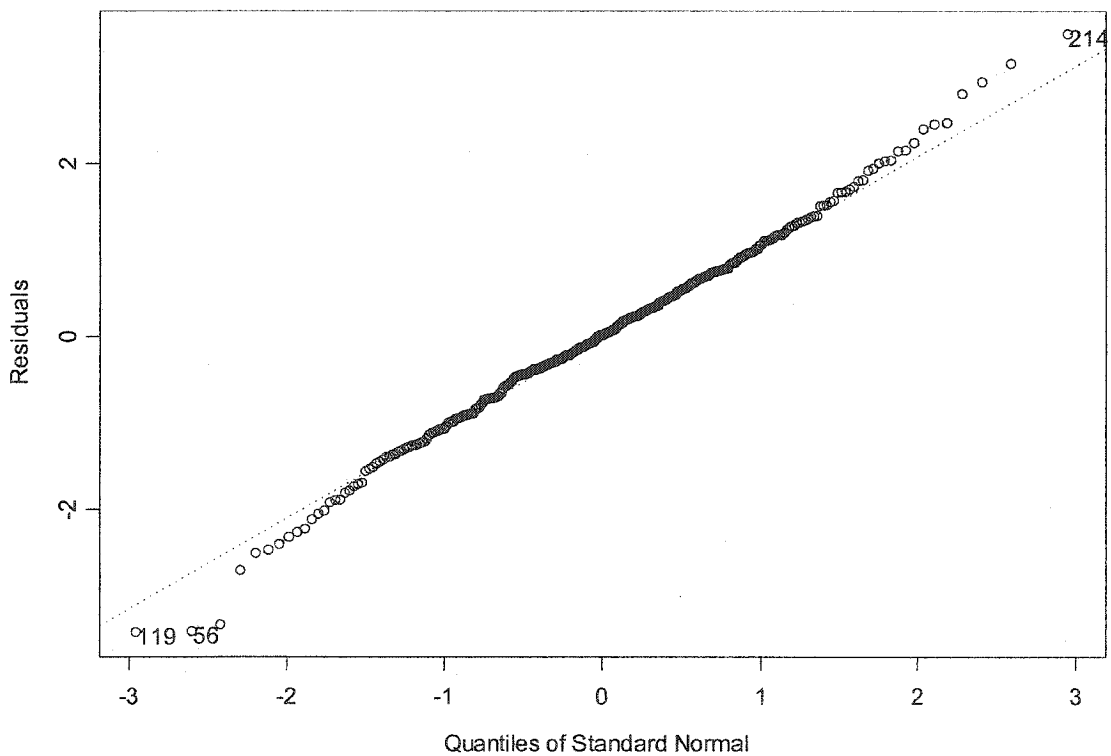

Figure 4.3.3: Distribution of the BTS regression model residuals.

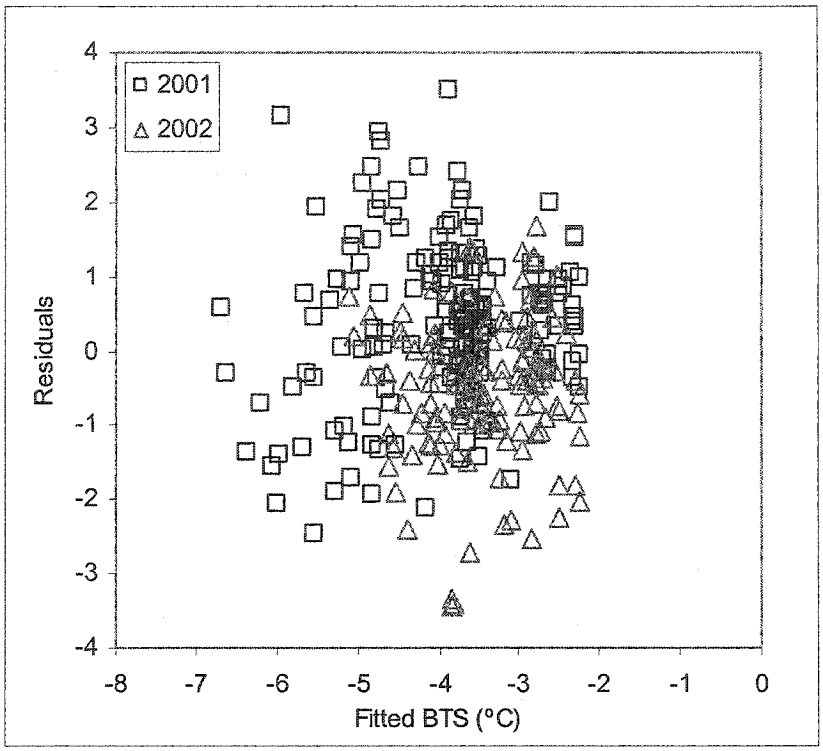

Figure 4.3.4: Plotted residual data from the BTS regression model.

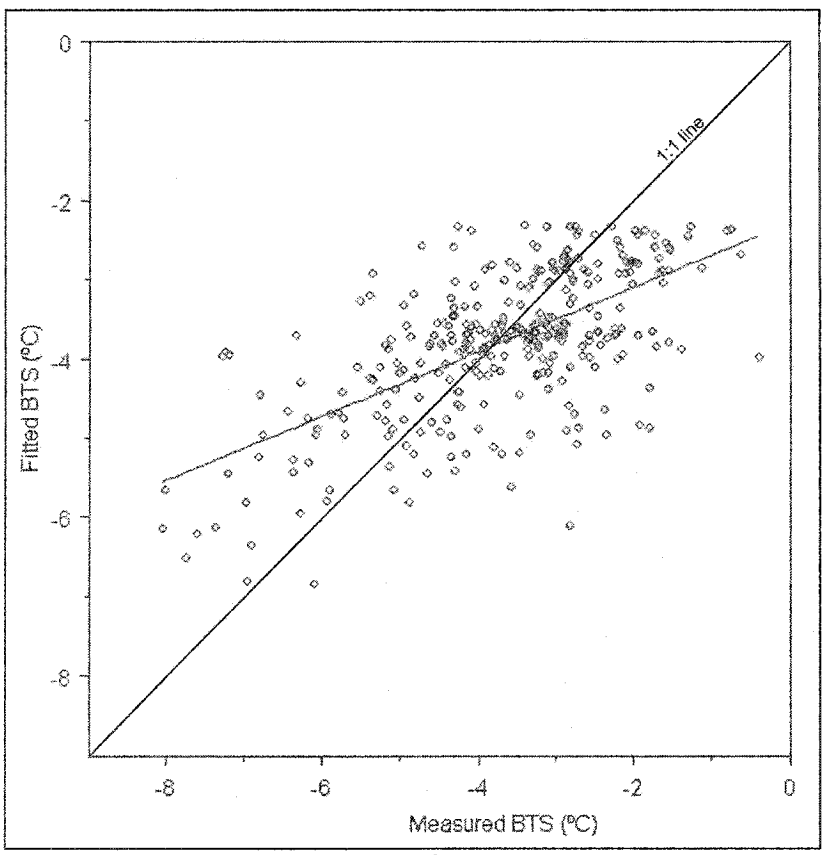

Figure 4.3.5: Measured BTS versus fitted BTS bands values.

The scatter in Figure 4.3.5 appears reasonable visually, but in fact, the best fit line does differ statistically from the 1:1 line. For this reason, modeling was undertaken with the best-fit equation (Table 4.3.2) and with ± 1 standard error in order to assess the sensitivity of the results to the exact relationships employed. ArcGIS was used to calculate BTS values for the entire basin using the DEM (to provide elevation values) and the potential incoming solar radiation map. The resulting grid (Figure 4.3.6) shows continuous predicted BTS values for the best-fit relationship; Figures 4.3.7 and 4.3.8 show the predicted BTS field employing ± 1 standard error. The modeled BTS values predicted using +1 standard error are warmer than best-fit BTS model and modeled BTS values predicted using -1 standard error are cooler.

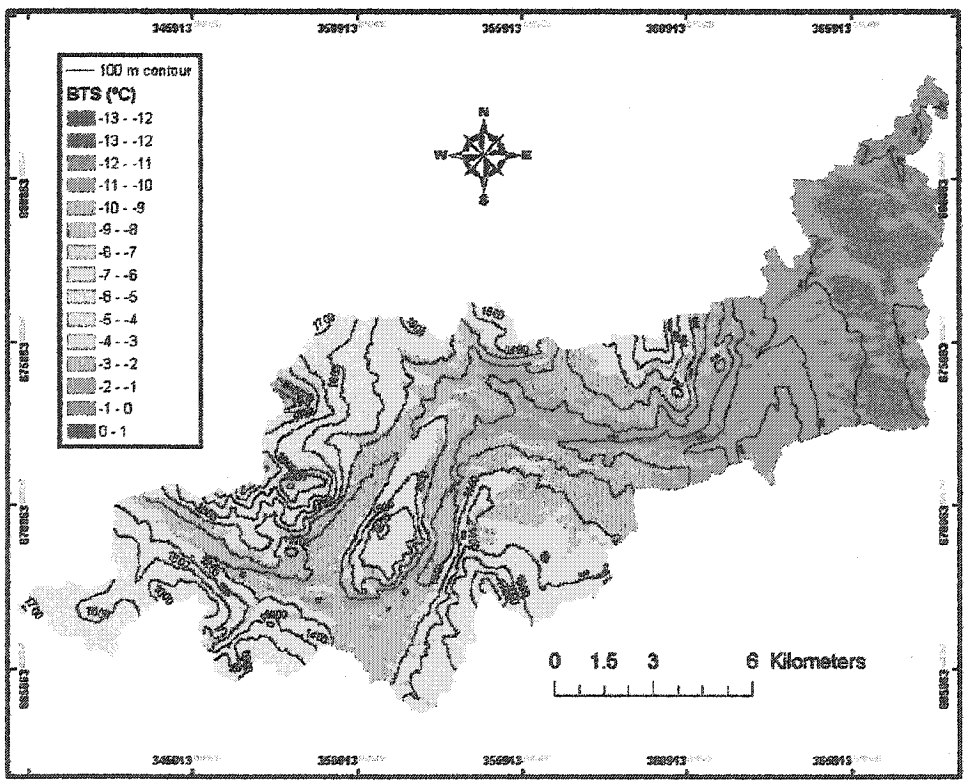

Figure 4.3.6: Map of modeled BTS values for Wolf Creek basin.

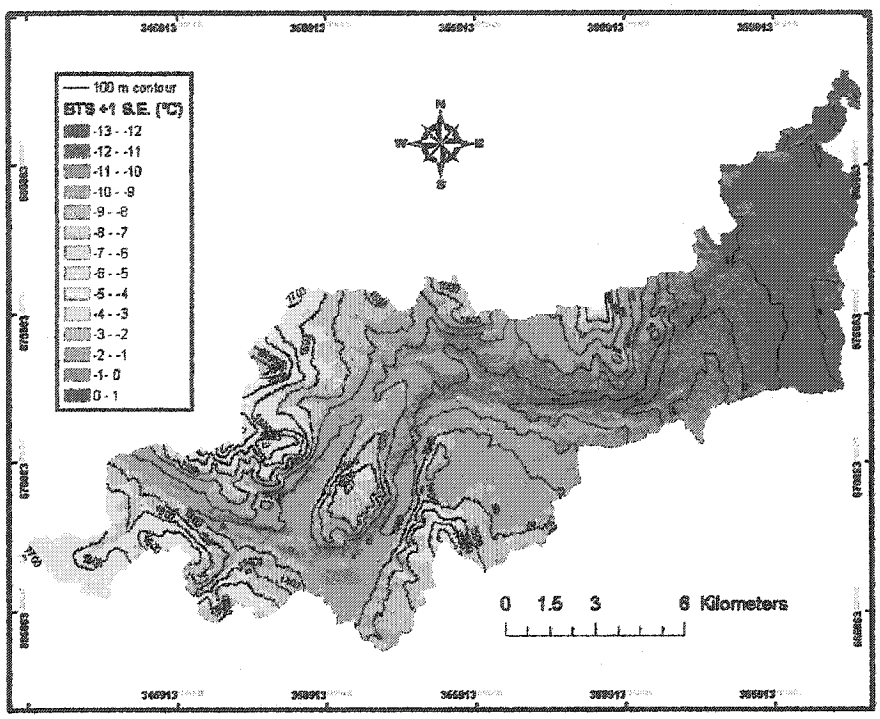

Figure 4.3.7: Map of modeled BTS values +1 standard error for Wolf Creek basin.

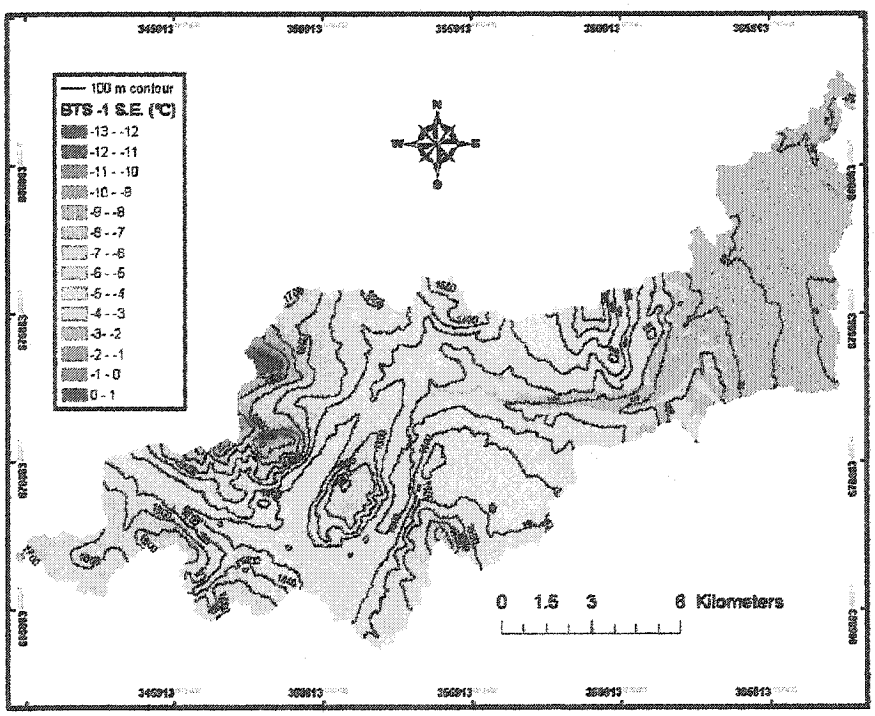

Figure 4.3.8: Map of modeled BTS values –1 standard error for Wolf Creek basin.

4.4. Observations of late-summer frozen ground

A total of 201 pits were excavated between July 20th and August 24th, 2002. Frozen ground was found to be present at 113 locations using either direct observation of frozen soil (Figure 4.4.1) (25 sites), or measured temperatures of 0°C (88 sites).

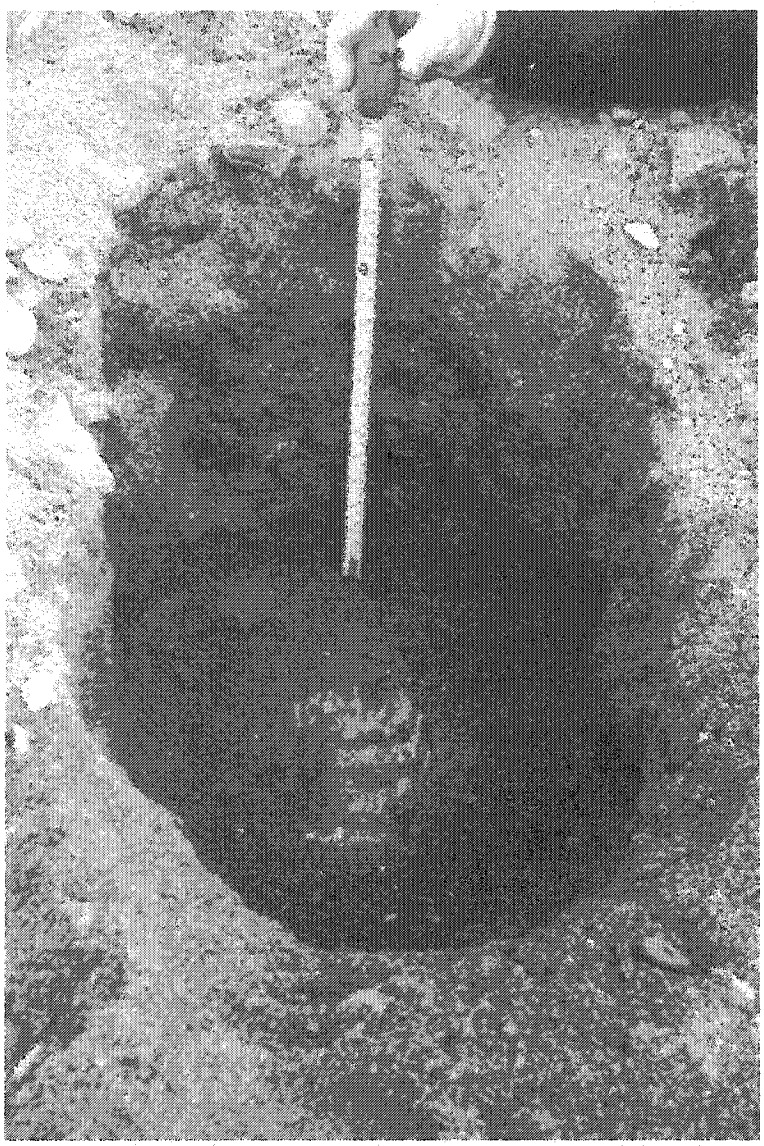

Figure 4.4.1: Frozen ground observed at a depth of 40 cm at site 2002/07/24/A24B. The pit was located at the base of a west-facing slope at an elevation of 1836 m.

A total of 88 of the excavated pits did not exhibit frozen ground at depths ≤150 cm. Ground temperature predictions based on the temperature profile were needed to identify whether each pit would be classified as having frozen ground within the top 2 m (Figure 4.4.2). The temperature profile analysis indicated that 18 out of the 88 pits were too close to confidently categorize the presence or absence of permafrost, leaving 70 pits that were categorized into either permafrost (15) or non-permafrost (55 sites).

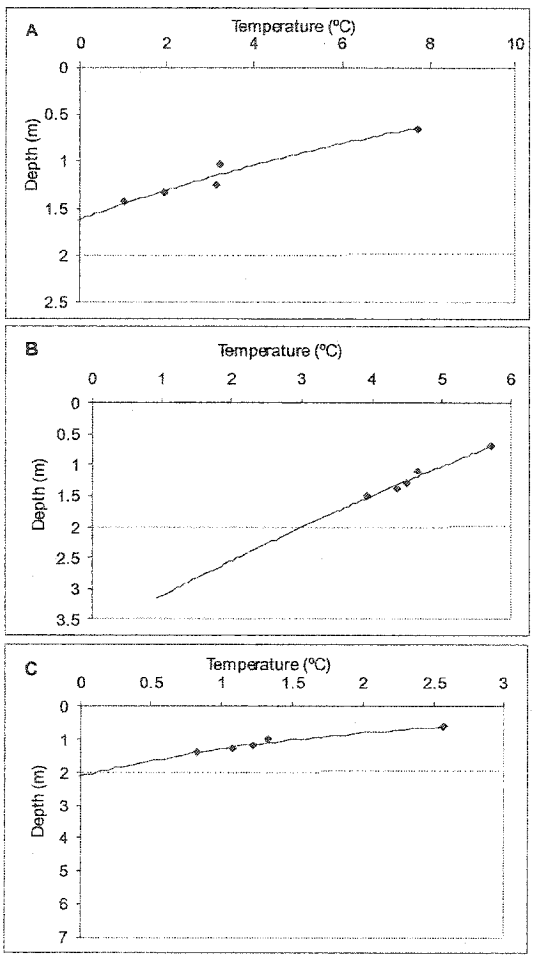

Figure 4.4.2: Examples of ground temperature predictions.
The line represents the 2 m maximum depth for frozen ground that would be classified as permafrost. Example A, site 2002/07/22/A9A, represents a pit where frozen ground was predicted around 1.6 m and therefore the site was classified as a permafrost location. Example B, site 2002/07/30/A35A, represents a pit where frozen ground was not predicted within 2 m of the surface and the site was therefore classified as being non-permafrost. Example C, site 2002/08/04/A51, represents a pit where frozen ground was predicted close to the 2 m cut-off depth and therefore was removed from the data-set prior to analysis.

The pits were excavated throughout a range of BTS values from -1°C through -11°C (Figure 4.4.3). The majority of the pits were located in the -4°C to -2°C modeled BTS categories. There are very few pits located in the -1°C range, as access to the lower part of the basin was logistically difficult. As a consequence, confidence in permafrost distribution predictions is greatest for the upper part of the basin.

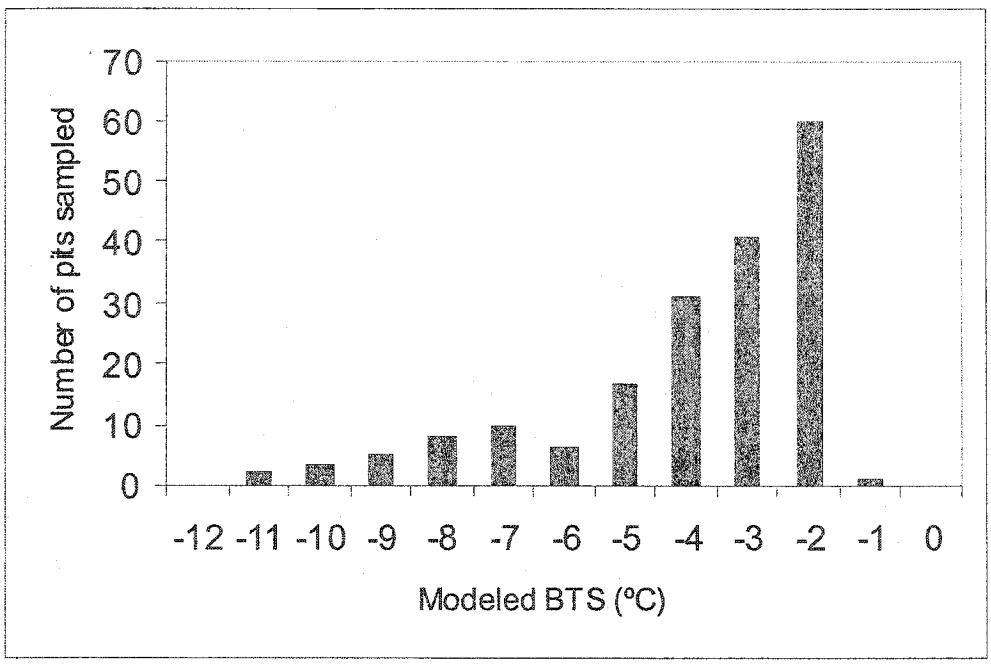

Figure 4.4.3: Histogram of excavated pits at modeled BTS values
Note: Values shown are the upper temperature in the range.

It is interesting to examine the relationship between organic layer thickness and the presence of permafrost at the pit sites. In lowland areas in the discontinuous zone, a thick organic layer is often a strong indicator of the existence of permafrost. The observations from the pits show that an organic layer thicker than 10 cm and the absence of an organic layer are usually, but not invariably, indicators of permafrost (Figure 4.4.4). The wide range of organic-layer thicknesses measured at permafrost locations is due on the one hand, to thin or non-existent organic layers at high elevations, and on the other, to permafrost being present at low elevations beneath thick organic mats. At the most typical organic-layer thicknesses of 2-8 cm, permafrost and

non-permafrost sites are equally common. Hence organic-layer thickness is not a good determinant for permafrost in the Wolf Creek basin.

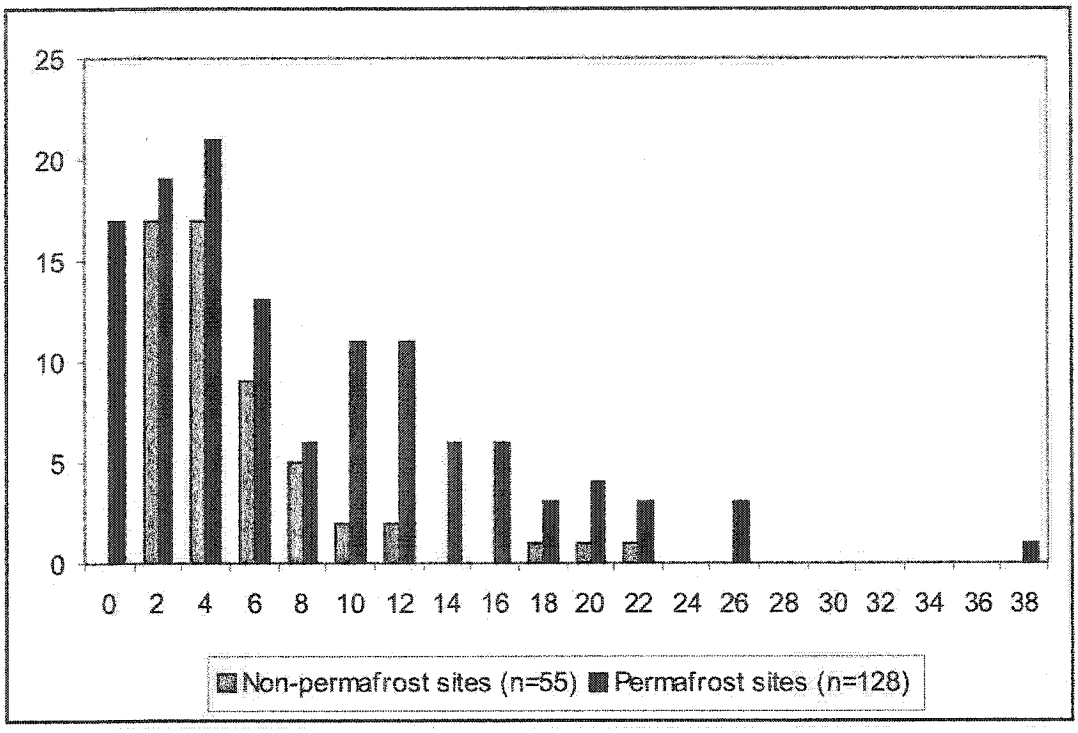

Figure 4.4.4: Organic mat thickness at permafrost and non-permafrost sites.

4.5. Use of logistic regression to predict permafrost probability

The probability of permafrost was calculated using the relation between best-fit modeled BTS (step 3) and the actual distribution of frozen ground according to step 5 of the Methodology. Using logistic regression, a model termed LM-1 was developed. The regression equation for the model is:

$$Y = -2.267 - 0.823(BTS)$$

where BTS values are those predicted from the multiple regression model, and

$$P = 1/(1+\exp(-Y))$$

where P is the probability of permafrost.

The results from LM-1 signify a relation between BTS and the presence or absence of permafrost as indicated by the pits. Both the BTS and the constant coefficients are considered significant at p=0.01 (99% confidence level) (Table 4.5.1).

Table 4.5.1: Variables defined in LM-1 regression model.

	ß Coefficient	Standard Error	Wald[a]	Degrees of freedom	Significance
Constant	-2.27	0.50	13.8	1	<0.01
BTS	-0.82	0.15	25.7	1	<0.01

[a] Wald value is obtained by comparing the maximum likelihood estimate of the slope to an estimate of its standard error (Hosmer and Lemeshow, 1989).

The overall model is also significant at the 0.01 level according to the model chi-square statistic. The resulting regression equation allows for a permafrost probability curve to be generated (Figure 4.5.1). The permafrost probability curve for LM-1 shows

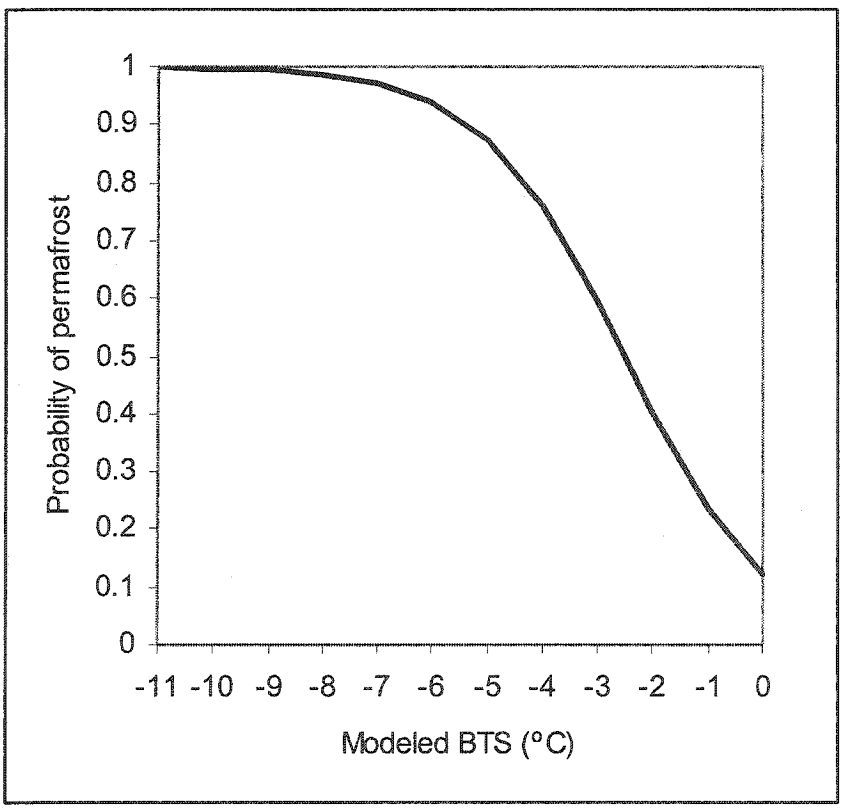

Figure 4.5.1: Permafrost probability curve generated from logistic regression analysis (LM-1) that uses all the accepted pits.

that there is a >90% probability of permafrost at modeled BTS values <-5.4°C, and a <10% probability of permafrost at modeled BTS values >0°C.

The modeled probability of permafrost was compared to measured averages of permafrost for each BTS category, -1°C through -8°C (Figure 4.5.2). The predicted probability of permafrost for BTS values of -3°C and -4°C is close to the measured values. At -1°C BTS the predicted probability of permafrost was 23% while the observed single site did not exhibit permafrost (Figure 4.5.2).

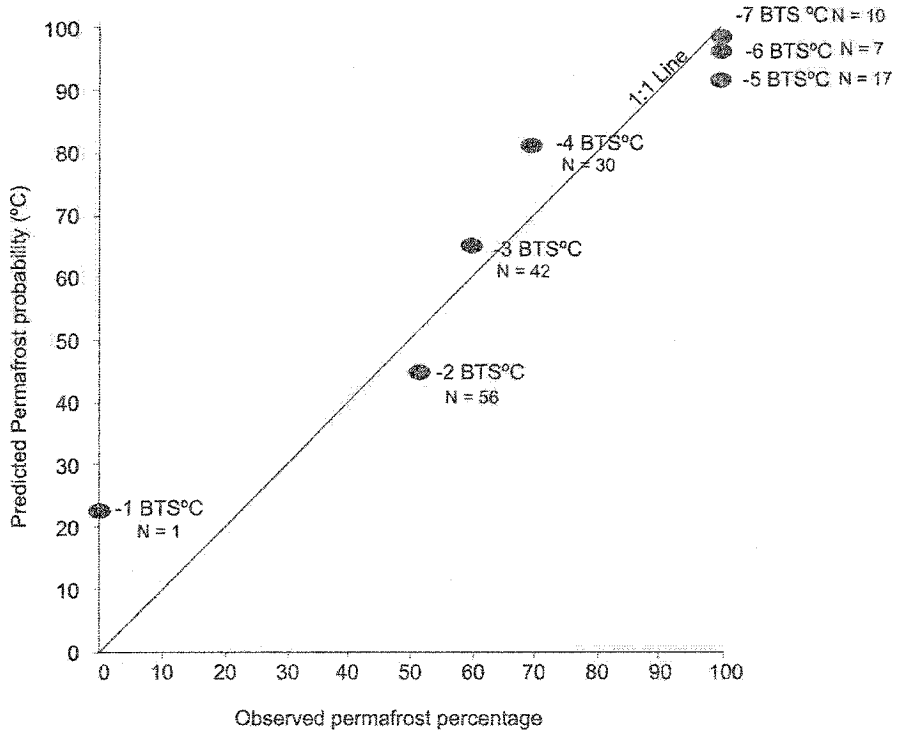

Figure 4.5.2: Observed permafrost percentages versus predicted permafrost probabilities for LM-1 at specific BTS values.
The number of observations is also presented. BTS values <-7 could not be shown as observed and predicted permafrost percentages are >99%. Note: the observed permafrost percentage is an average of each BTS category (*i.e.* -1 BTS category includes -1 to -1.999°C). Therefore, the predicted permafrost probability is also calculated for the average BTS values (*i.e.* -1 °C BTS = -1.5°C).

Based on LM-1, a map of predicted permafrost probabilities was calculated in Arc GIS (Figure 4.5.3).

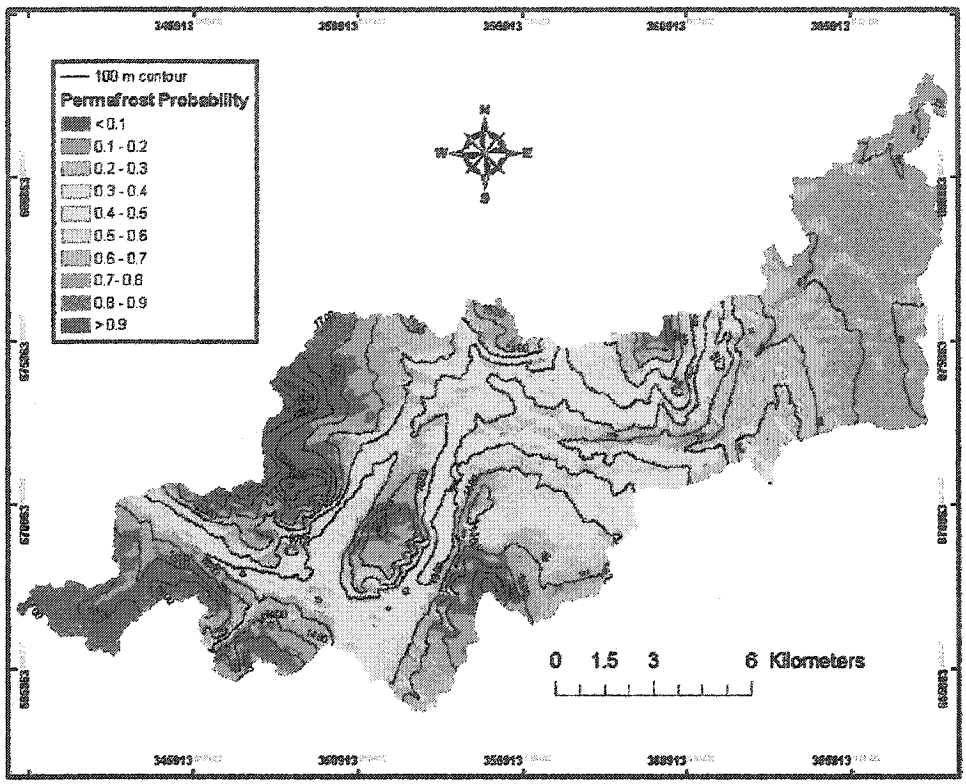

Figure 4.5.3: Map of permafrost probability for the Wolf Creek basin.

Figure 4.5.3 gives detailed information on where permafrost is likely to be present or absent within the basin. As expected, it shows that the probability of permafrost in the basin predicted by LM-1 increases dramatically as elevation increases, ranging from <0.1 in the lowest parts of the basin to >0.9 on the mountain peaks. The influence of insolation can also be seen, with high probabilities of permafrost occurring on north-facing slopes, while, at similar elevations on south-facing slopes, the probability is much lower. The probabilities shown can be converted into more conventional statistics on the amount of permafrost present in the basin, if it is assumed that there is a direct relationship between probability and percentage area (i.e. that half of the grid cells with a permafrost probability of 0.5 are underlain by permafrost and half are not). The

model predicts the area underlain by permafrost at the lowest elevations (600-700 m) in the basin is 18%. The area underlain by permafrost increases dramatically at higher elevations, reaching 93% at 1700-1800 m (Figure 4.5.4). Using conventional definitions of permafrost zones, LM-1 predicts that there is no terrain in the basin that would be classified as having isolated patches of permafrost (<10%). The 600-1300 m range constitutes the scattered discontinuous permafrost zone, the 1300-1700 m range constitutes widespread discontinuous permafrost zone, and permafrost above 1700 m would be classified as continuous permafrost (e.g. Heginbottom *et al.*, 1995).

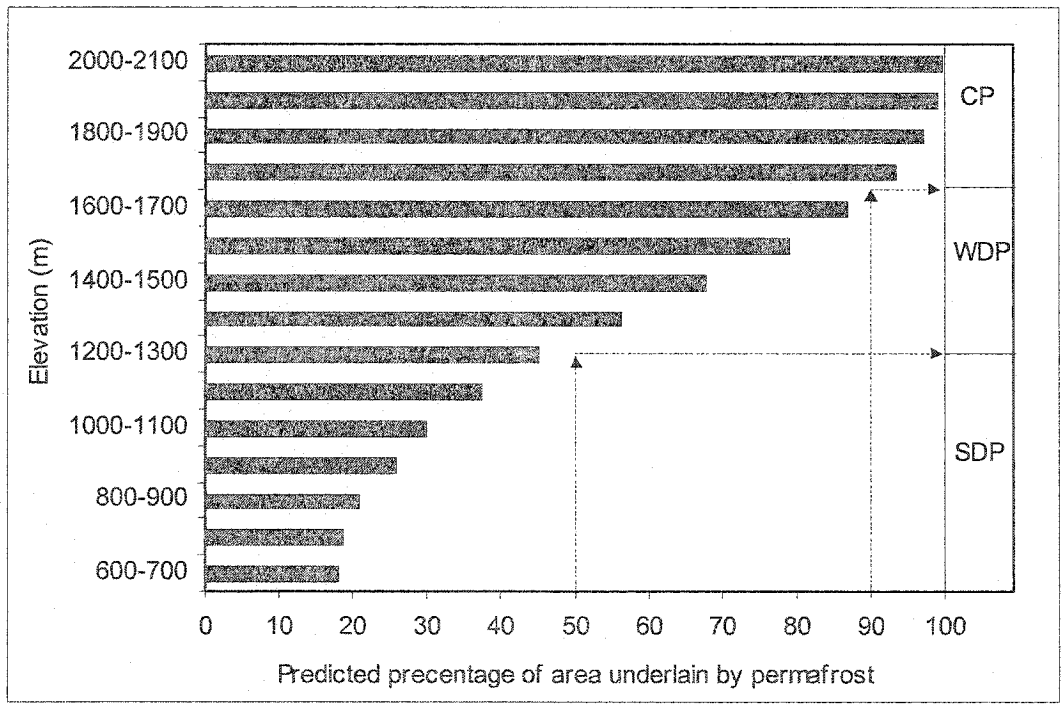

Figure 4.5.4: Percentage of elevation bands in Wolf Creek underlain by permafrost according to LM-1.
Permafrost zone definitions from Heginbottom *et al.* (1995). (SDP- Sporadic discontinuous permafrost, WDP-Widespread discontinuous permafrost, CP- Continuous permafrost).

The BTS modeling is robust because essentially the same permafrost probability curve pattern is observed using ± 1 BTS standard error (Figure 4.5.5)

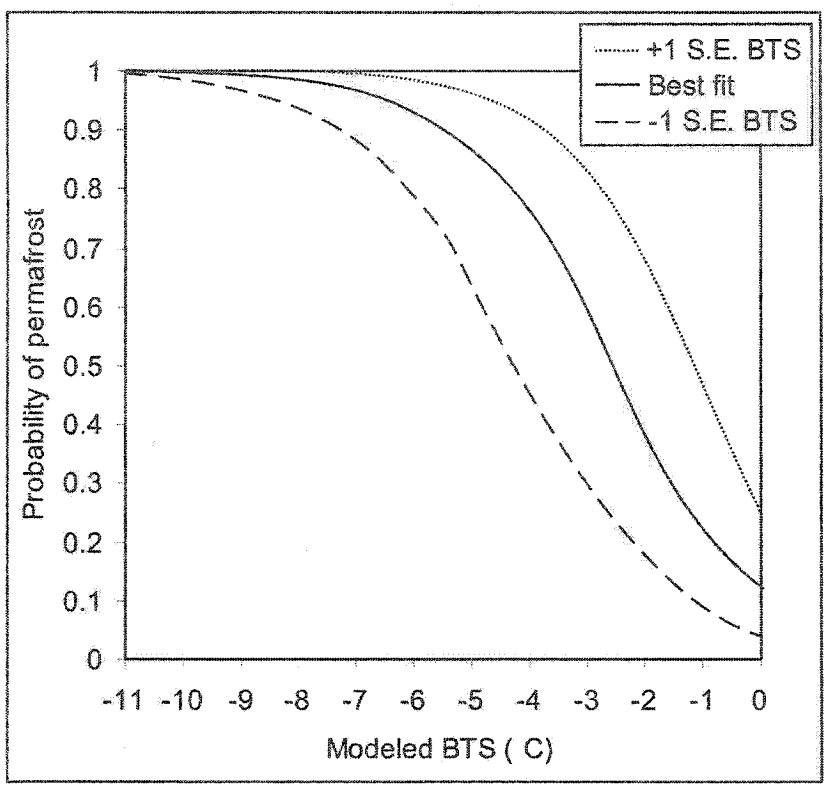

Figure 4.5.5: Permafrost probability curve of best fit and ± 1BTS standard error according to LM-1.

The resulting permafrost probability maps based on +1 BTS standard error (Figure 4.5.6) and -1 BTS standard error (Figure 4.5.7) indicate relatively little difference in actual permafrost distribution. According to +1 BTS standard error, 51% of the basin is underlain by permafrost and 55% is underlain by permafrost according to -1 BTS standard error. These values compare to 51% predicted using the best-fit BTS relationship.

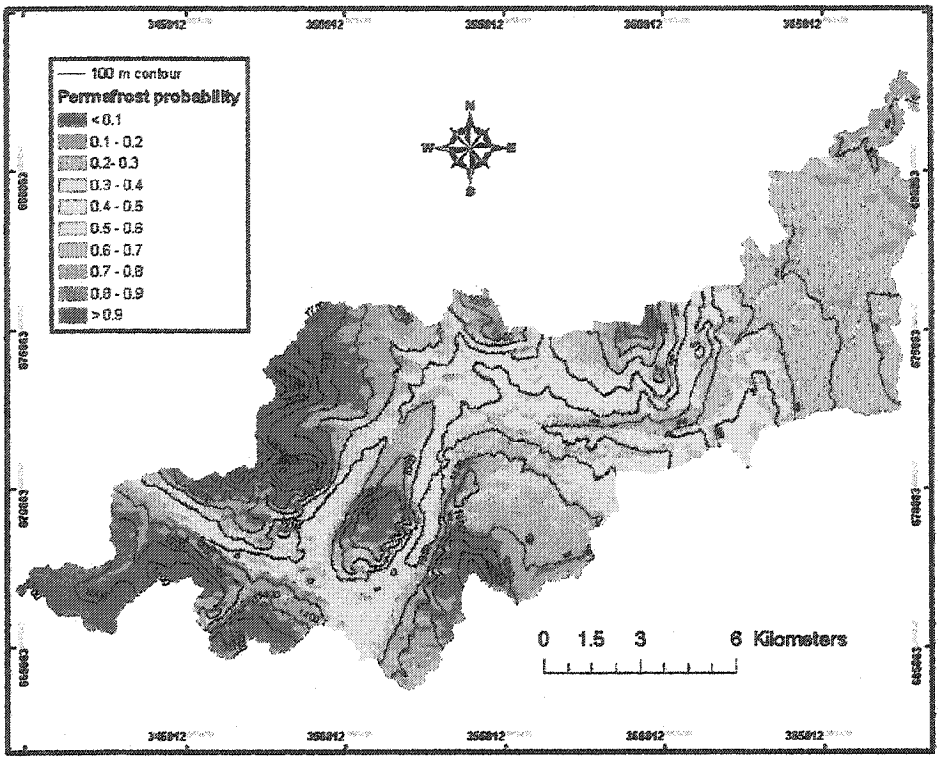

Figure 4.5.6: Map of permafrost probability calculated using +1 BTS standard error.

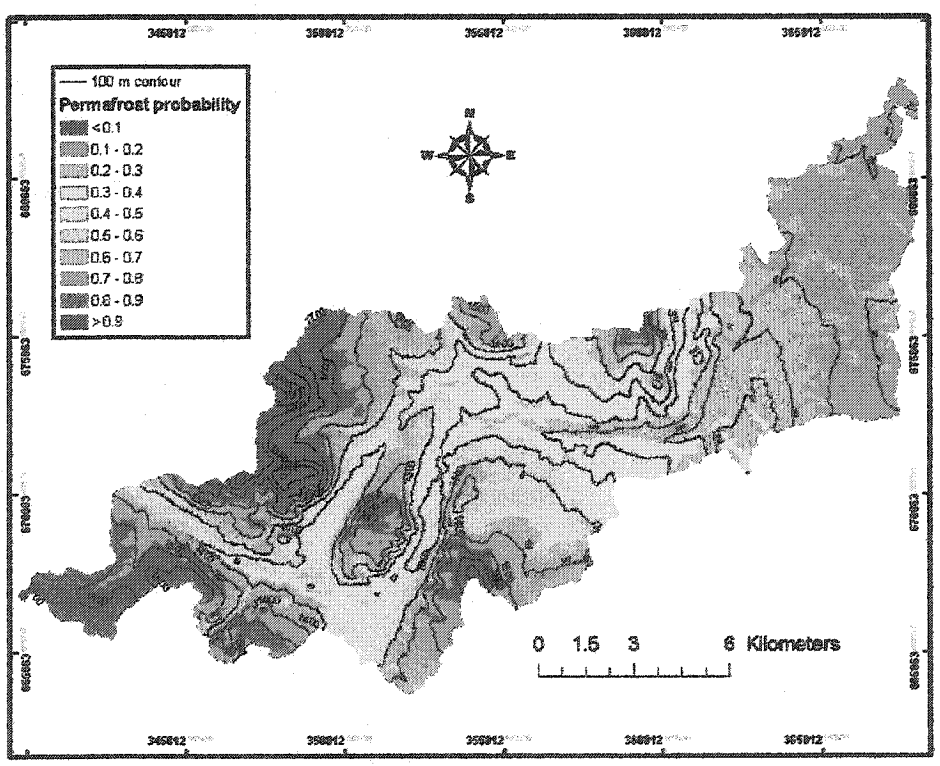

Figure 4.5.7: Map of permafrost probability calculated using -1 BTS standard error.

4.6. Refinement of predictive model

The curve in Figure 4.5.1 predicts a probability of permafrost of 10% for 0°C modeled BTS. However, six of the lowest sampled pits excavated north of Coal Lake, encountered no permafrost and predicted BTS values in this region range from -2°C through -1°C. Based on the permafrost probability curve, this area should have permafrost probabilities of 19-35%. This suggests that there is an error in the model to produce such high levels of permafrost in areas where it should be relatively scarce. Somewhere within the analysis there must be a factor pushing the model to predict greater than expected permafrost conditions (see Figure 4.5.1).

Probing and ground temperature measurements indicated widespread permafrost in the confined valley on the west side of Coal Ridge at relatively low elevations. Permafrost was present on the valley floor while being absent on the valley sides. Widespread permafrost together with the presence of well-developed palsas (Coultish, 2002) indicate conditions that contrast with elsewhere in the basin at similar elevations. The presence of an inverted tree line, composed of white spruce, within the confines of the valley, suggests the presence of cold air drainage resulting in temperature inversions which might reduce the length of the growing season. The white spruce trees are not present on the valley floor, which is covered by shrub willow and birch together with grasses and mosses, and are only encountered at various elevations above the valley (Figure 4.6.1). The inverted tree line is not observed at a particular elevation along the valley walls but reflects the topography of the valley floor. Cold air drainage could affect the distribution of permafrost on the valley floor, leading to a greater distribution of permafrost than would be expected based on elevation and PISR. Cold air drainage has been rarely investigated in mountainous regions, but occurs in northern Alberta, British Columbia and southern Yukon Territory (Harris, 1982; Taylor *et al.*, 1998). The occurrence of cold air drainage has been reported in Wolf Creek

(Janowicz, 1999).

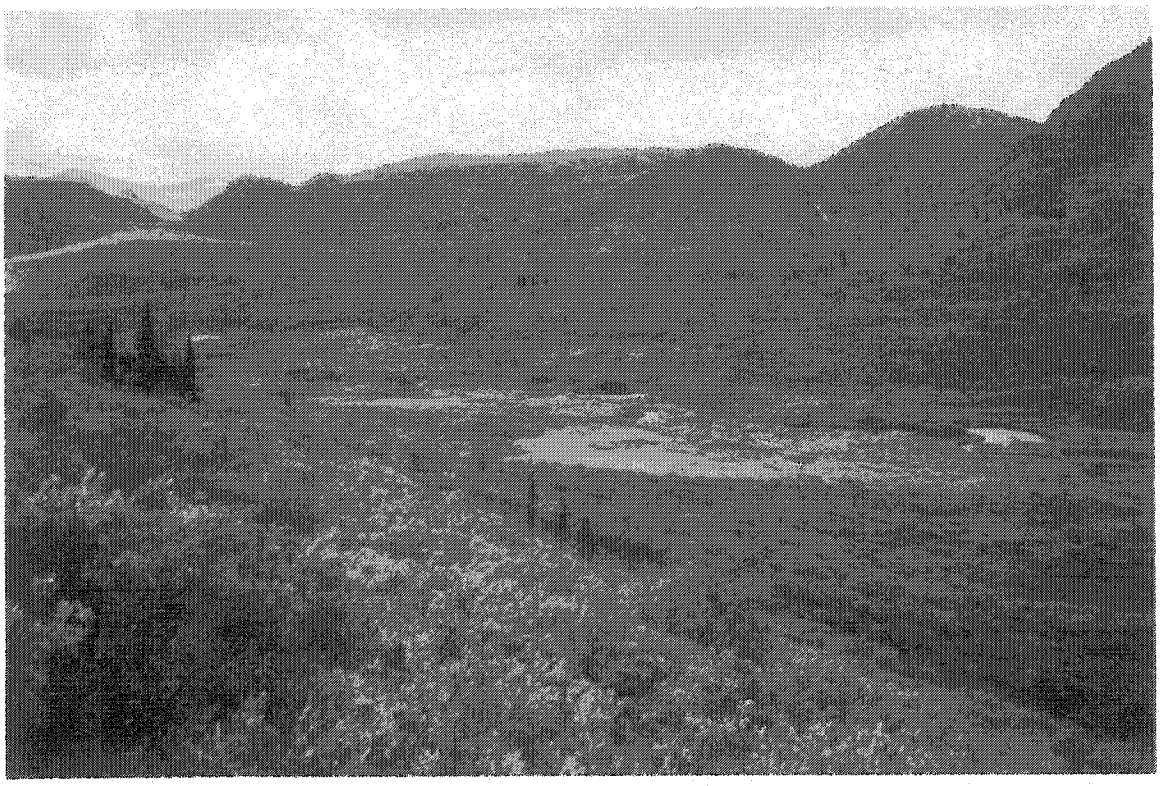

Figure 4.6.1: Southwest-facing picture of the confined valley that is subject to cold air drainage or atmospheric temperature inversions.
Note the absence of white spruce trees on the valley floor and their presence on the valley side slopes. A second altitudinal tree-line occurs at higher elevations.

The tree-line along the valley walls, mapped using aerial photography, was used as an indicator of the upper boundary of the hypothesized cold air drainage. The geo-referenced permafrost excavations were overlain with an air photograph to identify the specific pits that were located below the tree-line (Figure 4.6.2). A road along the west side of the valley was used for control points. A total of 110 geo-referenced points were recorded at 50 m intervals along the road. The road runs diagonally across the air photograph and near the bottom of the valley being investigated. It was not possible to use a single elevation to differentiate pits below and above this valley-bottom tree-line because it slopes down-valley (see Figure 4.6.2).

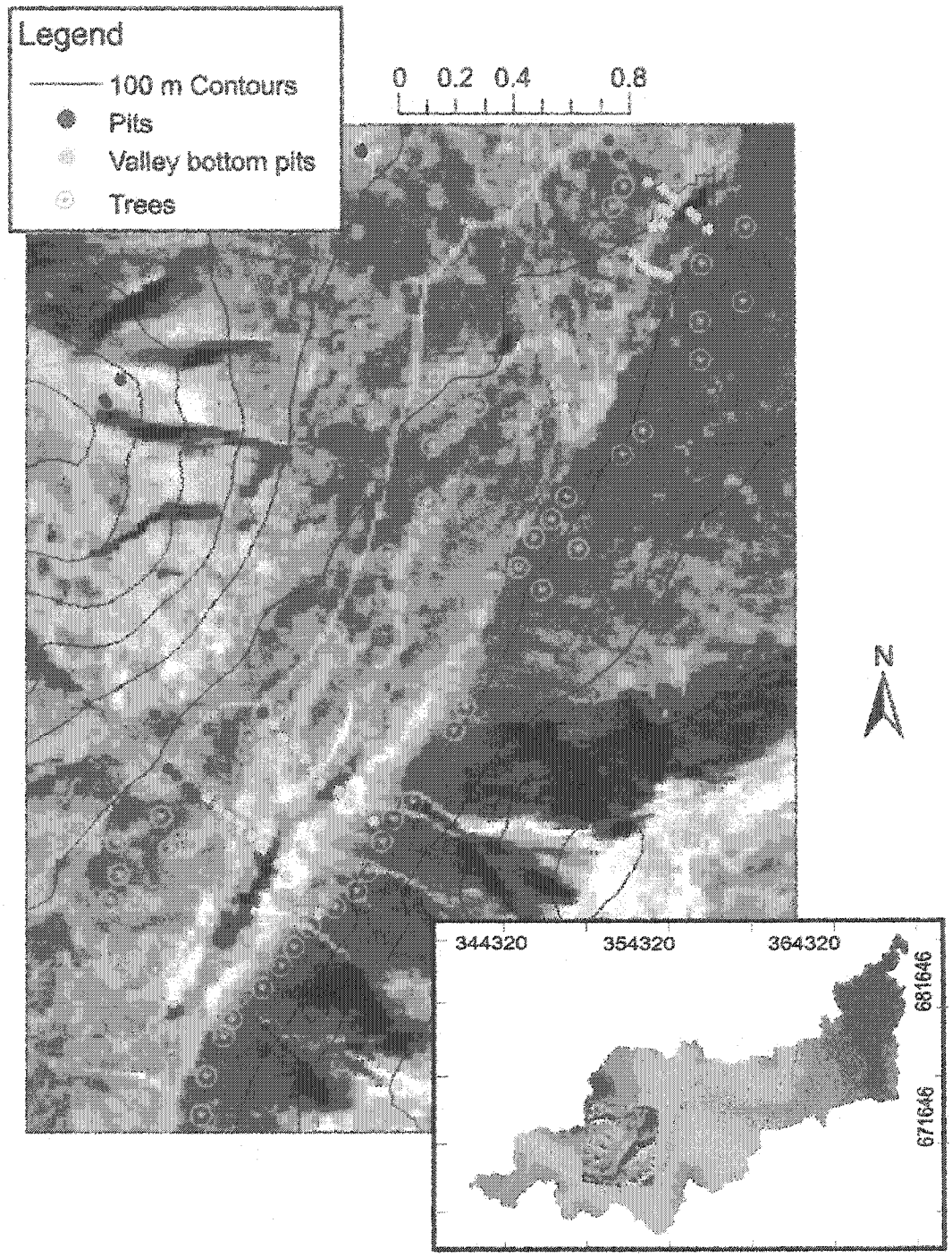

Figure 4.6.2: Overlay of excavated pits and digitized air photograph.
The yellow points are excluded from LM-2, as these points are located below the tree-line on the valley floor. The red points represent pits near the valley that were retained in LM-2 (among others). The green markers represent individual trees forming the tree-line.

The air photograph used in this analysis was taken in 2001 and has a scale of 1:15,000. At this scale, trees were easy to identify under magnification. The trees were circled and a lower boundary of the average tree line was estimated. An RMS error of 0.81 was generated between the road shape file and the air photograph.

A second linear logistic regression model (LM-2) was performed on the pit excavations excluding the 40 valley bottom pits. The modeling procedure was the same as with LM-1. The model coefficients for both BTS and the constant are significant at the 0.01 level with a critical value of 6.635 [df = 1] (Table 4.6). The overall model is also considered significant at the 0.01 level according to the model chi-square statistic. A comparison of predicted permafrost probabilities from LM-2 and the measured percentages of permafrost (Figure 4.6.3) gives similar results to those of LM-1 (see Figure 4.5.2), but LM-2 predicts lower permafrost probabilities at higher temperatures, that more accurately reflect the observations. Permafrost probabilities at BTS predictions <-5° are similar for both LM-2 and LM-1.

Table 4.6: Variables defined in LM-2 regression model.

	ß Coefficient	Standard Error	Wald	Degrees of freedom	Significance
Constant	-3.23	0.84	14.74	1	<0.01
BTS	-1.01	0.22	20.96	1	<0.01

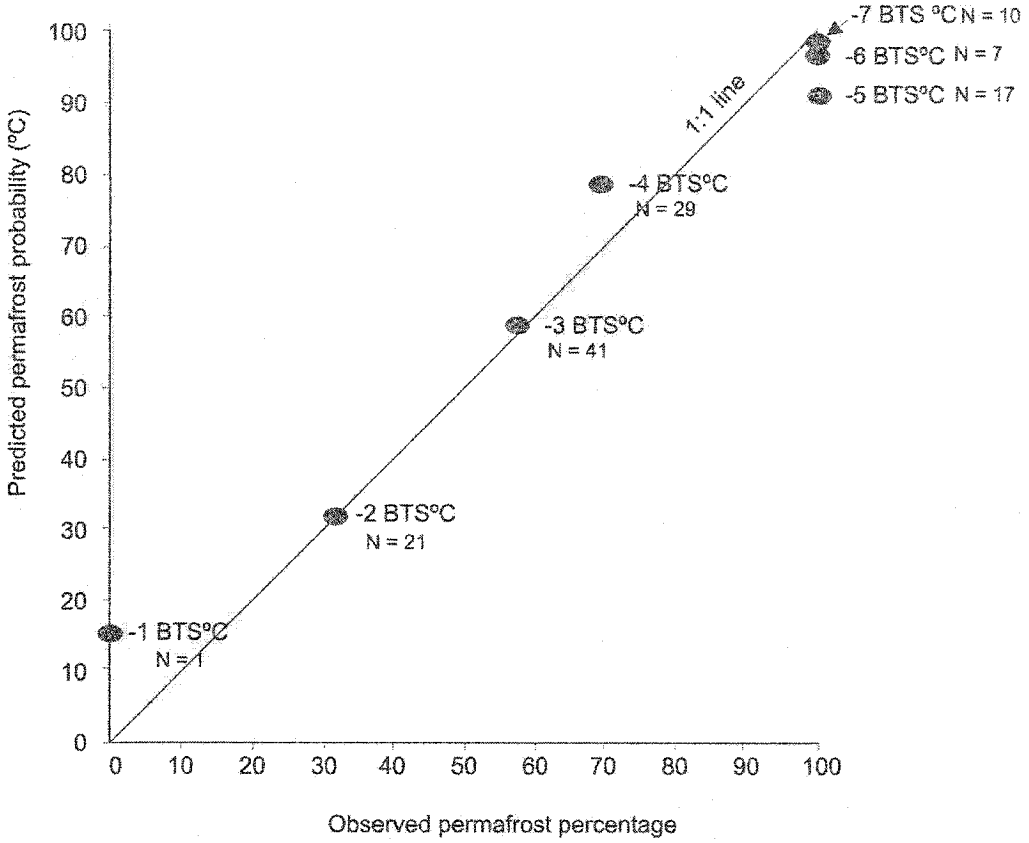

Figure: 4.6.3 Observed permafrost percentages versus predicted permafrost probabilities for LM-2 at specific BTS values.
The number of observations is also presented. BTS values <-7 could not be shown as observed and predicted permafrost percentages are >99%. Note: the observed permafrost percentage is an average of each BTS category (*i.e.*-1 BTS category includes -1 to -1.999°C). Therefore, the predicted permafrost probability is calculated for the average BTS values (*i.e.* -1 °C BTS represents -1.5°C).

The predicted permafrost curves from both models are shown in Figure 4.6.4. LM-2 predicts slightly greater probability of permafrost at BTS values of -11°C through -5°C and lower probabilities at BTS values >-5°C. For example, at -4°C, LM-1 predicts a 74% probability of permafrost while LM-2 predicts 69%; at 0°C modeled BTS, LM-2 predicts a permafrost probability of 3% while LM-1 predicts 9%.

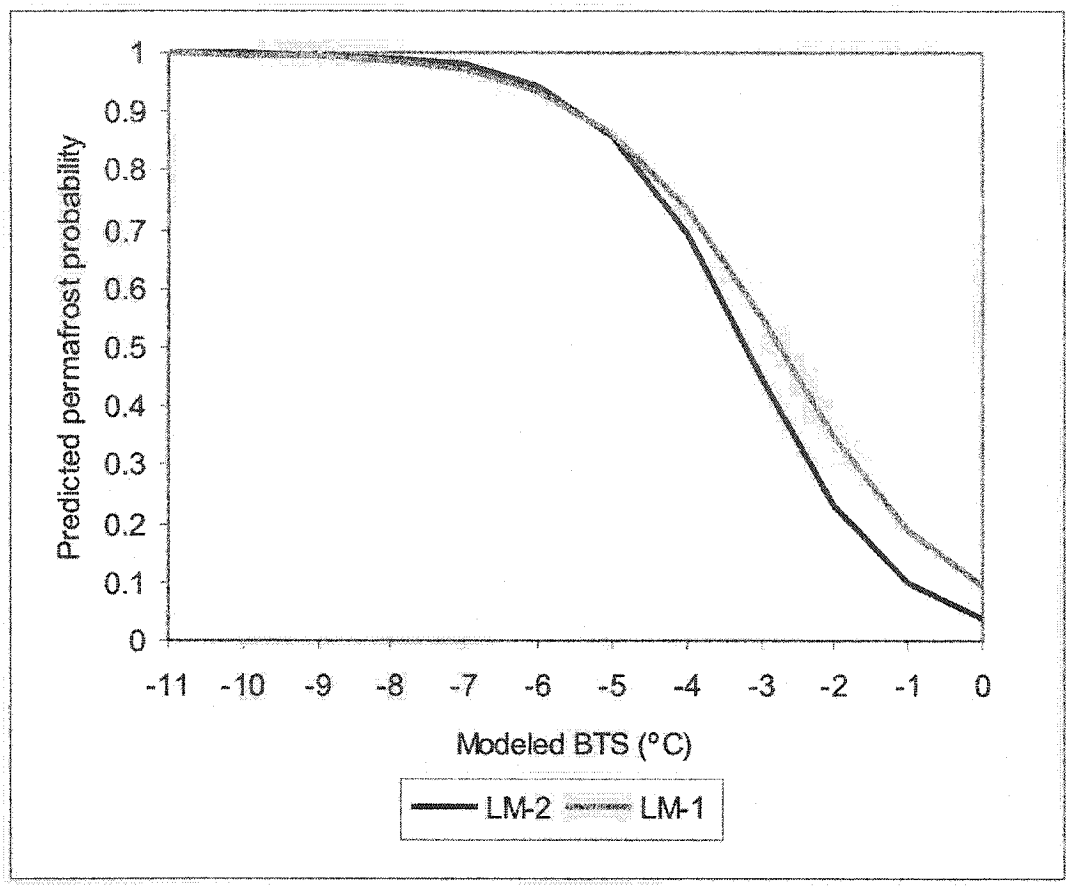

Figure 4.6.4: Permafrost probability curves for LM-1 and LM-2.

LM-2 appears to more accurately reflect the probability of permafrost for the majority of the basin but there still remains the problem of calculating the probability of permafrost within the confined valley under the influence of cold air drainage. Within this area, the model predicts 25%–35% probability of permafrost whereas 62% of the pits excavated on the valley floor had permafrost. Therefore, a third linear logistic regression model (LM-3) was calculated comparing the 40 pits located in the shrub-zone below the tree-line and the BTS values modeled from elevation and PISR. The resulting model coefficients indicated that the constant was not significant while the slope coefficient was significant at a 0.05 level. Since the constant was not significant, the model cannot be used to represent permafrost probabilities in the valley. In place of the model, permafrost distribution was set to the percentage of permafrost calculated from the 40

pits excavated in the valley. The area below the inverted tree line, as identified in Figure 4.6.2, was given a uniform permafrost percentage of 62%.

LM-2 and the percent permafrost calculated for the valley bottom were combined using Arc Map calculator to create a map of the probability of permafrost within the valley and throughout the Wolf Creek basin (Figure 4.6.5). Based on this permafrost probability map, 43% of the basin is underlain by permafrost.

A more detailed map of the area subjected to cold air drainage shows the greater probability of permafrost within the valley bottom when compared to higher elevations on the valley sides (Figure 4.6.6). However, the full extent of the area subjected to cold air drainage in the Wolf Creek basin is unknown. There may be other un-sampled areas where cold air drainage significantly increases the probability of permafrost and these are not represented by the model. Therefore, it is possible that the area underlain by permafrost in the basin is underestimated. A more detailed investigation into the extent of cold air drainage throughout the basin is needed to increase the accuracy of the permafrost probability map.

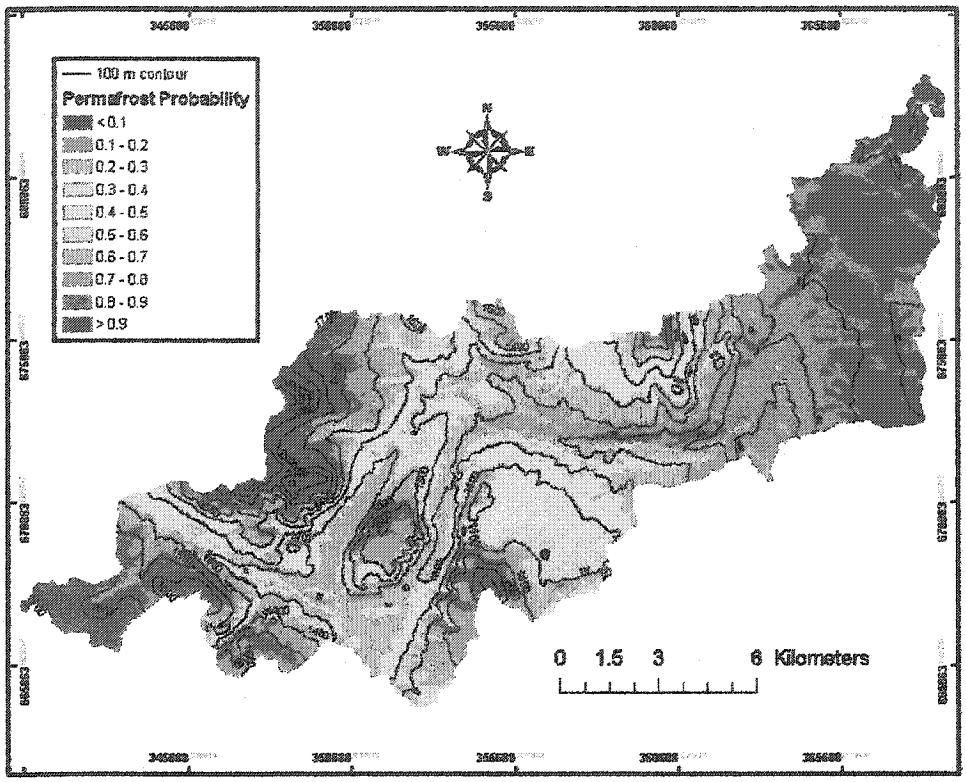

Figure 4.6.5: Permafrost probability map of the Wolf Creek basin created using LM-2 and measured probabilities in the valley west of Coal Ridge.

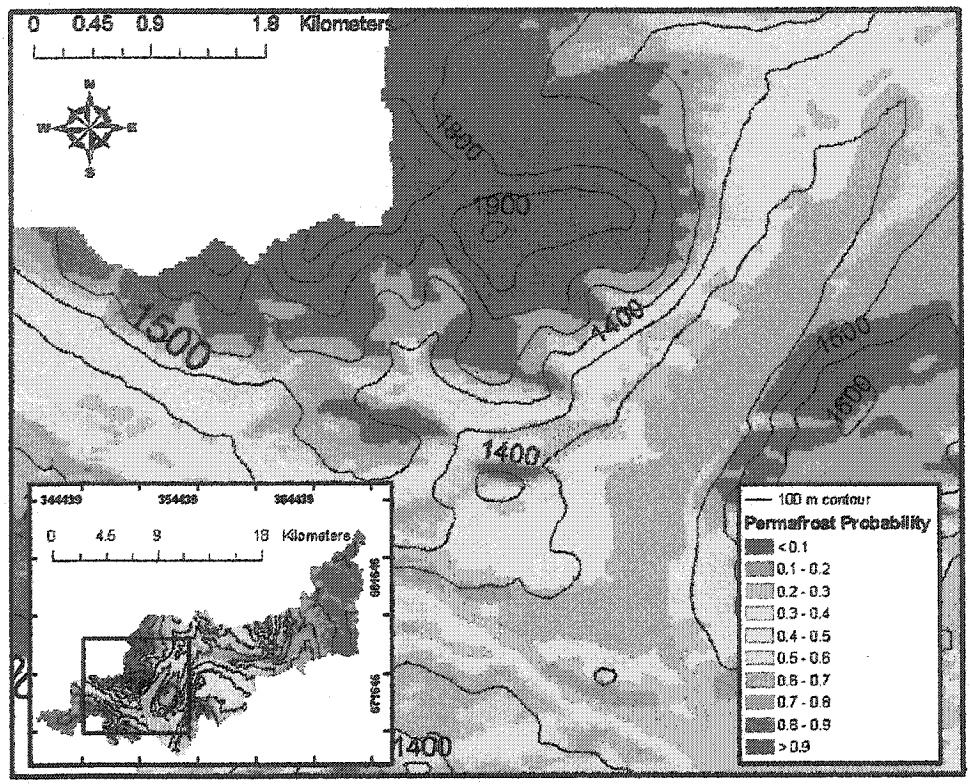

Figure 4.6.6. Large-scale map of the area affected by cold air drainage.

In terms of area underlain by permafrost, LM-2 (Figure 4.6.7) predicts a smaller extent of permafrost in the lower part of the basin than LM-1. Using conventional definitions of permafrost zones (e.g. Heginbottom *et al.*, 1995), isolated patches of permafrost (IP) are predicted for elevations of 600-800 m. The 800-1400 m range constitutes scattered discontinuous permafrost (SDP); the 1400-1700 m range is widespread discontinuous permafrost (WDP), and continuous permafrost (CP) begins at 1700 m. Compared to LM-1 (see Figure 4.5.4) the boundary between continuous and widespread discontinuous permafrost fell by 100 m. However, the scattered discontinuous permafrost zone increased from 600-1300 m to 800-1400 m. Isolated

permafrost was not present within the basin according to LM-1 but was predicted at 600-800 m by LM-2.

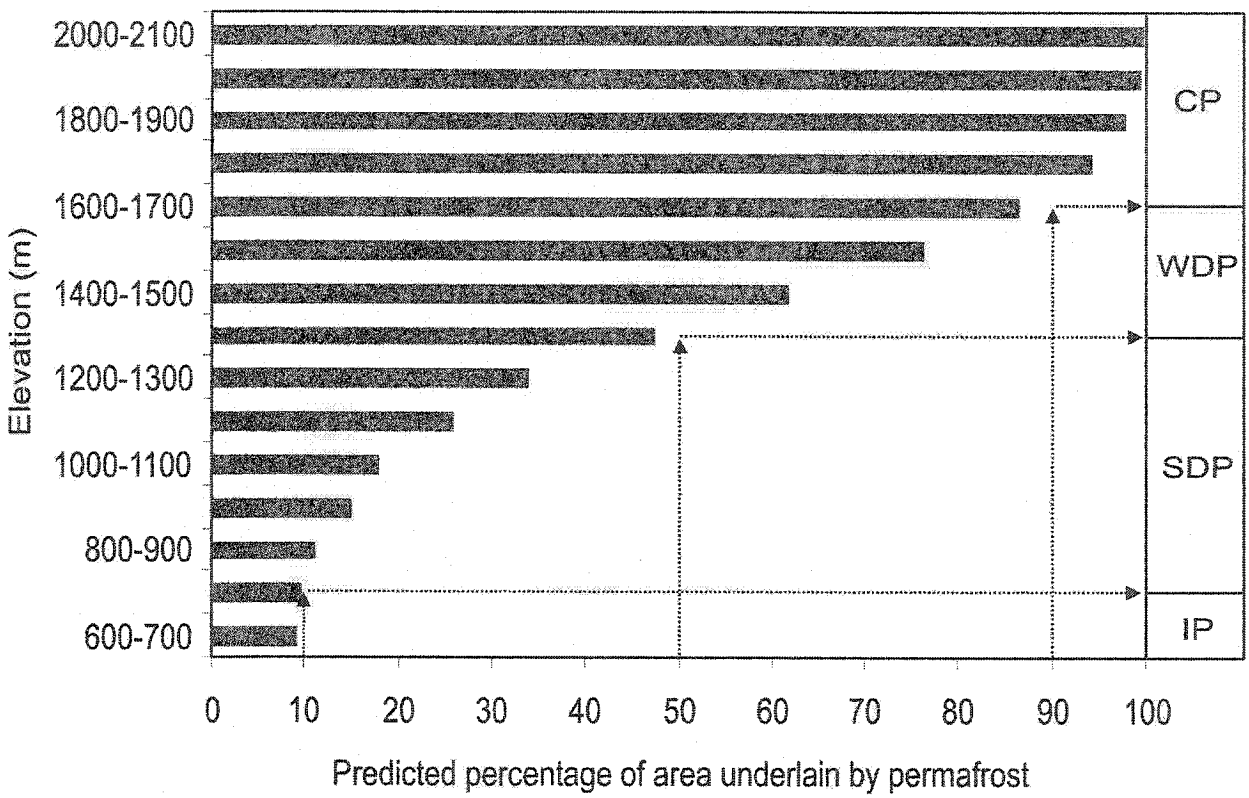

Figure 4.6.7: Predicted percentage of area underlain by permafrost for LM-2.

4.7. Description of permafrost distribution

The construction of a permafrost probability map of Wolf Creek basin permits a detailed analysis of the modeled distribution of permafrost. In this analysis, the permafrost probability is taken as being equivalent to areal extent because the sample size is so large (more than 180,000 grid squares in the basin). For example, neglecting the intra-grid square variability, an individual grid square that has an assessed probability of 40% likelihood of permafrost, either does or does not posses permafrost (*i.e.* either has 0% or 100% permafrost). However, one thousand grid squares are

assessed at the same probability level, 400 are expected to be underlain by permafrost and 600 to be non-permafrost.

Figure 4.7.1 shows the trends in permafrost distribution. The upper reaches of the basin are underlain by continuous permafrost regardless of orientation and slope: above 1800 m, all sites have >90% probability of permafrost. From 600 m to 1800 m, there is a wide range of permafrost probabilities. At elevations less than 800 m, the probability of permafrost is very low: the majority of the basin is less than 10%. In this elevation band, permafrost would be expected to be present only on steep north-facing slopes where conditions are suitable for the growth and preservation of permafrost.

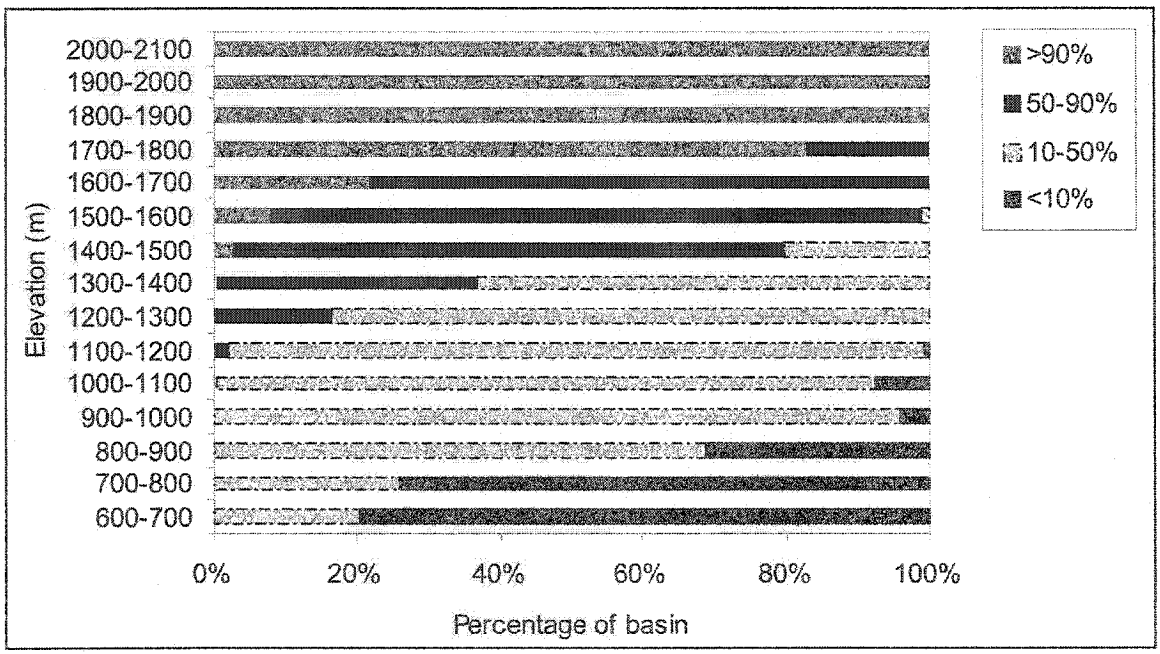

Figure 4.7.1: Trends in permafrost probabilities in relation to elevation.
Note the chart is based on data from the combined LM-2 and LM-2 permafrost probability map.

An alternative description of the distribution of permafrost in the basin in terms of area (km^2) is presented in Figure 4.7.2. This figure illustrates similar points to those in Figure 4.7.1 but shows that elevation bands constitute unequal percentages of the basin.

Consequently, while above 1800 m a.s.l, all the terrain has a permafrost probability of >90%, these areas make up only 5% of the basin area. The majority of the basin between 1400 m and 1700 m is underlain by 50-90% probability of permafrost or widespread discontinuous permafrost. Between 800 m and 1400 m the majority of area is underlain by sporadic discontinuous permafrost (10-50%) and below 800 m the majority of the area is classified as isolated permafrost (<10%).

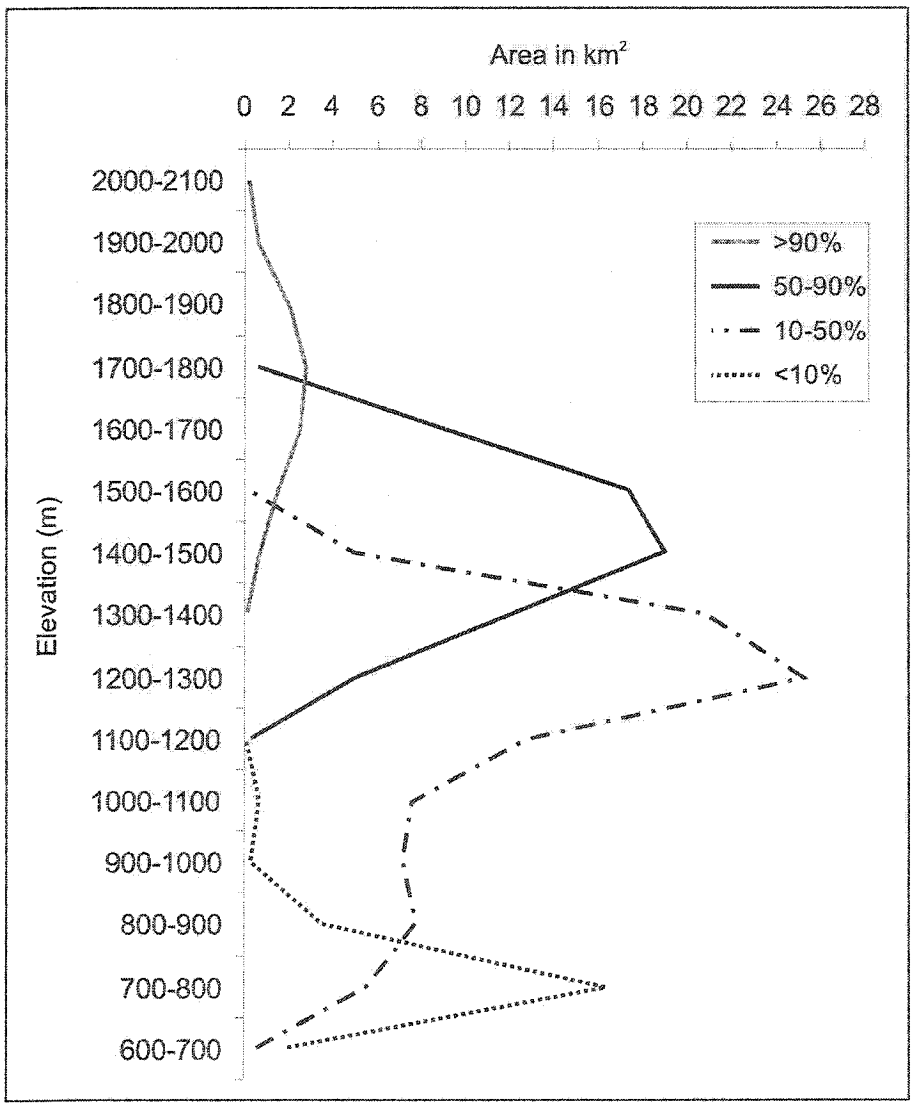

Figure 4.7.2: Extent of permafrost probability classes in km^2.

The angle of the slope was found to significantly influence the modeled probability of permafrost. As shown in Figure 4.7.3, a change in slope angle affects the amplitude of the elevation difference between north-facing and south-facing slopes for permafrost limits. On gentle slopes (*e.g.* a 5° gradient) the elevation difference between north-facing and south-facing aspects for 90% permafrost probability is relatively small, around 58 m. As slope increases, the difference between north-facing and south-facing aspects gets larger, and for a 20° slope is greater than 244 m. The difference in elevation between north-facing and south-facing aspects increases with decreasing probabilities of permafrost, from small difference at 90% permafrost probability to a very large difference at 10% probability of permafrost. Thus according to LM-2, orientation matters more at low probabilities than at high probabilities.

The fluctuation in the lower limit of permafrost on south-facing slopes with changes in slope angle was expected. As south-facing slopes increase in angle, the amount of radiation received also increases. North-facing slopes experience the opposite trend so that an increase in slope angle causes the lower boundary of the permafrost to fall in elevation. On west-facing and east-facing slopes there is virtually no dependency of permafrost probability on slope angle. This summary figure would allow engineers or permafrost researchers to roughly assess the probability of permafrost based on slope angle and elevation in the basin.

The same data were used to produce Figure 4.7.4. This radar chart shows the lower limit of each permafrost category and gives a visual impression of the permafrost distribution around a hypothetical mountain in the basin. The influence of slope angle on north-south asymmetry is clear. The slight east-west asymmetry is caused by extracting results from actual slopes in the basin and reflects differential shading.

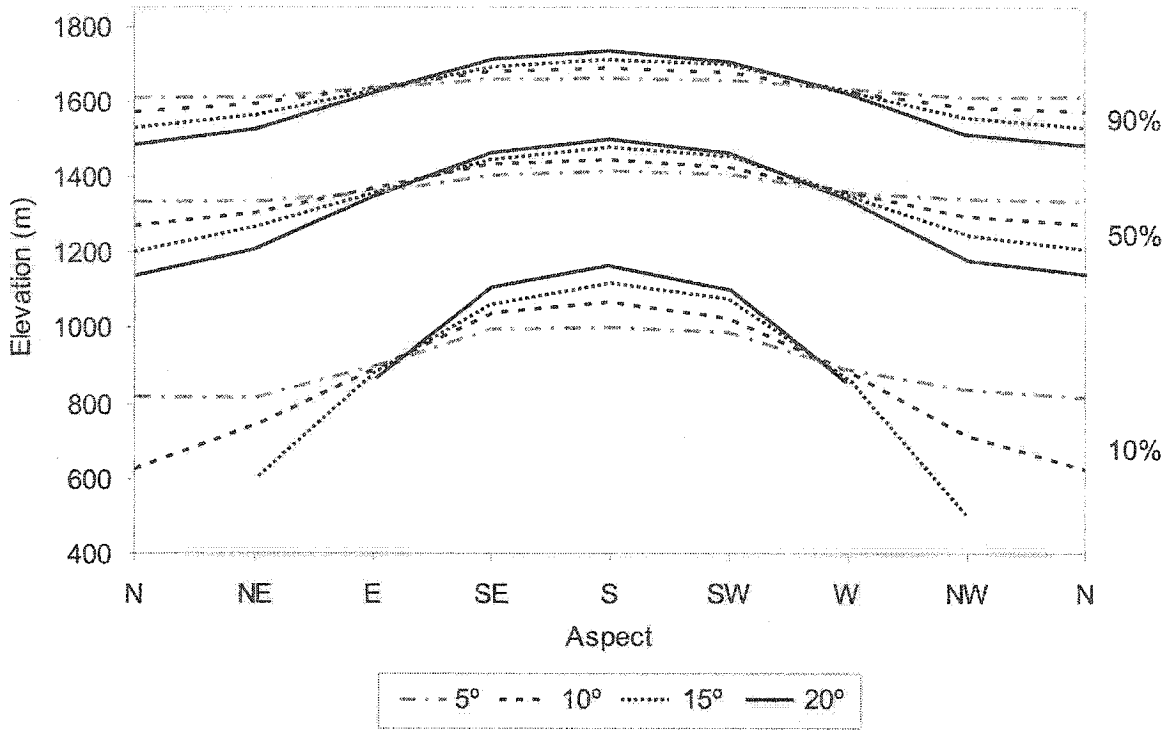

Figure 4.7.3: The lower limit of permafrost probabilities (90%, 50%, 10%) in relation to slope angle and aspect.
Note: North aspect appears twice on the x-axis of the figure to add symmetry and facilitate interpretation. North, north-west, and north-east values could not be calculated for 10% permafrost probability due to elevation being cubed (*i.e.* they fall outside the limits for the basin elevation).

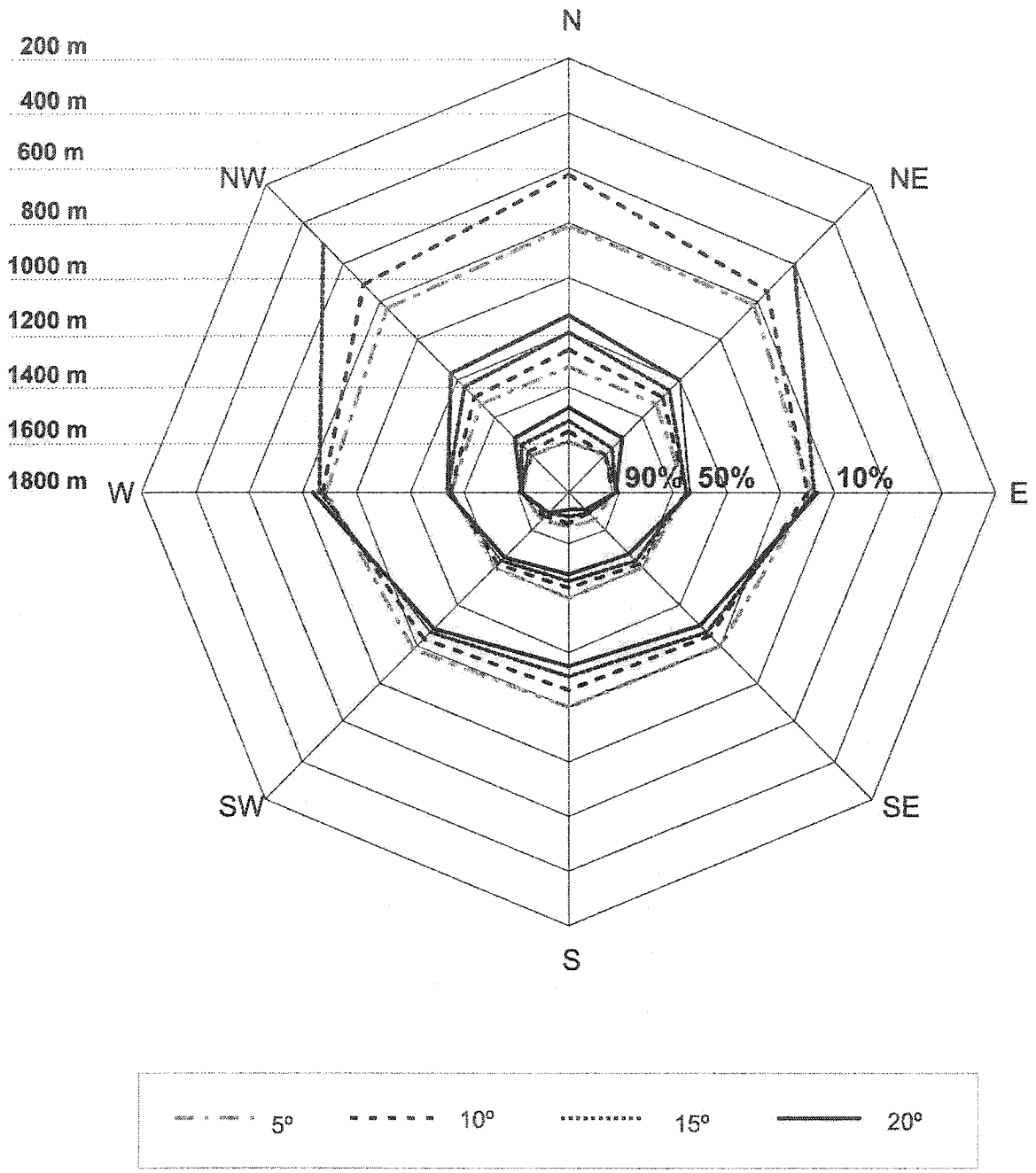

Figure 4.7.4: Radar chart showing the lower limit of permafrost probability (90%, 50%, 10%) on different slope angles over 8 compass directions.
Note: North, north-west, and north-east values could not be calculated for 10% permafrost probability due to elevation being cubed.

4.8. Micro-scale variations in permafrost distribution

In order to examine micro-scale variations (sub 30x30 m or within a single grid cell of the DEM) a total of 36 pairs of pits were excavated with each pair within 30 m of each other. The paired pits were excavated to examine the influence of snow depth (a factor not included in the basin-wide model) on the presence or absence of permafrost. One of each pair was at a location expected to have deep snow (>80 cm) while the other pit was at an estimated shallow snow location (<80 cm). Topography and vegetation were used as indicators of deep and shallow snow depths. Deep snow sites were in hollows or depressions where snow might accumulate and/or had a cover of *Cassiope tetragona*, an indicator of late lying snow cover *(e.g.* Evans *et al.*, 1989). Shallow snow sites were in flat exposed locations that would be wind-swept, preventing snow accumulation and/or had short vegetation covers (<80 cm willow/birch shrubs).

Many of these double pits were located on two transects south and north of Mt. Granger on generally east-facing slopes. Numerous cross-slope benches consisting of a flat crest, a steep riser, and a gentle tread are present in this area (Figures 4.8.1 and 4.8.2). In Figure 4.8.1, darker vegetation is generally located on the gentle topography between the benches and consists of willows and birch trees ranging in height up to 200 cm. The lighter vegetation, mostly composed of short grasses and *Cassiope tetragona*, covers the riser and the upper part of the bench tread. Exposed sites were located on the flat terrain upslope of the slope crest (Figure 4.8.2). The vegetation was composed mainly of dwarf willows and birch ranging in height from 1-30 cm with a ground cover of mosses and grasses. Bare mudboils were present at many sites. Deep snow sites were located in the concavity at the base of the terrace riser. Vegetation here mainly consisted of grasses and *Cassiope tetragona* with some mosses (Figure 4.8.3).

A small number of paired sets of pits were excavated at higher elevations where snow depths were estimated solely on topography and exposure to wind. At low elevations, it was difficult to estimate the depth of snow due to the more developed stands of willow and birch shrubs.

Figure 4.8.1: Picture showing the north slopes of Mount Granger.
The gentle sloping topography is interspersed with short steep slopes referred to a bench steps, light green in colour.

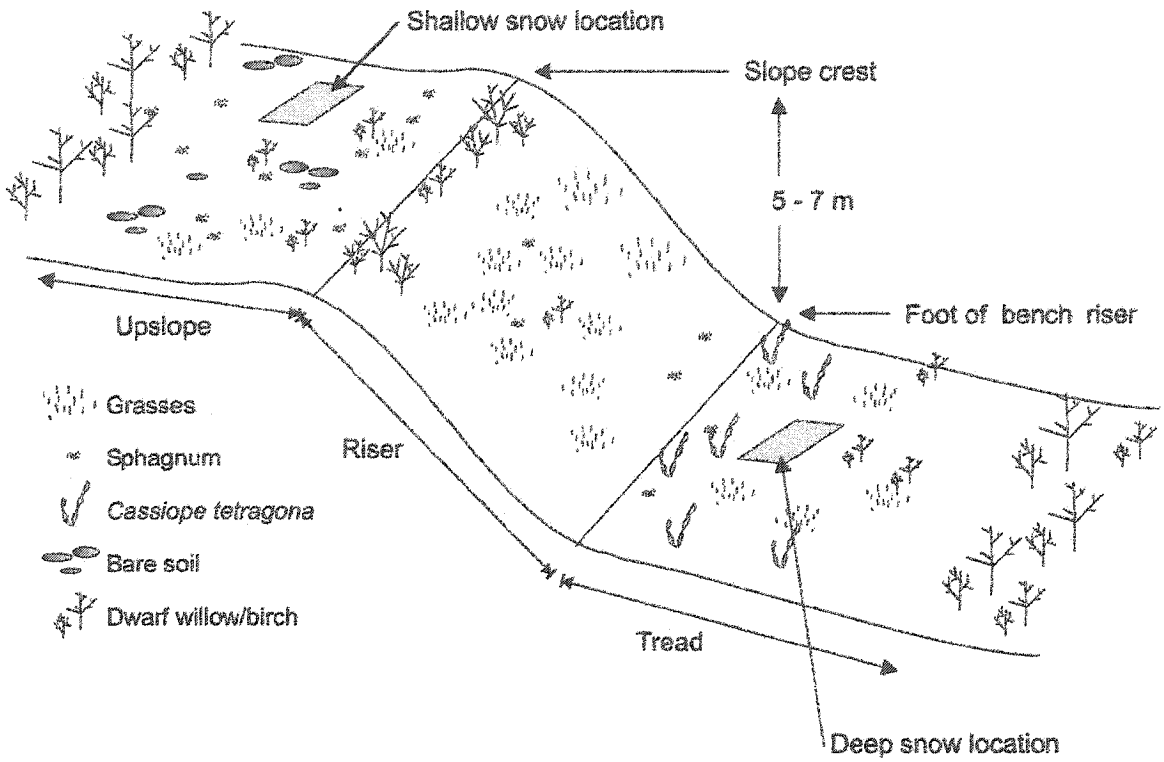

Figure 4.8.2: Schematic of typical bench characteristics.

Figure 4.8.3: The presence of *Cassiope tetragona* indicates the existence of late-lying snow cover.
The pit shown (2002/08/11/A76B, 1470 m) was classified as non-permafrost while the exposed pit of the pair (2002/08/11A76A, 1470 m), located upslope of the crest indicated the presence of frozen ground at 158 cm.

Of the 36 pairs of thin snow/deep snow pits, all of the double pits above 1660 m had permafrost present at both shallow and deep snow locations (18 pairs). Below 1660 m, 13 out of 18 pairs of pits had permafrost conditions at all the shallow snow sites located on the flat terrain just upslope of the riser where slope angles are low, and no permafrost was found at the pits located in the concavity at the foot of the bench riser. Based on a t-test, organic-mat-layer thickness between shallow and deep snow sites was not significantly different, leaving snow depth as the controlling factor of the presence or absence of permafrost.

The results from the paired pit excavations indicate an elevation band where permafrost is controlled by snow depth. Above roughly 1660 m, elevation conditions are suitable for the presence of permafrost and snow depth is irrelevant except on steep south-facing slopes as demonstrated in Section 4.7. Below this elevation, the presence of permafrost is strongly controlled by PISR and depth of snow, the latter varying over short distances. The lower limit of this zone could not be calculated, as snow depth in the tall willow and birch vegetation at lower elevations was impossible to estimate. Results from southern Norway indicate a similar permafrost transition zone ranging from 1300 m to 1550 m, where permafrost distribution is dependent upon snow depth (Sollid *et al.*, 2003).

The results from the paired pits indicate a weakness in the BTS method when employed in the permafrost transition zone. Where snow depths are sufficient to take a BTS measurement, the local area may not be underlain by permafrost due to the thermal characteristics of the deep snow pack. Nearby exposed areas may be underlain by permafrost but BTS measurements cannot be recorded in these areas due to thin snow cover. However, when BTS values are compared to the actual distribution of permafrost (pit excavations with roughly half being in shallow snow and half being in deep snow) the

errors can be eliminated. The problem would have been acute if the European BTS system of three categories was followed.

CHAPTER 5. DISCUSSION

5.1. Impact of snow on permafrost distribution

The inference of possible snow cover at each pit excavation allowed the calculation of predicted permafrost probability of both deep and shallow snow covers scenarios for the Wolf Creek basin. The pits were separated into two categories: deep snow locations (estimated snow depth >80 cm) and shallow snow locations (estimated snow depth of <80 cm). The valley bottom pits below the tree-line removed in LM-2 were also removed from both the shallow and deep snow data sets.

A total of 80 pits were identified as having a deep snow cover. The resulting logistic regression (LM-4), between the presence or absence of permafrost at these 80 pits and modeled BTS gave a slope coefficient and a constant that were significant at the 0.01 level with a critical value of 6.635 [df = 1] (Table 5.1.1)

Table 5.1.1: Variable defined in LM-2, LM-4 and LM-5 regression models.

Model		ß Coefficient	Standard error	Wald	Degrees of Freedom	Significance
LM-2	Constant	-3.23	0.84	14.7	1	<0.01
	BTS	-1.01	0.22	21.0	1	<0.01
LM-4	Constant	-1.87	0.50	13.8	1	<0.01
	BTS	-0.76	0.15	25.7	1	<0.01
LM-5	Constant	-7.92	3.41	5.40	1	0.01
	BTS	-3.09	1.21	6.56	1	0.02

The overall model is also significant at the 0.01 level according to the model chi-square statistic. The model provides a reasonable fit to the observed data but slightly under-predicts permafrost probabilities from -2°C to -3°C BTS and <-5°C (Figure 5.1.1). The model over-predicts the probability of permafrost at the -1°C BTS category (but there is only one observation) and more importantly in the -4° BTS category where it predicts a probability of 61% while only 31% of the pits exhibited permafrost.

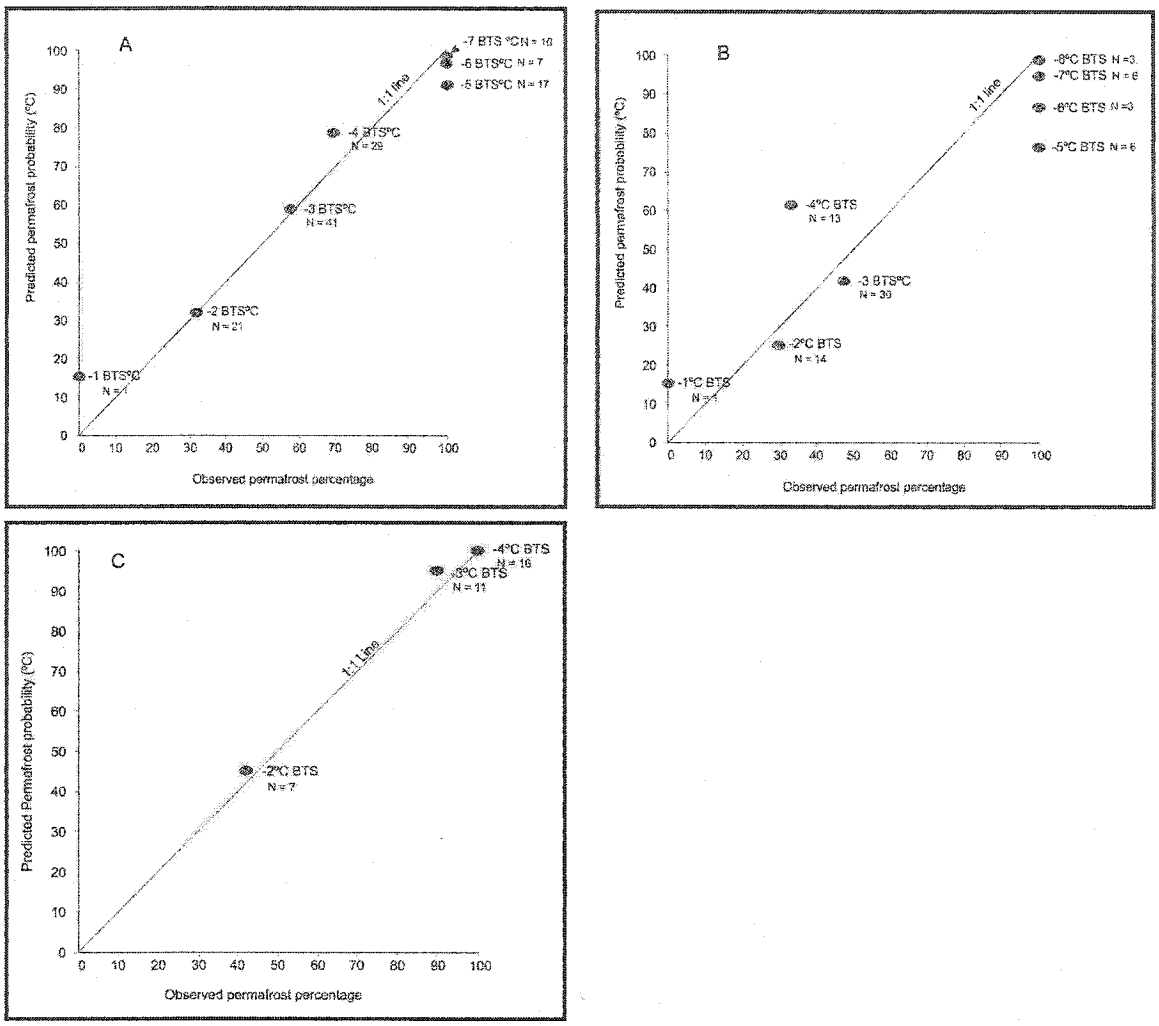

Figure 5.1.1: Observed permafrost percentages versus predicted permafrost probabilities for (A) LM-2, (B) LM-4, and (C) LM-5 at specific BTS values. The number of observations is also presented. Note: the observed permafrost percentage is an average of each BTS category (*i.e.*-1 BTS category includes -1 to -1.999°C). Therefore, the predicted permafrost probability is calculated for the average BTS values (*i.e.* -1 °C BTS = -1.5°C).

The regression equation allows for a permafrost probability curve to be generated (Figure 5.1.2). The permafrost probability curve for LM-4 shows that there is a >90% probability of permafrost at modeled BTS values of <-7°C, and a <10% probability of permafrost at modeled BTS values >-1°C. Compared to LM-2, deep snow conditions decrease the probability level at a given BTS value by 0.1°C to 1.5°C between -6°C and

-3°C BTS. The probability of permafrost predicted by LM-4 and LM-2 becomes similar around -1°C BTS, most likely due to the lack of exploratory pits in the -1°C BTS range.

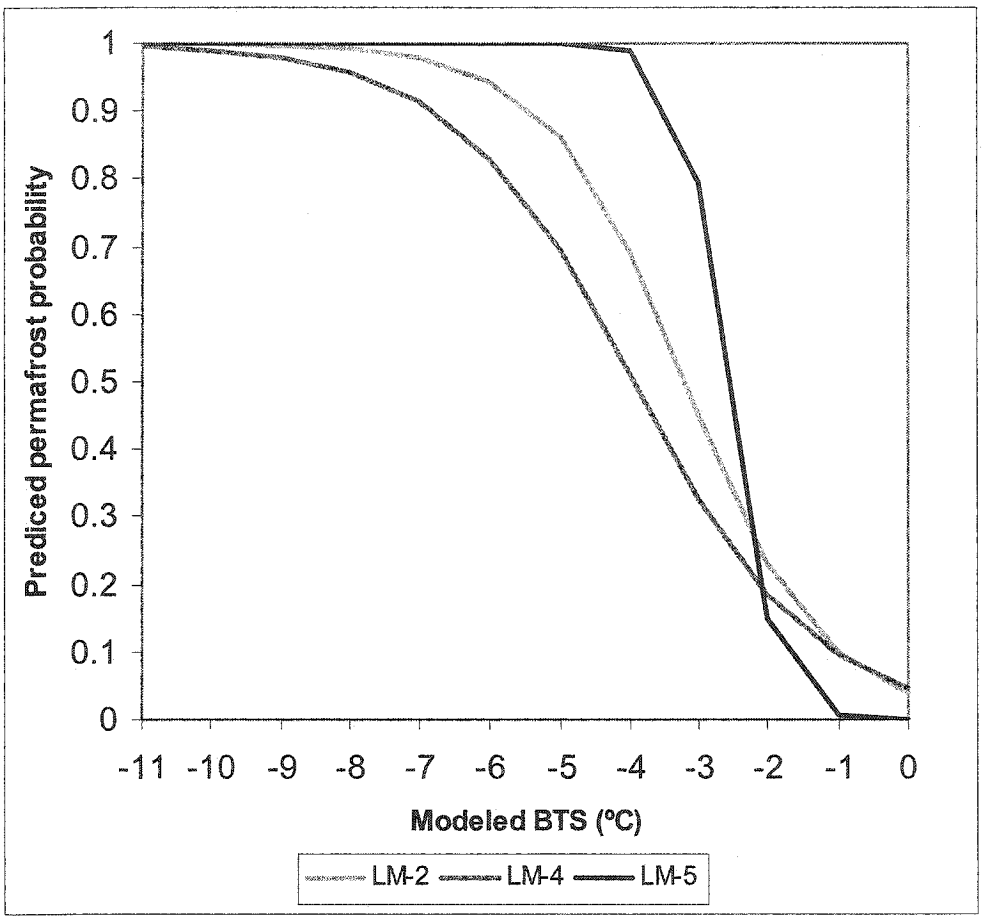

Figure 5.1.2: Permafrost probability curves generated from logistic regression analyses LM-2, LM-4 and LM-5.

The probability curves, as with other logistic models, can be converted into permafrost probability maps of the basin (Figure 5.1.3). According to LM-4, 33% of the basin would be underlain by permafrost if deep snow prevailed throughout.

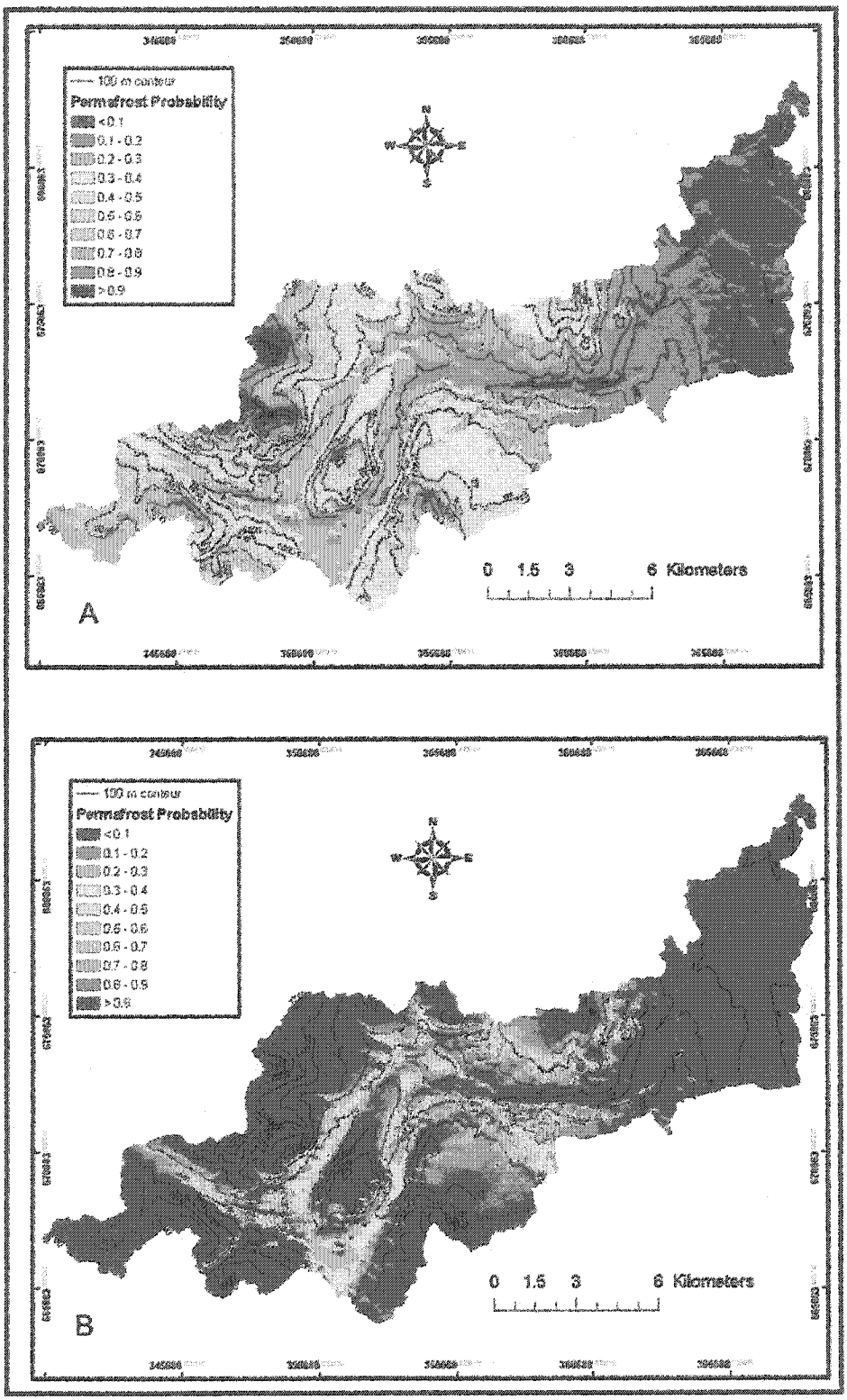

Figure 5.1.3: Map of permafrost probability for the Wolf Creek basin under (A) deep snow conditions and (B) shallow snow conditions.
Note: Cold air drainage in the valley adjoining Coal Ridge is not considered.

In terms of area underlain by permafrost, LM-4 predicts a smaller concentration of permafrost in the lower parts of the basin than does LM-2 (Figure 5.1.4). Using conventional definitions of permafrost zones, isolated patches of permafrost (IP) are predicted in the 600-800 m range. The 800-1500 m range constitutes scattered discontinuous permafrost (SDP), the 1500-1800 m range constitutes widespread discontinuous permafrost (WDP), and the 1800-2100 m range constitutes continuous permafrost (CP).

The distribution of permafrost predicted by LM-4 may be used to estimate the change in permafrost conditions under differing snow accumulation scenarios. The use this model to predict changes in permafrost is tentative as snow depths are estimates only. Under a thick snow cover, the permafrost probability curves produced from LM-4 give a lower concentration of permafrost in the mid-range BTS values. The result is that there is an upward shift of about 100 m in the elevation boundaries of permafrost distribution classes (Table 5.1.2). The greatest difference between the LM-2 and LM-4 is between 1300 m and 1900 m elevation (Figure 5.1.5). Below and above this elevation, there is little change in the area underlain by permafrost.

Table 5.1.2: Elevation boundaries of permafrost classifications for LM-2,LM-4 and LM-5.

	LM-2	LM-4	LM-5
IP	600-800 m	600-800 m	600-1000 m
SDP	800-1400 m	800-1500 m	1000-1200 m
WDP	1400-1700 m	1500-1800 m	1200-1400 m
CP	1700-2100 m	1800-2100 m	1400-2100 m

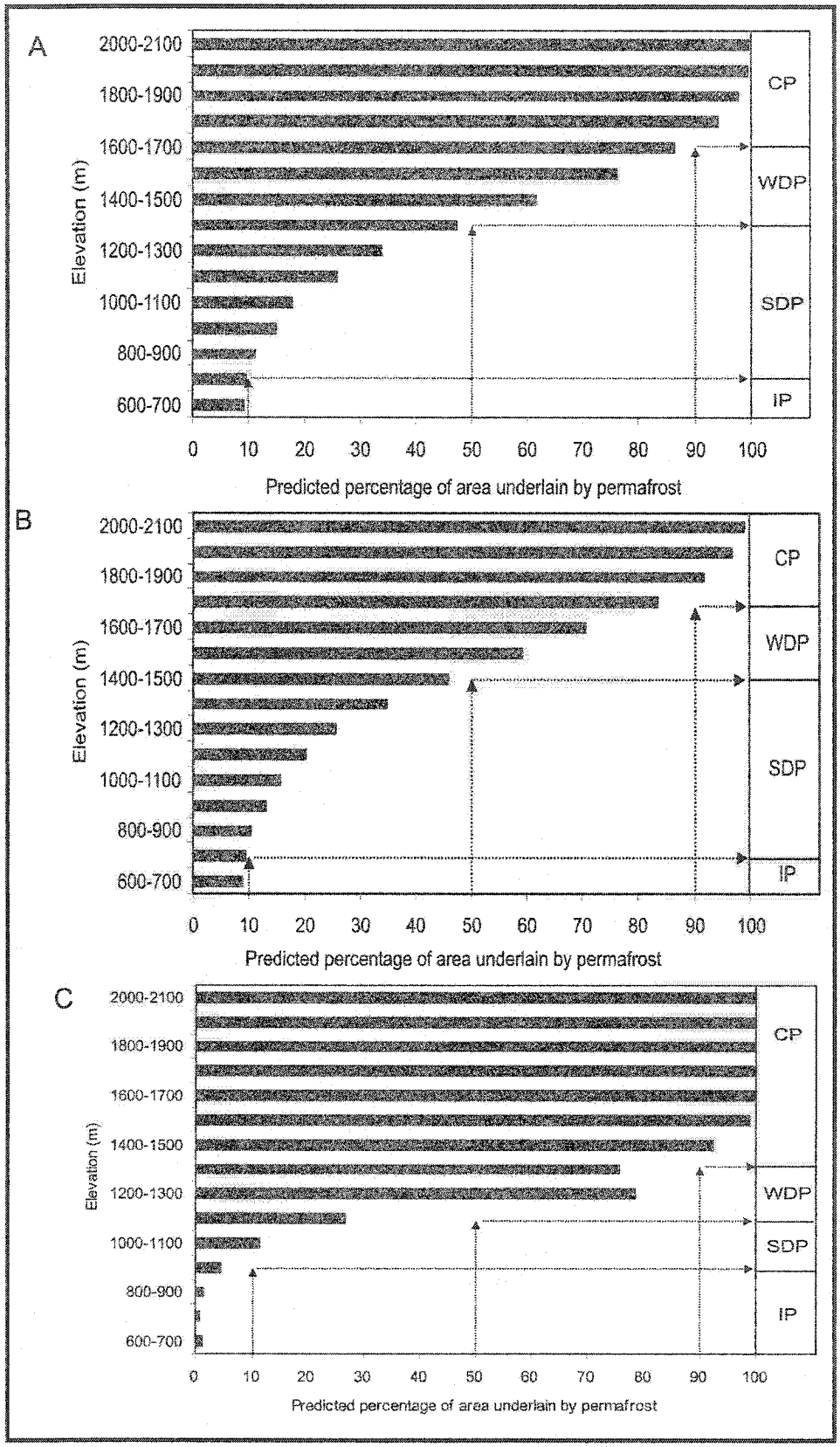

Figure 5.1.4: Predicted percentage of area underlain by permafrost for (A) LM-2, (B) LM-4, and (C) LM-5.

A total of 65 pits were identified as having a shallow snow cover. The resulting logistic regression (LM-5), between the presence or absence of permafrost at these 65 pits and modeled BTS gave a slope coefficient and a constant that were significant at the 0.05 level with a critical value of 3.84 [df = 1] (see Table 5.1.1) The overall model is also significant at the 0.05 level according to the model chi-square statistic.

The model provides a reasonable fit to the observed data but slightly over-predicts the probability of permafrost in the -2°C and -3°C BTS ranges (see Figure 5.1.1). There are no shallow snow pits in the -1°C BTS category. At the -4°C BTS category, the modeled and the observed permafrost are both close to 100%. At modeled BTS values <-4°C the model predicts >99% probability of permafrost and observed permafrost was 100%.

The regression equation allows a permafrost probability curve to be generated (see Figure 5.1.2). The permafrost probability curve for LM-5 shows that there is a >90% probability of permafrost at modeled BTS values of <-3.3°C and a <10% probability of permafrost at modeled BTS values of >-1.9°C. Compared to LM-2, shallow snow conditions increase the probability level for a given BTS value by up to 0.3 between -3°C and -5°C BTS. The slope of LM-5 is steep and crosses LM-2 at -2°C BTS, dropping to virtually zero probability of permafrost at 0°C. The crossing of the curves was unexpected and is probably an artifact of the lack of sample points at the warmer BTS values.

The probability curve can be converted into a permafrost probability map of the basin (see Figure 5.1.3). According to LM-5, 54% of the basin would be underlain by permafrost if shallow snow conditions prevailed throughout. A large increase in the area underlain by continuous (>90% probability) permafrost is predicted by LM-5 compared to LM-2.

In terms of area underlain by permafrost, LM-5 predicts a smaller concentration of permafrost in the lower regions of the basin than both LM-2 and LM-4 (see Figure 5.1.4). Isolated patches of permafrost are predicted in the 600-1000 m range. As noted above, this is probably the result of a lack of sample points at warm temperatures. The 1000-1200 m range constitutes scattered discontinuous permafrost, the 1200-1400 m range represents widespread permafrost, and continuous permafrost is present above 1400 m.

The distribution of permafrost predicted by LM-5 may be used to estimate the change in permafrost conditions under differing scenarios. As with LM-4, the use of this model is tentative as snow depths are only estimated. Under a thin snow cover (LM-5), the permafrost probability curve gives a greater concentration of permafrost in the mid and high-range BTS values, while at BTS >-2°C, permafrost concentrations are lower than in both LM-2 and LM-4. The result is a greater area of the lower part of the basin classified as isolated patches of permafrost (see Table 5.1.2). There is a 200 m upward shift in the isolated patches of permafrost boundary compared to LM-2. The widespread discontinuous permafrost boundary begins 200 m lower than predicted by LM-2. Continuous permafrost covers more of the area than predicted by LM-2, beginning around 1400 m.

5.2. Inter-annual variations in BTS values

Data-loggers were used to record hourly fluctuations in surface and ground temperatures at 60 cm depth (Figure 5.2.1 A-C). They validate the timing of the BTS measurements, supply data about the evolution of temperatures over the winter season, and provide comparative information on temperature in the two seasons of 2000-2001 and 2001-2002. Through average annual temperatures, they also provide an indication of whether permafrost is present. A total of 9 data-loggers recorded surface and ground temperature (60 cm depth) for a minimum of one year and five of these recorded two years of data. At six of these sites, pits were excavated in order to ascertain the presence or absence of permafrost.

Data-loggers are useful for checking on the timing of the BTS survey. BTS surveys were conducted in March/April 2001 and 2002. According to the majority of the loggers, the timing of the BTS surveys was optimal. The ground surface reached a minimum quasi-equilibrium state temperature between March/April. In some cases, such as in data-loggers Cassiope 1 (Figure 5.2.1A) and Semi-permanent snow bank (Figure 5.2.1C), steady state temperatures were not reached until late April. The BTS surveys may have registered a warmer BTS value than later in the month as in the case of the data-logger Semi-permanent snowbank or a colder BTS value, as in the case of logger Cassiope 1 (2001 BTS survey).

The second function of the data-loggers was to supply information on the evolution of surface and ground temperatures throughout the winter season. The information from the data-loggers may be used to reconstruct BTS values. The reconstructions of BTS values were simple in some cases. The data-loggers in Figure 5.2.1C exhibited steady-state ground surface temperatures allowing BTS values to be easily identified. In other cases, reconstruction of BTS values was difficult or impossible due to lack of sufficient snow cover to insulate the ground surface from atmospheric

temperature variations. At C40 for example, the ground surface exhibited large rapid temperatures fluctuations over a wide range during both winters 2000-01 and 2001-02 (Figure 5.2.1B). At this site, a BTS value could not be reconstructed.

Data-logger C6 is located on a steep north-facing slope. The ground at 60 cm depth froze only briefly during winter 2000-01 and temperatures never dropped below 0°C in winter 2001-02. Closer examination of the temperature trends indicates the possibility of ground water at 60 cm (Figure 5.2.2). In late June, there was a dramatic surface warming that was paralleled at 60 cm depth. This may be a result of water flowing through the ground from upslope, warming the surface and ground temperature at the same time. Despite the warming ground temperature at 60 cm, a BTS value of -4.3°C was reconstructed from the data-logger and a modeled BTS value of -4.0°C. According to the permafrost probability curve generated by LM-2, this site would have a 75% probability of permafrost for the reconstructed BTS value and 67% for the modeled value. A pit dug at the site indicated that permafrost was not predicted, as a temperature of 2.2°C was measured at 152 cm.

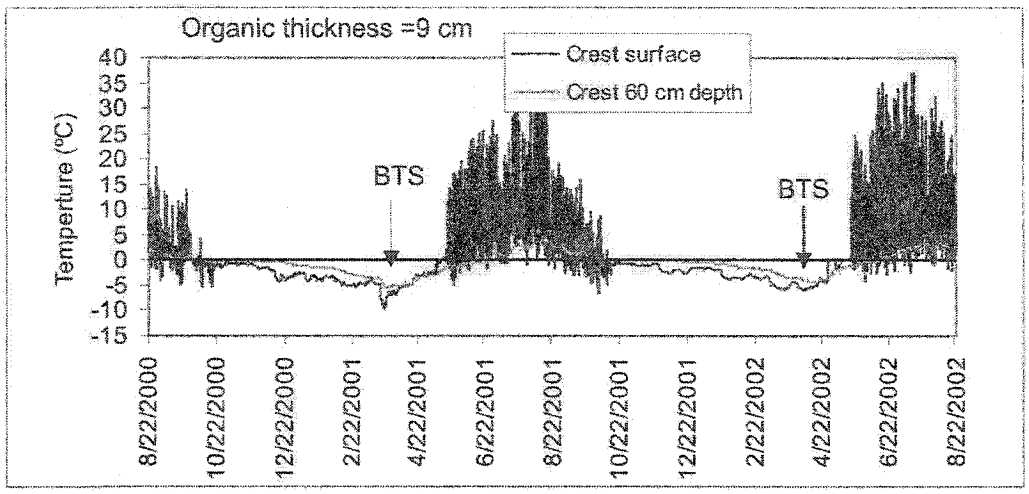

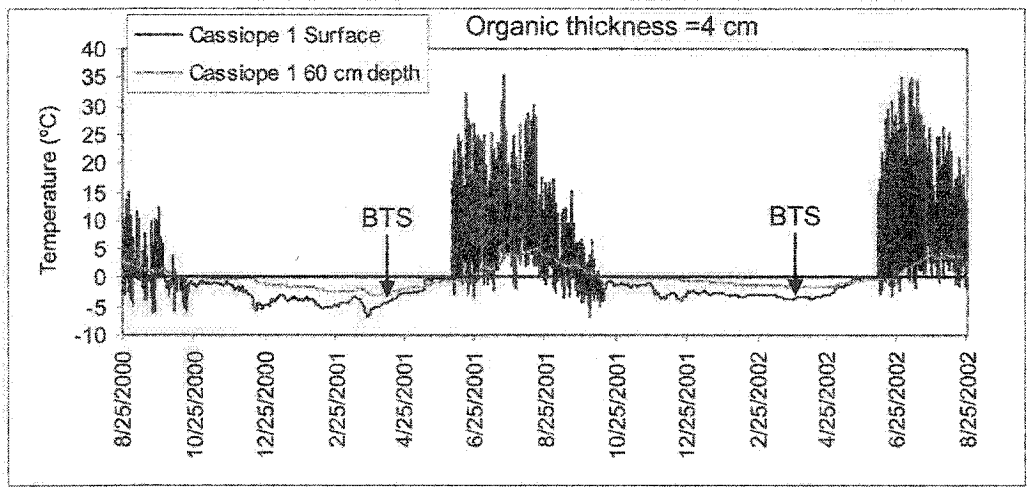

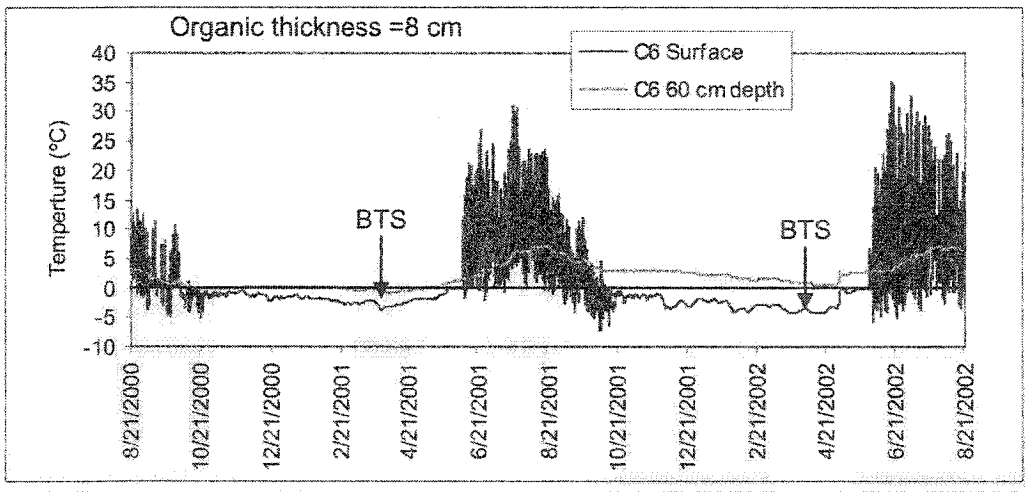

Figure 5.2.1A: Surface and ground temperature from data-loggers Crest, Cassiope 1, and C6.
Note: The organic thickness depth is noted above the graph.

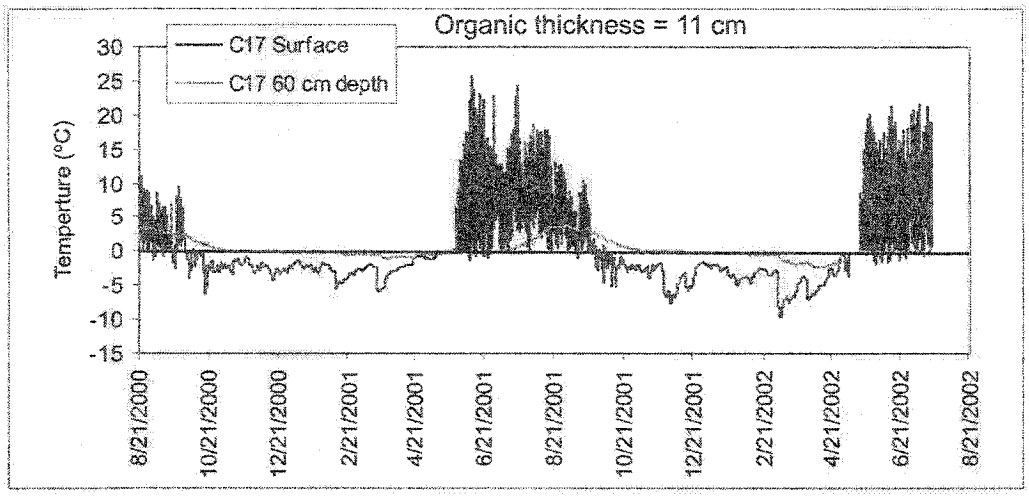

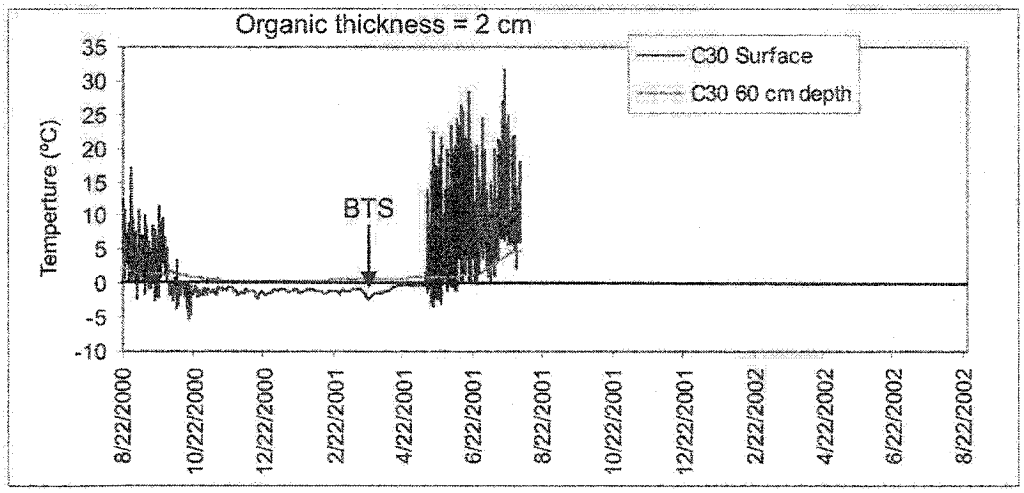

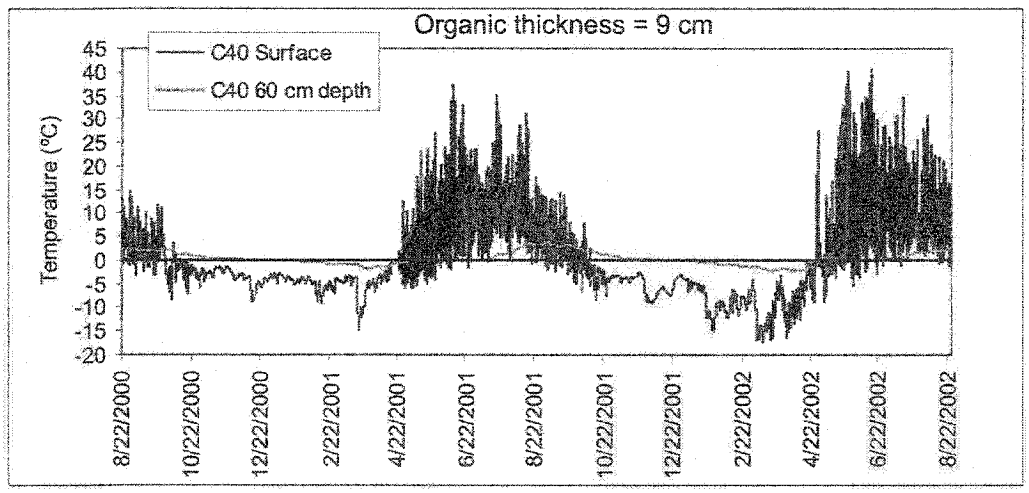

Figure 5.2.1B: Surface and ground temperature from data-loggers C17, C30, and C40. Note: The organic thickness depth is noted above the graph.

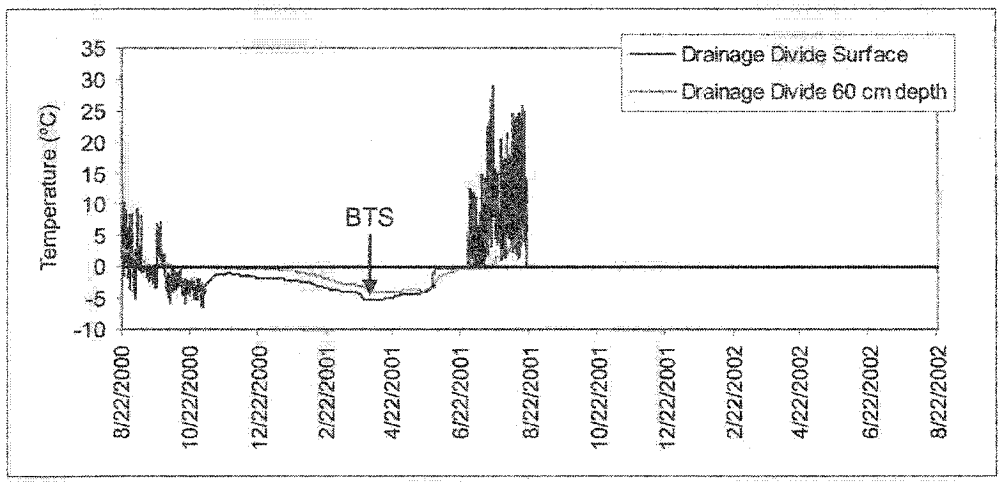

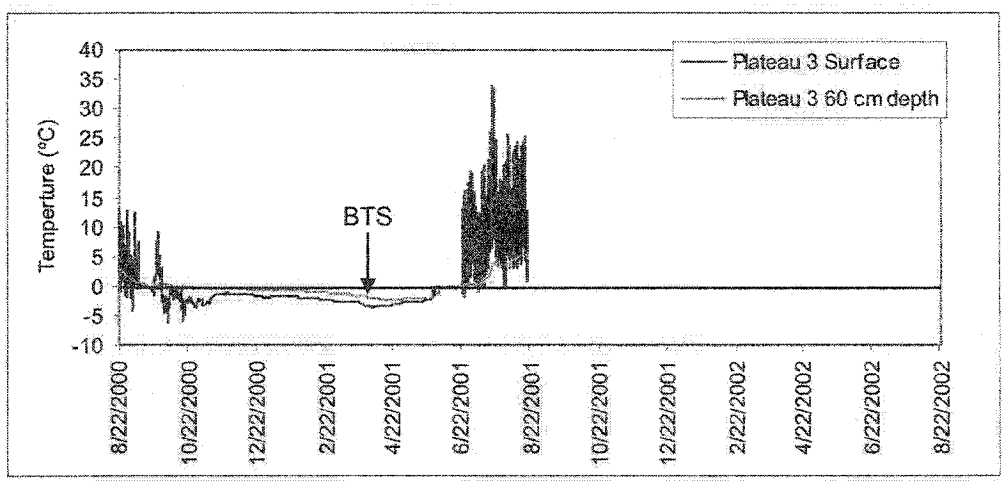

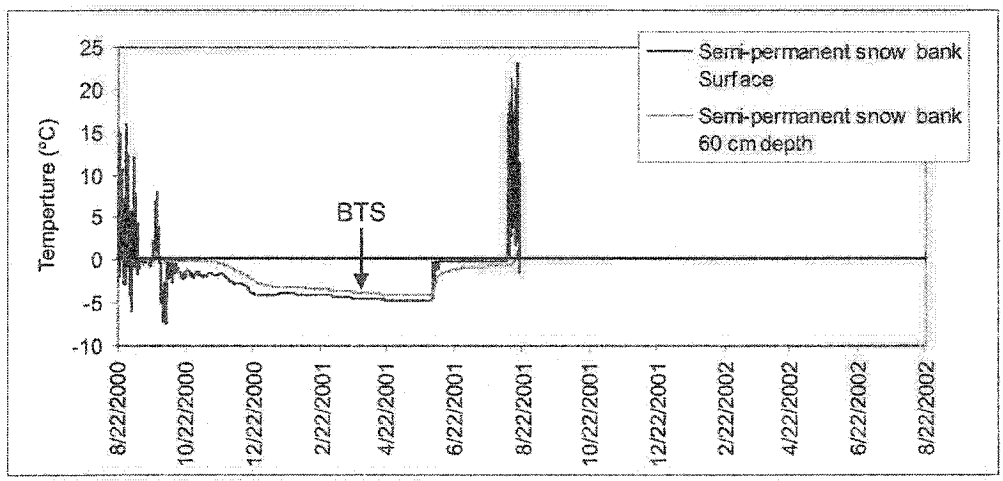

Figure 5.2.1C: Surface and ground temperature from data-loggers Drainage divide, Plateau 3, and Semi-permanent snow bank.
Note: The organic thickness depths are not noted, as pits were not excavated in these locations.

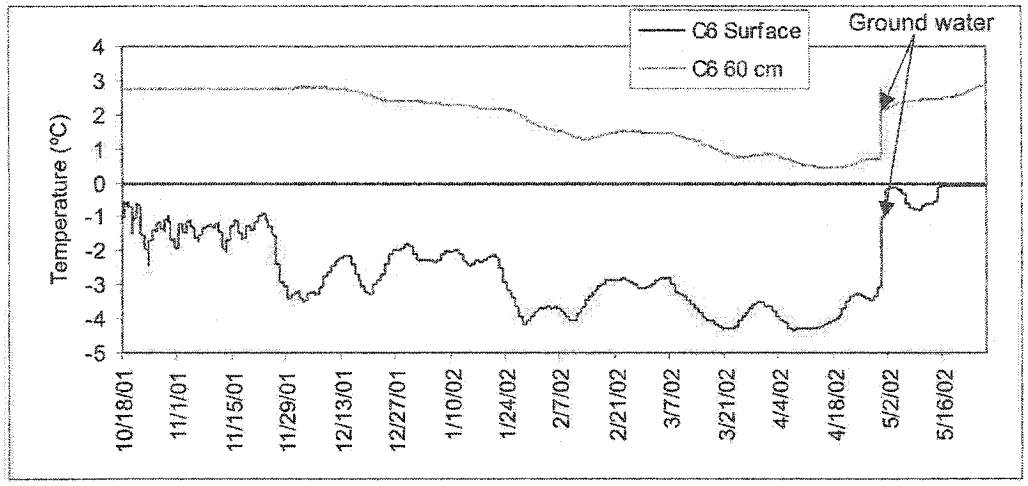

Figure 5.2.2: Possible effect of ground water infiltration on surface and ground temperatures at data-logger C6.

Using the 2-year data set, variations in average temperatures can be compared between years. When temperatures are calculated it is apparent that ground surface and 60 cm depth temperatures were 0.4 - 0.6°C colder in 2000-2001 than in 2001-2002. (Table: 5.2.1). The cooler ground and surface temperatures result from differing snow accumulation patterns as well as atmospheric differences between the two years. For example, diurnal temperature fluctuations at the Crest data-logger flattened out around mid-October during winter 2001-2002. On the other hand, during winter 2000-2001, the fluctuations existed to a greater degree throughout the entire snow cover period. Similar trends were observed in the Cassiope 1 data-set. This indicates that snow accumulation was greater at this site during winter 2001-2002 than in 2000-2001. The average temperature records at the Cassiope 1 site show a temperature offset of 0.4°C between the surface and 60 cm depth for both years. In 2000-01, the average negative temperature at 60 cm suggests that frozen ground could have been present at depth. The next year, 2001-02, surface and 60 cm temperatures were above 0°C. BTS values for both winters were cool, indicating permafrost is probable, yet there is a difference of

2.5°C between winters, with winter 2000-01 being colder. These results suggest that permafrost may be marginal at the Cassiope 1 site and may vary through time. Permafrost might develop at this site during winters with low snow accumulation or extended cold periods. Following warmer winters, such as in 2001-02, permafrost might begin to degrade. The Crest site, located just upslope of Cassiope 1, maintained temperature conditions indicative of frozen ground in both years, suggesting that permafrost is not as marginal.

Table 5.2.1: Average yearly temperature for data-loggers.

Data-logger	2000-01 Temperature (°C)				2001-02 Temperature (°C)			
	Surface	Ground (60 cm)	BTS[a]	Depth to permafrost[b]	Surface	Ground (60 cm)	BTS	Depth to permafrost
Cassiope 1	0.2	-0.2	-5.2	I.P	0.7	0.3	-3.4	N.P
Crest Pit	0.5	-0.7	X	159 cm	1.2	-0.2	-5.8	159 cm
C6	1.1	1.1	-3.6	N.P	0.7	3.1	-4.3	N.P
C17	0.8	0.4	-2.8	N.P	X	X	X	N.P
C30	1.4	1.0	-2.3	N.P	X	X	X	N.P
C40	0.5	0.4	X	N.P	-1.0	0.3	X	N.P
Plateau 3	0.04	-0.3	-3.5	I.P	X	X	X	X
Semi-permanent snowbank	-2.1	-1.9	-4.3	I.P	X	X	X	X
Drainage-divide	-2.1	-1.9	-5.3	I.P	X	X	X	X

Note: X= no valid BTS obtained or no record.
[a]: Reconstructed BTS values from data-loggers.
[b]: I.P = average yearly ground temperature at 60 cm depth is <0°C and is indicative of permafrost at depth. N.P = permafrost was observed or predicted from pit data.

CHAPTER 6. CONCLUSION

6.1. Conclusions

The following conclusions can be reached:

1. BTS values in the study basin vary in a predictable fashion, despite the uncertainties due to heterogeneous snow cover. Consequently, it was possible to develop relations between elevation, potential incoming solar radiation, and BTS values, that have a similar strength to those in Europe (*i.e.* an r^2 value of about 0.40). This is the first time that these relations have been demonstrated in North America.

2. The predicted BTS values relate to the distribution of permafrost as found through probing and inspections pits. Thus the BTS method can be used as a predictor of permafrost distribution. In Wolf Creek, the best estimate is that permafrost underlies 43% of the basin.

3. The successful application of logistic regression to provide a quantitative probabilistic view of mountain permafrost is a significant advance over the standard BTS divisions of "permafrost probable/possible/improbable". The full methodology employed in this thesis is summarized in Figure 6.1.1.

4. Investigation of paired deep-snow and shallow-snow sites, suggests that permafrost presence can vary over short distances. Modeling showed that uniformly deep snow in Wolf Creek would reduce permafrost extent significantly (from 43% to 34%), while widespread shallow snow would increase the extent of permafrost (from 43% to 55%).

5. The winter of 2000-01 produced colder ground surface temperatures beneath the snow than in 2001-02. Values recorded by data-loggers suggest that at some sensitive sites, permafrost may form in some years, exist for a few years, and then disappear.

6. Localized climatologically conditions, such as hypothesized cold air drainage, can affect permafrost distribution in way that the BTS modeling cannot predict at present. Further work will be needed to identify locations affected in this manner and to apply appropriate adjustments to the model.

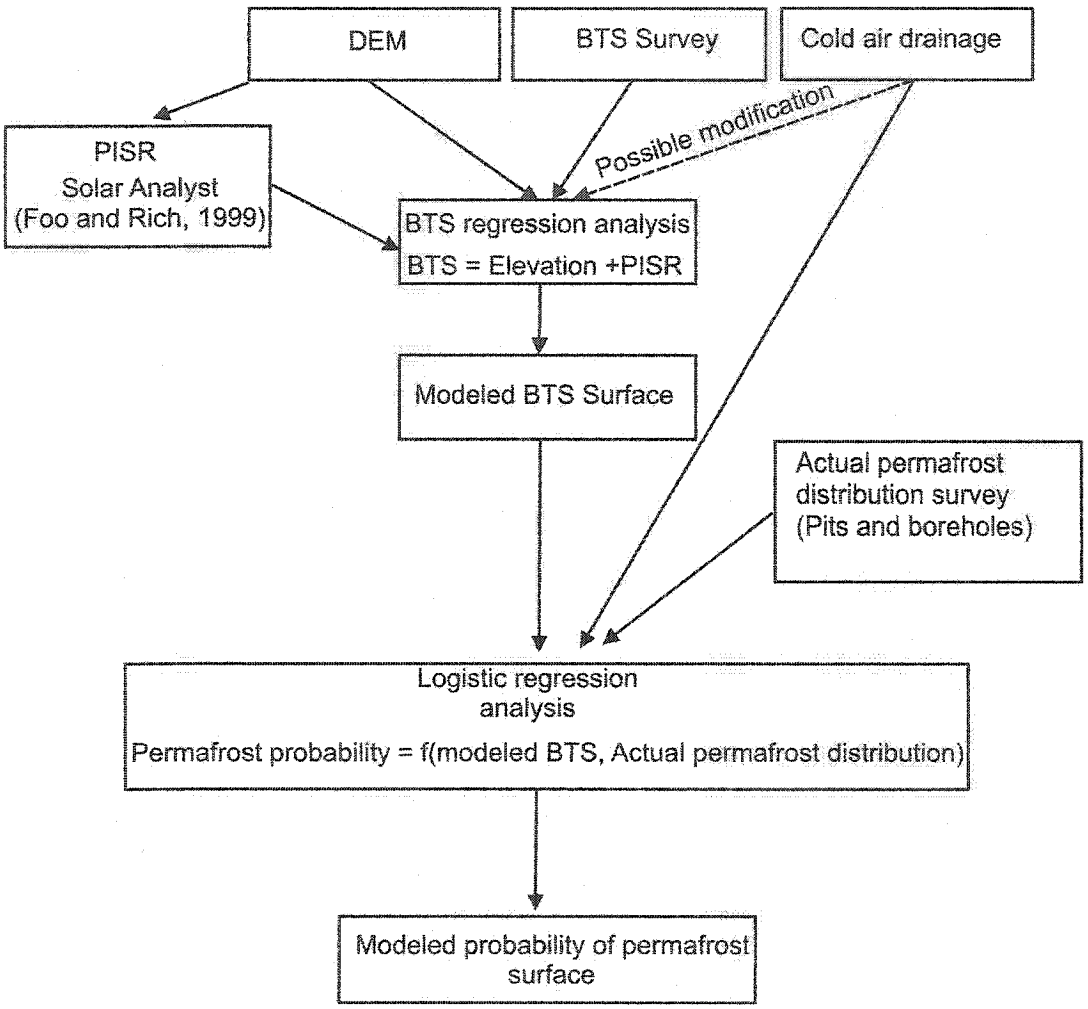

Figure 6.1.1: Steps of the methodology employed by the study.

6.2. Future research

Within Wolf Creek, modeling could be improved by obtaining a better knowledge of actual permafrost distribution for the lower part of the basin. Permafrost predictions to date are based on data from elevations above 1190 m, and 61 km^2 or 32% of the basin is below this. Little is therefore known about permafrost within the boreal forest zone, and the modeling, for example, does not take into account albedo differences or the influence of shading from trees.

The validity of 80 cm snow depth to insulate the ground surface from atmospheric temperature variations was not evaluated in this study. The snow depth limit used was taken from previous investigations in the European Alps and needs to be evaluated in the North American context.

More research is also needed to measure cold air drainage and to identify areas affected by it within the basin. A model needs to be developed to predict where cold air drainage would most likely occur so it could be included in initial BTS modeling and increase the accuracy of the permafrost probability model.

Outside Wolf Creek, there is potential to expand BTS measurements to map permafrost throughout the mountains of Yukon, wherever snow depths are great enough to permit valid measurements. Sufficient sites would be needed to determine the degree to which the relationships between BTS, PISR and elevation, and between BTS and permafrost probability (using logistic regression), are transferable.

References

ACGR 1988: *Glossary of Permafrost and Related Ground-Ice Terms.* National Research of Canada, Technical Memorandum No. 142. pp.64.

Burn, C.R. and Smith, C.A.S. 1988: Observations of the "thermal offset" in near-surface mean annual ground temperatures at several sites near Mayo, Yukon Territory, Canada. *Arctic*, 41(2): 99-104.

Canadian Climate Normals 1994: Canadian monthly climate data and 1943-1993 normals: Ottawa: Environment Canada. CD-rom.

Coultish, T.L. 2002: Long-Term Development of palsas and other permafrost-cored mounds in mountainous terrain, Wolf Creek, southern Yukon. Unpublished M.Sc thesis, University of Ottawa, Ottawa Ontario, pp.125.

Dobinski, W. 1998: Permafrost occurrences in the alpine zone of the Tatra Mountains, Poland. *In* A.G. Lewkowicz and M. Allard, (eds.) *Proceedings, Seventh International Conference on Permafrost, Yellowknife, June 23-27, 1998.* Nordicana, Centre d'Etudes Nordiques, Quebec City. 231- 237.

Duk-Rodkin, A.1999: *Glacial Limits map of Yukon Territory* in Yukon digital geology, S.P. Gordey and A.J. Makepeace (comp.); Geological Survey of Canada Open File D3826 and Exploration and Geological Services Division, Yukon, Indian and Northern Affairs Canada, Open File 1999-1(D)

Etzelmuller, B., Berthling, I., and Ludvig Sollid, J. 1998: The distribution of permafrost in southern Norway- a GIS approach. *In* A.G. Lewkowicz and M. Allard, (eds.) *Proceedings, Seventh International Conference on Permafrost, Yellowknife, June 23-27, 1998.* Nordicana, Centre d'Etudes Nordiques, Quebec City. 251- 256.

Evans, B.M., Walker, D.A., Benson, C.S., Nordstrand, E.A. and Peterson, G.W. 1989: Spatial interrelationships between terrain, snow distribution and vegetation patterns at an arctic foothills site in Alaska. *Holarctic-Ecology*, 12(3): 270-278.

Evans, S.G. and Clague, J.J. 1994: Recent climatic change and catastrophic geomorphic processes in mountain environments. *Geomorphology*, 10: 107-128.

Francis, S. 1997. Data Integration and Ecological Stratification of Wolf Creek Watershed, South-Central Yukon. Report prepared for Indian & Northern Affairs Canada and Agriculture Canada. Applied Ecosystem Management Ltd., Whitehorse, 23 pp.

Fu, P. and Rich, P.M. 1999: Design and implementation of the Solar Analyst: an Arcview extension for modeling solar radiation at landscape scales. http://www.esri.com/library/userconf/proc99/proceed/papers/pap867/p867.htm>

Getis, A. and Griffith, D.A. 2002: Comparative spatial filtering in regression analysis. *Geographical Analysis*, 34(2): 130-140.

Gordey, S.P. and Makepeace, A.J. (comp.) 1999: *Yukon bedrock geology.* Yukon digital geology, S.P. Gordey and A.J. Makepeace (comp.); Geological Survey of Canada Open File D3826 and Exploration and Geological Services Division, Yukon, Indian and Northern Affairs Canada, Open File 1999-1(D)

Granger, R. J.1999: Partitioning of energy during the snow-free season at the Wolf Creek Research Basin. *In* Pomeroy, J.W., Granger, R.J (eds.) *Wolf Creek Research Basin: Hydrology, Ecology, Environment.* Saskatoon: National Water Research Institute. 55-78.

Gruber, S. and Hoelzle, M. 2001: Statistical modeling of mountain permafrost distribution: Local calibration and incorporation of remotely sensed data. *Permafrost and Periglacial Processes*, 12: 69-77.

Haeberli, W. 1973: Die basis-temperatur der winterlichen schneedecke als moglicher indikator fur die verbeitung von permafrost in den aplen. *Zeitschrift fur Gletscherkunde und Glazialgeologie*, 1-2: 221-227.

Haeberli W. and Epifani F. 1986: Mapping the distribution of buried glacial ice- an example from Lago Delle Locce, Monte Rosa, Italian Alps. *Annals of Glaciology*, 8: 78-81.

Haeberli, W., Guodong, C., Gorbunov, A.P. and Harris, S.A. 1993: Mountain permafrost and climatic change. *Permafrost and Periglacial Processes*, 4: 165-174.

Harris, C., Davies, M.C.R. and Etzelmuller, B. 2001: The assessment of potential geotechnical hazards associated with mountain permafrost in a warming global climate. *Permafrost and Periglacial Processes*, 12: 145-156.

Harris, S.A. 1982: Cold air drainage west of Fort Nelson, British Columbia. *Arctic*, 35(4): 537-541.

Harris, S.A. 1988: The alpine periglacial zone. *In* Clark, M.J. (ed.), *Advances in periglacial Geomorphology.* Wiley, Chichester. 369-405.

Harris, S.A. and Corte, A.E. 1992: Interactions and relations between mountain permafrost, glaciers, snow and water. *Permafrost and Periglacial Processes*, 3: 103-110.

Heginbottom, J.R., Dubreuil, M.A., Hanker, P.T., Caron, A., Paul, P. and Rose, I. 1995: Canada Permafrost, 5th edition. 1:7,500,000. The national atlas of Canada, sheet MCR 4177. Ottawa: National Resources Canada.

Hoelzle, M., 1992: Permafrost occurrence from BTS measurements and climatic parameters in the Eastern Swiss Alps. *Permafrost and Periglacial Processes*, 3: 143-147.

Hoelzle, M., Haeberli, W. and Keller, F. 1993: Application of BTS measurements for modeling mountain permafrost distribution. In *Proceedings of the Sixth International Conference on Permafrost, Beijing.* South China University of Technology, Beijing. Vol.1: 272-277.

Hoelzle, M., Mittaz, C., Etzelmuller, B. and Haeberli, W. 2001: Surface energy fluxes and distribution models of permafrost in European Mountain areas: an overview of current developments. *Permafrost and Periglacial Processes*, 12: 53-68.

Hosmer, D.W. and Lemeshow, S. 1989: *Applied logistic regression*. John Willey & Sons, New York, U.S.A. 16-17.

Imhof, M., Pierrehumert, G., Haeberlie, W. and Kienholz, H. 2000: Permafrost investigation in the Schilthorn Massif, Bernese Alps, Switzerland. *Permafrost and Periglacial Processes*, 11: 189-206.

IPCC 1996: Climate change 1995 -The Science of Climate Change. Contribution of Working Groupl to the Second Assessment Report of the Intergovernmental Panel on Climate Change. Editors J.J.Houghton, L.G. Meiro Fillio, B.A. Callander, N. Harris, A. Kattenberg and K. Maskell. Cambridge University Press, Cambridge.

Ishikawa, M.and Hirakawa, K. 2000: Mountain permafrost distribution based on BTS measurements and DC resistivity soundings in the Daisetu Moutains, Hokkaido, Japan. *Permafrost and Periglacial Processes*, 11: 109-123.

Janowicz, J.R. 1999: Wolf Creek Research Basin - Overview. Wolf Creek Research Basin: Hydrology, Ecology, Environment. *In* Pomeroy, J.W., Granger, R.J (eds.) *Wolf Creek Research Basin: Hydrology, Ecology, Environment*. Saskatoon: National Water Research Institute. 125-134.

Jeckel, P.P. 1988: Permafrost and its altitudinal zonation in N. Lapland. In *Proceedings of the Fifth International Conference on Permafrost, Trondheim*. Tapir, Trondheim. Vol.1: 332-337.

Johnson, J.P. and Nickling W.G. 1979: Englacial temperature and deformation of a rock glacier in the Kluane Range, Yukon Territory, Canada. *Canadian Journal of Earth Sciences*, 16: 2275-2283.

Keller, F. and Gubler, H. 1993: Interaction between snow cover and alpine permafrost, Murtle Corvatsch. Swiss Alps. *In Proceedings of the Sixth International Conference on Permafrost, Beijing*. South China University of Technology, Beijing. Vol. 1: 332-337.

Kerr, J.T., Southwood, T.R.E. and Cihlar, J. 2001: Remotely sensed habitat diversity predicts butterfly species richness and community similarity in Canada. *Proceedings of the National Academy of Science of the United States of America (PNAS)*, 98(20): 11365-11370.

King, L. 1990: Soil and rock temperatures in discontinuous permafrost: Gornergrat and Unterrothorn, Wallis, Swiss Alps. *Permafrost and Periglacial Processes*, 1: 177-188.

King, L. 1992: Prospecting and mapping of mountain permafrost and associated phenomenon. *Permafrost and Periglacial Processes*, 3: 73-81.

Kleinbaum, D.G., Kupper, L.L., Muller, K.E., and Nizam, A. 1998: *Applied regression anlaysis and other multivariable methods*. Pacific Grove, Duxbury Press, 656 pp.

Leverington, D.W. and Duguay, C.R. 1996: Evaluation of three supervised classifiers in mapping "depth to late-summer frozen ground" Central Yukon Territory. *Canadian Journal of Remote Sensing*, 22(2): 163-174.

Luoto, M. and Seppäla, M. 2003: Thermokarst ponds as indicators of the former distribution of palsas in Finnish Lapland. *Permafrost and Periglacial Processes*, 14: 19-27.

Mackay, J.R. and Burn, C.R. 2002: The first 20 years (1978-1979 to 1998-1999) of active-layer development, Illisarvik experimental drained lake site, western Arctic coast, Canada. *Canadian Journal of Earth Sciences*, 39: 1657-1674.

Mikusinski, G., Gromadzki, M., and Chylarecki, P. 2000: Woodpeckers as indicators of forest bird diversity. *Conservation Biology*, 15(1): 208-217.

Nelson, F.E. and Outcalt, S.I. 1987: A computational method for prediction and rationalization of permafrost. *Arctic and Alpine Research,* 3: 279-288.

Pereira, J.M.C. and Itami, R.M. 1991: GIS-based habitat modeling using logistic multiple regression: A study of the Mt. Graham red squirrel. *Photogrammetric Engineering & Remote Sensing*, 57(11): 1475-1486.

Sawada, M. 1999: ROOKCASE: An Excel 97/2000 visual basic (VB) add-in for exploring global and local spatial autocorrelation. *Bulletin of the Ecological Society of America*, 4: 231-234.

Seguin, M-K., Stein, J., Nilo, O., Jalbert, C. and Ding, Y.1999: Hydrogeophysical Investigation of the Wolf Creek Watershed, Yukon Territory, Canada. *In* Pomeroy, J.W., Granger, R.J (eds.) *Wolf Creek Research Basin: Hydrology, Ecology, Environment.* Saskatoon: National Water Research Institute. 33-43.

Smith, M.W. and Riseborough, D.W. 1983: Permafrost sensitivity to climatic change. In *Proceedings of the Fourth International Conference on Permafrost.* National Academy Press, Washington, DC. Vol. 1: 450-455.

Smith, M.W. and Riseborough, D.W. 1996: Permafrost monitoring and detection of climate change. *Permafrost and Periglacial Processes*, 7: 301-309.

Smith, M.W. and Riseborough, D.W. 2002: Climate and limits of permafrost: A zonal analysis. *Permafrost and Periglacial Processes*, 13: 1-15.

Sokal, R. and Oden, N. 1978: Spatial autocorrelation in biology 1. Methodology. *Biological Journal of the Linnean Society*, 10: 199-228.

Solid, J.L., Isaksen, K., Eiken, T. and Ødegård, R.S. 2003: The transition zone of mountain permarfrost on Dovrefjell, southern Norway. *In Proceedings, 8th International Conference on Permafrost.* In press.

Taylor, A., Nixon, M., Eley, J., Burgess, M. and Egginton, P. 1998: Effects of atmospheric temperature inversions on ground surface temperatures and discontinuous permafrost, Norman Wells, Mackenzie Valley, Canada. *In* A.G. Lewkowicz and M. Allard, (eds.) *Proceedings, Seventh International Conference on Permafrost, Yellowknife, June 23-27, 1998.* Nordicana, Centre d'etudes nordiques, Quebec City. 1043-1048.

Vonder Mühll, D., Stucki, T. and Haeberli, W. 1998: Borehole temperatures in alpine permafrost: A ten year study. *In* A.G. Lewkowicz and M. Allard, (eds.) *Proceedings, Seventh International Conference on Permafrost, Yellowknife, June 23-27, 1998.* Nordicana, Centre d'Etudes Nordiques, Quebec City. 1089-1095.

Vonder Mühll, D., Hauck, C., Gubler, H., McDonald, R. and Russill, N., 2000: New geophysical methods of investigating the nature and distribution of mountain permafrost with specific references to radiometry techniques. *Permafrost and Periglacial Processes*, 12: 27-38.

Washburn, A.L. 1979: *Geocryology.* Edward Arnold, London. 406pp.

Wheeler, J.O. 1961: *Whitehorse Map-area, Yukon Territory 105 D.* Geological Survey of Canada, Memoir 312.

Woo, Ming-ko., and Carey, S. K. 1999: Permafrost, seasonal frost and slope hydrology, Central Wolf Creek Basin, Yukon. *In* Pomeroy, J.W., Granger, R.J (eds.) *Wolf Creek Research Basin: Hydrology, Ecology, Environment.* Saskatoon: National Water Research Institute, pp. 45-53.

Yukon. Dept. of Renewable Resources. Geographic Information System. *2000: RRGIS 30 m digital elevation model [electronic resources].* Yukon Department of Renewable Resources, Geographic Information Systems.